

AD-E 300 064

12

DNA 4348T

AD A U 48872

# THE ARBITRARY BODY OF REVOLUTION CODE (ABORC) FOR SGEMP/IEMP

IRT Corporation  
P.O. Box 80817  
San Diego, California 92138

1 July 1976

Topical Report for Period September 1975—June 1976

CONTRACT NO. DNA 001-75-C-0071

APPROVED FOR PUBLIC RELEASE;  
DISTRIBUTION UNLIMITED.

THIS WORK SPONSORED BY THE DEFENSE NUCLEAR AGENCY  
UNDER DTIC RMSS COLL B323076464 R99QAXE B06903 H2590D.

Prepared for  
Director  
DEFENSE NUCLEAR AGENCY  
Washington, D. C. 20305

DDC  
RECEIVED  
JAN 18 1978  
B

AD NO. 1  
JDC FILE COPY

Destroy this report when it is no longer  
needed. Do not return to sender.



(18) DNA, SBIE

(19) 4348TAD-E344 464

UNCLASSIFIED

SECURITY CLASSIFICATION OF THIS PAGE (When Data Entered)

REPORT DOCUMENTATION PAGE		READ INSTRUCTIONS BEFORE COMPLETING FORM
1. REPORT NUMBER DNA 4348T	2. GOVT ACCESSION NO.	3. RECIPIENT'S CATALOG NUMBER
4. TITLE (and Subtitle) <b>THE ARBITRARY BODY OF REVOLUTION CODE (ABORC) FOR SGEMP/IEMP.</b>		5. TYPE OF REPORT & PERIOD COVERED Topical Report Sep 1975-Jun 1976
7. AUTHOR(s) Andrew J./Woods Thomas N./Delmer		6. PERFORMING ORG. REPORT NUMBER INTEL-RT-8141-028
9. PERFORMING ORGANIZATION NAME AND ADDRESS IRT Corporation P.O. Box 80817 San Diego, California 92138		8. CONTRACT OR GRANT NUMBER(s) DNA 001-75-C-0071
11. CONTROLLING OFFICE NAME AND ADDRESS Director Defense Nuclear Agency Washington, D.C. 20305		10. PROGRAM ELEMENT, PROJECT, TASK AREA & WORK UNIT NUMBERS Subtask R99QAXEB069-03
14. MONITORING AGENCY NAME & ADDRESS (if different from Controlling Office)		12. REPORT DATE 1 Jul 76
		13. NUMBER OF PAGES 144
		15. SECURITY CLASS. (of this report) UNCLASSIFIED
16. DISTRIBUTION STATEMENT (of this Report) Approved for public release; distribution unlimited.		15a. DECLASSIFICATION/DOWNGRADING SCHEDULE
17. DISTRIBUTION STATEMENT (of the abstract entered in Block 20, if different from Report)		
18. SUPPLEMENTARY NOTES This work sponsored by the Defense Nuclear Agency under RDT&E RMSS Code B323076464 R99QAXEB06903 H2590D.		
19. KEY WORDS (Continue on reverse side if necessary and identify by block number) SGEMP ABORC Computer Code Photo-Compton Currents IEMP Maxwell's Equations Space-Charge-Limiting EMP Particle in Cell Resonant Structures		
20. ABSTRACT (Continue on reverse side if necessary and identify by block number) The ABORC computer code for the solution of electromagnetic currents and fields around arbitrary bodies of revolution in SGEMP/IEMP problems is documented. Detailed descriptions of the physics and modeling used in the code are provided, and validation tests are discussed. Sample problems of interest in SGEMP, including results obtained for a wide range of object sizes and photon excitations, as well as geometry effects calculations, are explained. Considerations in choosing numerical grid sizes are outlined, and a complete user's manual is provided.		

## CONTENTS

1. INTRODUCTION . . . . .	3
2. ABORC COMPUTER CODE DESCRIPTION . . . . .	4
3. ABORC VERIFICATION . . . . .	6
3.1 Empty Cylinder Field Solution . . . . .	6
3.2 Double-Cylinder Field Solution . . . . .	10
3.3 Particle Emission Tests . . . . .	12
3.4 Checkouts Including Particle Motion . . . . .	16
3.4.1 Analytical Comparisons for Particle Motion . . . . .	16
3.4.2 Comparisons of ABORC with Other SGEMP Codes . . . . .	17
3.4.3 Summary of Code Verifications . . . . .	23
4. SUMMARY . . . . .	24
REFERENCES . . . . .	26
APPENDIX A - DESCRIPTION OF THE PHYSICS AND MODELING EMPLOYED IN THE ABORC CODE . . . . .	27
APPENDIX B - SAMPLE ABORC CALCULATIONS: SCALING LAWS FOR SGEMP . . . . .	45
APPENDIX C - SAMPLE ABORC CALCULATIONS: SGEMP GEOMETRY EFFECTS . . . . .	53
APPENDIX D - NUMERICAL SENSITIVITY CONSIDERATIONS IN ABORC CALCULATIONS . . . . .	79
APPENDIX E - USER'S MANUAL FOR ABORC AND PERIPHERAL COMPUTER CODES . . . . .	97

ACCESSION for		
HTIS	White Section	<input checked="" type="checkbox"/>
DOC	Buff Section	<input type="checkbox"/>
UNANNOUNCED		<input type="checkbox"/>
JUSTIFICATION		
BY		
DISTRIBUTION/AVAILABILITY CODES		
Dist.	AVAIL	and/or SPECIAL
A		

## 1. INTRODUCTION

The ABORC (arbitrary body of revolution) computer code for the solution of system-generated electromagnetic pulse (SGEMP) and internal electromagnetic pulse (IEMP) on arbitrary bodies of revolution is documented in this report. The code is designed primarily for the solution of electromagnetic currents and fields produced by arbitrary axisymmetric emission of electrons due to photons incident on objects such as satellites or missiles. The complete set of Maxwell's equations is solved and coupled with particle motion representing currents. Self-consistent, time-dependent solutions of currents and fields are obtained in two dimensions.

This report contains a description of code capabilities and various tests which have been performed to determine the validity of its solutions by comparing ABORC fields and currents with analytical solutions, where available, and also with other computer codes.

Detailed descriptions of the physics and modeling are contained in Appendix A. Sample ABORC calculations on problems of interest in SGEMP are found in Appendices B and C. Results in Appendix B permit order-of-magnitude estimates for SGEMP responses over wide ranges of object size and photon excitation. Appendix C contains pertinent considerations of geometry effects under space-charge-limited (SCL) conditions. The appendices show by illustration the range of applicability of ABORC to SGEMP calculations.

Some numerical sensitivity considerations are discussed in Appendix D. These are designed to aid the user in producing results containing minimal statistical noise. A complete user's manual for ABORC and related graphics is provided in Appendix E.

## 2. ABORC COMPUTER CODE DESCRIPTION

The ABORC code solves Maxwell's equations with self-consistent electron motion in a vacuum for axisymmetric geometries. Direct finite-differencing of the field equations is done employing generalized coordinates, and finite "particles" of charge are followed through the spatial mesh of zones to obtain currents. Emission of arbitrary energy, angular, spatial, and time distributions of currents can be specified, including fully time-dependent spectrum and spatial distributions. Randomizing techniques are employed for all distributions for efficient numerical representation.

Boundary conditions currently available in the code require the specification of an outer, perfectly conducting cylinder. Free-space solutions can be obtained by moving the outer boundary out so the clear time (the time in which reflections from the outer wall return to the structure) is larger than the problem time of interest. The shape of the inner wall of the outer conductor can be modified to an arbitrary body of revolution by specifying conductivities within the outermost cylinder, but the final spatial extent of the calculation is the above-mentioned perfectly conducting cylinder.

Finite conductivities can be specified representing imperfect conductors, and dielectric structures may be treated by specifying proper dielectric constants. While the former is programmed into ABORC and is implemented by simple input card specification, the latter capability is somewhat limited. Dielectrics with  $\epsilon = \epsilon_0$  (free space permittivity) can be specified throughout the volume of the calculation by simply specifying conductors of very low conductors. Resistors are specified in this way, where the conductivity is chosen to give the sought-after resistance value. Care must also be taken here to ensure that the skin depth of the resistor is large enough to allow proper field penetration. Dielectrics with  $\epsilon \neq \epsilon_0$  present a different problem, however, in that no

provision has been made for them in the field equations. Programming changes are therefore necessary to add this capability. For certain cases with small, well defined volumes of dielectrics, however, this change can be relatively minor.

While most SGEMP/IEMP calculations are performed assuming complete absorption of photo-electrons upon impact with surfaces, back-scattering of electrons can be specified in ABORC if desired. Variable amounts of charge with modified energy and direction of propagation can be re-emitted from surfaces upon contact. This feature is presently limited to back-scattering from a simple cylinder with energy- and angle-independent reflection fractions, energy dissipation, and specular angle. Studies undertaken with this code option have shown considerable effect on SGEMP response under certain conditions (Ref. 1).

Graphics features include the capability of simple specification of most major calculational quantities at arbitrary locations to be disposed to various plotting routines. These routines include printer plots, pen plots, CKT plots, and 16mm computer-generated movies of electron trajectories. Files of data from different ABORC runs can be overlaid conveniently, allowing accurate analysis of calculations. Time histories and spatial distributions of fields and currents can be correlated directly with particle trajectories using the movie capability. The movies provide a helpful tool in debugging complicated geometry calculations where electrons are emitted from many surfaces and space-charge-limiting may occur.

---

<sup>1</sup>E. P. Wenaas and A. J. Woods, "Electron Backscattering Effects on SGEMP Responses," INTEL-RT 8141-025, March 10, 1976; to be presented at IEEE Conference on Nuclear & Space Radiation Effects, July 1976.

### 3. ABORC VERIFICATION

ABORC has been checked against known solutions of Maxwell's equations and against other computer codes. The results of the checkouts are discussed here. Comparisons are for both non-space-charge-limited and space-charge-limited currents.

#### 3.1 EMPTY CYLINDER FIELD SOLUTION

ABORC has been compared with analytic solutions for electric fields in an empty cylinder. These analytic solutions can be derived when a sinusoidal axial current density having a Bessel function radial dependence is specified:

$$J_z = J_0 \left( \frac{x_{01} r}{R} \right) \sin \left( \frac{\pi u}{L} \right) \quad \text{for } 0 < u < L, \text{ zero otherwise,} \quad (1)$$

where

- R = cylinder radius,
- L = cylinder length,
- r, z = radial, axial coordinates,
- u = vt - z,
- v = phase velocity,
- $x_{01}$  = first zero of Bessel function  $J_0$ .

The solutions for the radial and axial electric fields at time = L/V are

$$E_r = \frac{x_{01} J_1 \left( \frac{x_{01} r}{R} \right) \sin \left( \frac{\pi z}{L} \right)}{\epsilon_0 R v \left[ \left( \frac{x_{01}}{R} \right)^2 + \left( \frac{\pi}{L} \right)^2 \right]} \quad (2)$$

and



$$E_z = \frac{-J_0 \left( \frac{x_{01} r}{R} \right) \cos\left(\frac{\pi z}{L}\right)}{\epsilon_0 L v \left[ \left( \frac{x_{01}}{R} \right)^2 + \left( \frac{\pi}{L} \right)^2 \right]} . \quad (3)$$

A test problem was run with ABORC where the axial current was specified according to Eq. 1. The test problem had the following characteristics.

Cylinder radius (R) = 0.5 m

Cylinder length (L) = 1.0 m

Phase velocity (v) = 0.2c

These parameter inputs resulted in an electron flight time of 16.7 nsec across the cavity, which was used as the maximum running time.

ABORC was run with both constant and variable spatial zones as a check of the variable-zone capability of the code. The following inputs pertaining to grid sizes were employed.

Number of radial zones: 10

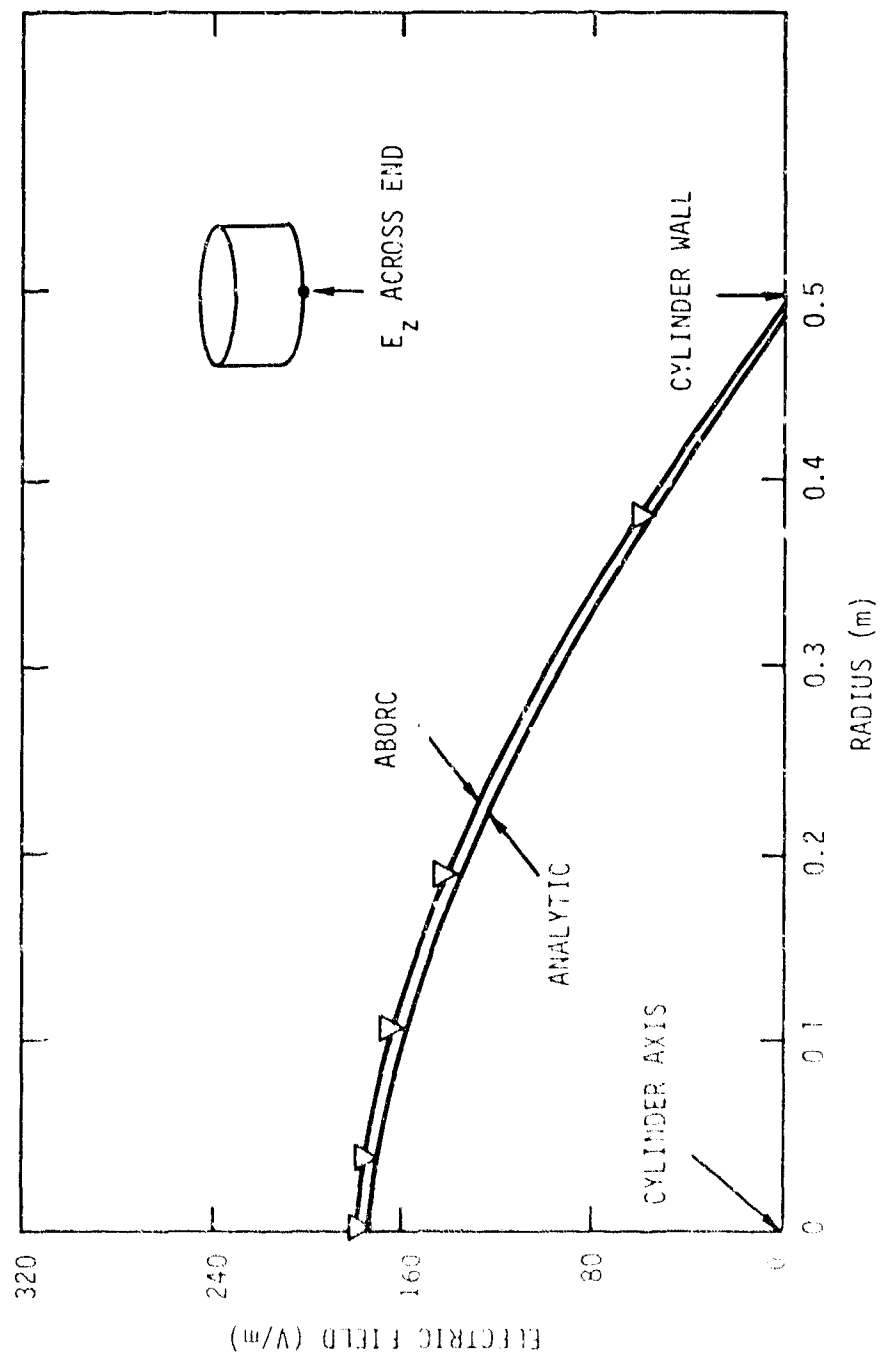
Number of axial zones: 20

Time step:  $2.09 \times 10^{-11}$  sec

Zone sizes varied by up to a factor of 10 in the variable-zoned case.

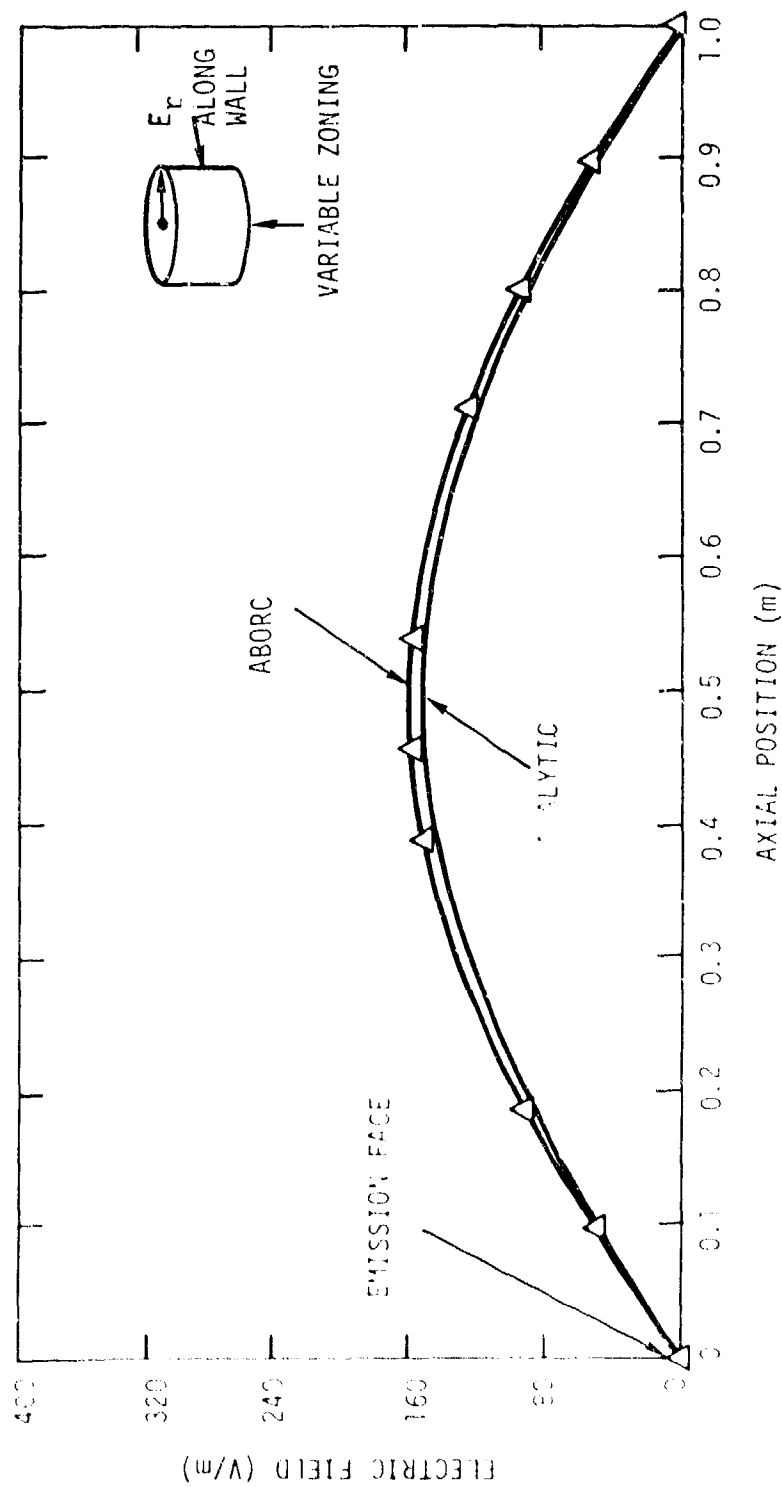
Equation 1 was used to update the axial current density each time step. Fields from the code were compared with the analytic solutions (Eqs. 2 and 3) at 16.7 nsec. The results of the comparisons are seen in Figures 1 and 2 for the axial electric field at the emitting end of the cylinder and the radial electric field at the side of the cylinder, respectively. The arrows on the geometry figures indicate the electron direction of propagation.

ABORC results are from the variable-zone case, which agreed well with the constant-zone case. Agreement of the code and analytic results is very good. Slight differences may be attributed to numerical inaccuracies resulting from finite grid spacings. This test of the code indicates that the field calculation portion is operating correctly, given the current in an empty cylinder.



RT-10599

Figure 1 Comparison of ABORC with analytic solution for empty cylinder; axial electric field at emission face versus radial position at time = 16.67 nsec for variable-increment spatial zoning



RT-10522

Figure 2. Comparison of ABORC with analytic solution for empty cylinder; radial electric field at cylinder wall versus axial position at time = 16.67 nsec for variable-increment spatial zoning

### 3.2 DOUBLE-CYLINDER FIELD SOLUTION

ABORC has been compared with analytic solutions for E- and H-fields in a double-cylinder geometry (Figure 3). Analytical solutions to Maxwell's equations are particularly easy to determine for the symmetry and initial conditions considered here. This simplification follows from the fact that the H-field in the azimuthal direction satisfies the boundary condition on a perfect conductor automatically. Any specification of the E-field which satisfies the boundary conditions and is zero initially implies a value of the magnetic field from the curl E equation. The combination of E- and H-fields then determines the value of the current density from the curl H equation, and it is that current which must be used to drive the computer solution to produce the E- and H-fields.

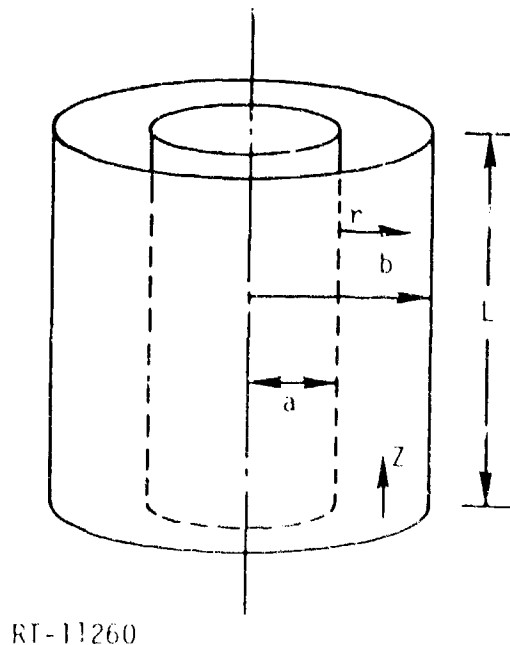


Figure 3. Double-cylinder configuration used for ABORC analytic field check out

An example of these solutions is shown in the following test problem. Analytic solutions are known by the above methods when an axial current density having the following dependence is specified.

$$J_z = [J_0(k_i r/a) Y_0(k_i) - J_0(k_i r/a) \sin\left(\frac{\pi u}{L}\right)] \quad (4)$$

for  $0 < u < L$ , zero otherwise,

where

- $k_i = 3.1228$  for  $b/a = 2$ ,
- $b$  = outer cylinder radius,
- $a$  = inner cylinder radius,
- $L$  = cylinder length,
- $r, z$  = radial, axial coordinates,
- $u = vt - z$ ,
- $v$  = phase velocity,
- $J_0, Y_0$  are Bessel functions of order zero.

The value of  $k_i$  causes the quantity in brackets to vanish at  $r = a$  and  $r = b$ . The axial and radial electric fields at a time equal to the flight time for electrons down the length of the cylinders are given by

$$E_z = \frac{-\pi}{L} \frac{1}{\epsilon_0 v} \left[ \frac{Y_0(k_i) J_0(k_i r/a) - J_0(k_i) Y_0(k_i r/a)}{\left(\frac{k_i}{a}\right)^2 + \left(\frac{\pi}{L}\right)^2} \right] \cos \frac{\pi z}{L} \quad (5)$$

and

$$E_r = \frac{k_i}{a} \frac{1}{\epsilon_0 v} \left[ \frac{Y_0(k_i) J_1(k_i r/a) - J_0(k_i) Y_1(k_i r/a)}{\left(\frac{k_i}{a}\right)^2 + \left(\frac{\pi}{L}\right)^2} \right] \sin \frac{\pi z}{L} \quad (6)$$

A test problem was run with ABORC where the axial current density was specified according to Eq. 4. The problem had the following characteristics.

- Inner cylinder radius,  $a$ : 0.25 m
- Outer cylinder radius,  $b$ : 0.5 m
- Cylinder length,  $L$ : 1 m
- Peak current density,  $J_{\text{PEAK}}$ :  $\approx 0.164 \text{ amp/m}^2$   
(occurs at a time of one-half an electron flight time at a radial position midway between cylinders)

Phase velocity, $v$ :	0.2c
Number of radial zones between cylinders:	10
Number of axial zones:	20
Constant spatial zone sizes:	$\Delta r = 0.25 \text{ m}$ $\Delta z = 0.05 \text{ m}$
Time step:	$4.17 \times 10^{-11} \text{ sec}$

The problem characteristics resulted in an electron flight time of 16.7 nsec.

The electric fields normal to the inner and outer cylinder walls and the end away from the emission surface are plotted at the time of 16.7 nsec in Figures 4, 5, and 6. The arrows on the geometry figures indicate the electron direction of propagation. The analytic curves are also shown. Agreement of the code and analytical results is excellent, with minor differences attributable to finite grid sizes used in ABORC. This test indicates that the field solution is operating correctly in cylinders with objects inside.

### 3.3 PARTICLE EMISSION TESTS

Several checkouts of the particle-emission portion of the ABORC code have been made. Some of the tests are described here. The particle emitter has built-in coding to store information on each emission energy distribution used in a given calculation. This information can be plotted at the end of a run and compared with the desired input energy distributions to test statistics. Comparisons of these "desired" and "obtained" distributions have shown agreements within permissible statistical deviations. The deviations are due to the Monte Carlo techniques employed by the code.

Emissions of currents from a variety of geometric objects have been studied. In many cases, the total charge emitted was analytically calculable (such as emission from simple cylinders or cones). The emitter has been verified under these comparisons, with pulses both long and short compared to object dimensions. The latter case provides a test of the delayed emission capability of the code.

A particularly complete checkout of the particle emitter was afforded by modeling a time-dependent spectrum in an electron-beam simulation calculation. The beam was modeled with a triangular pulse shape, and the

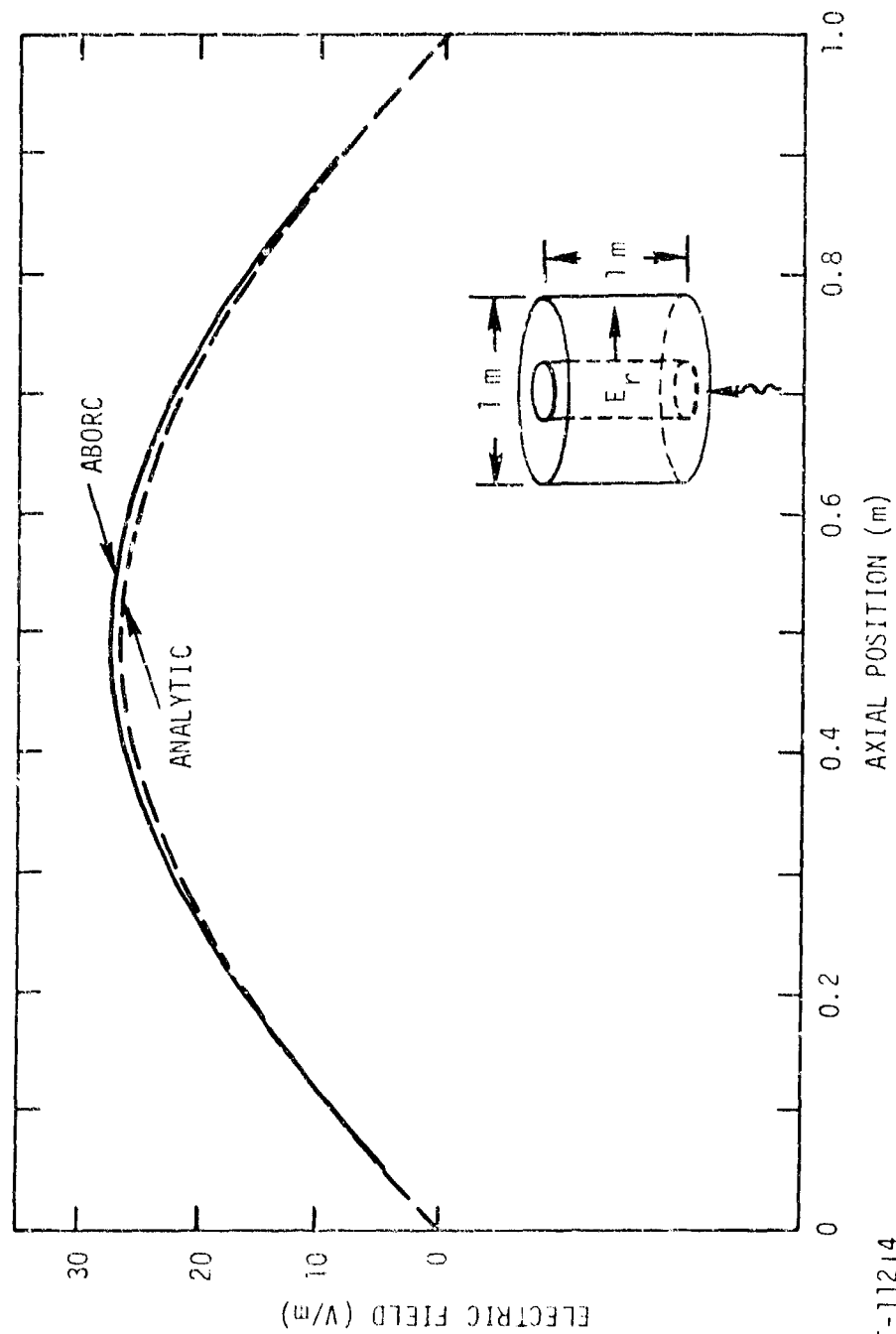


Figure 4. Comparison of ABORC with analytic solution for double cylinders; radial electric field versus axial position on inner conductor at time = 16.7 nsec

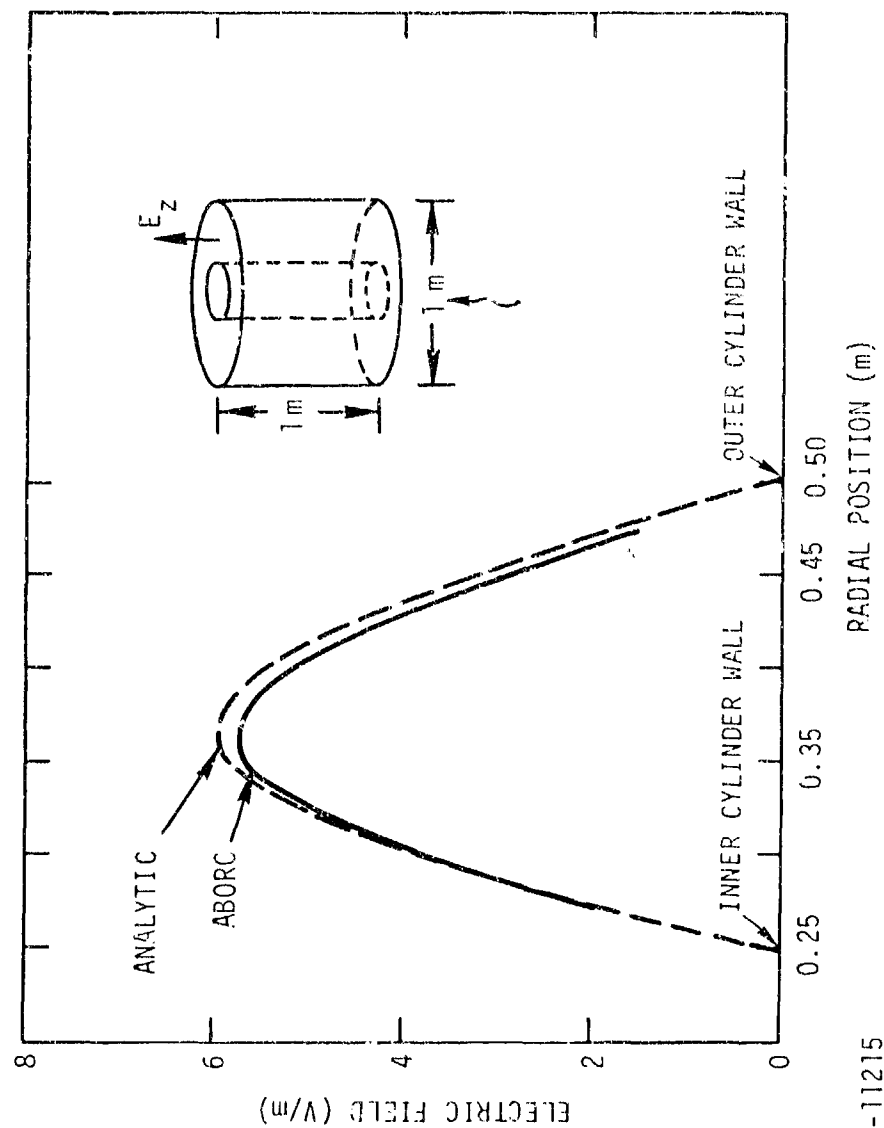
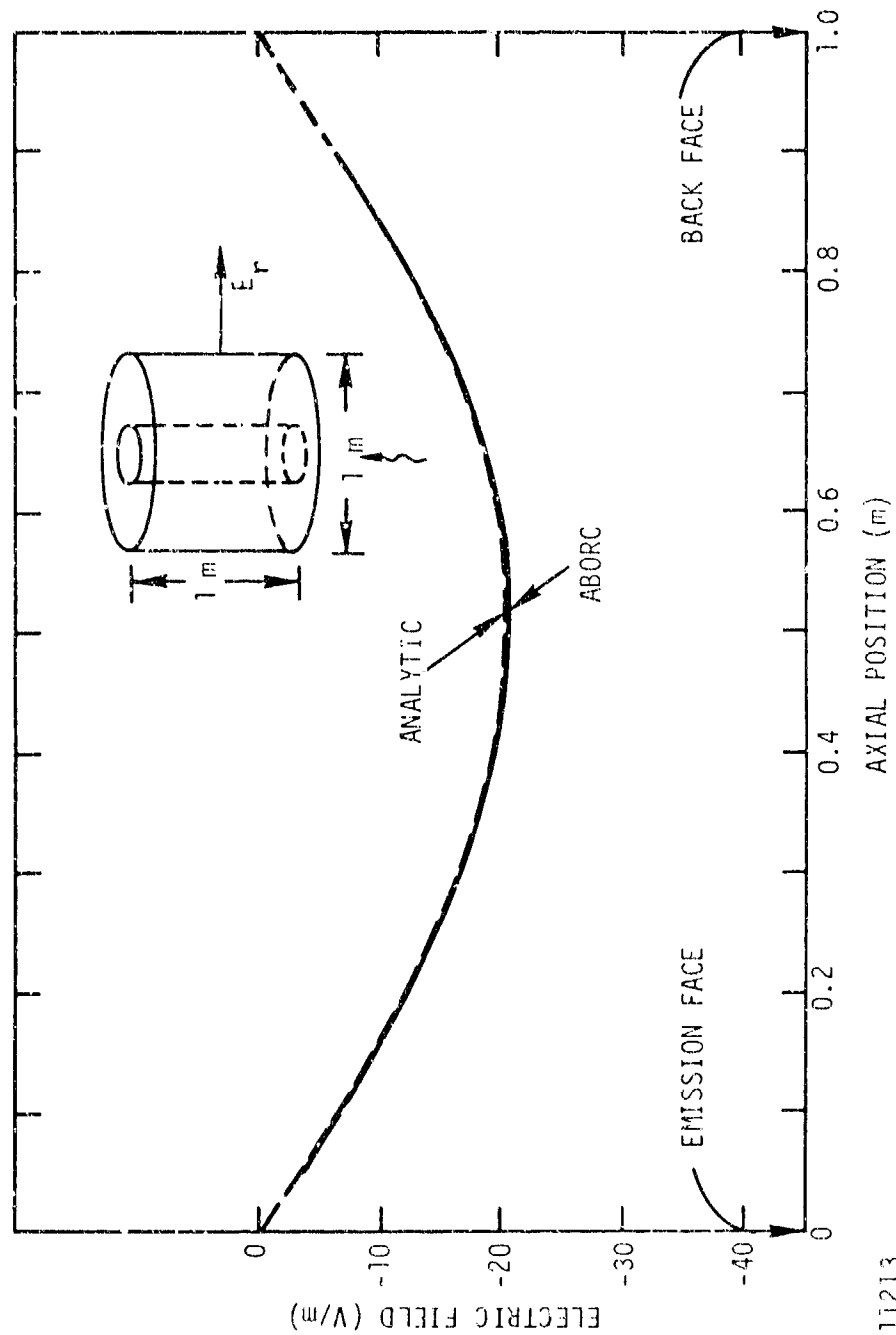


Figure 5. Comparison of ABORC with analytic solution for double cylinders; axial electric field at end away from emission position versus radial position at time = 16.7 nsec





RT-11213

Figure 6. Comparison of ABORC with analytic solutions for double cylinders; radial electric field at outer boundary versus axial position at time = 16.7 nsec

energy of the electrons was specified as triangular in time. These simplified representations permitted an analytical solution to be obtained for the time-averaged beam energy. This energy agrees with that obtained from ABORC when the total electron kinetic energy emitted is divided by the total charge emitted. The latter numbers are standard ABORC printout quantities.

### 3.4 CHECKOUTS INCLUDING PARTICLE MOTION

Several checkouts of the particle motion of ABORC have been made against analytic solutions and existing computer codes in both non-space-charge-limited and space-charge-limited situations.

#### 3.4.1 Analytical Comparisons for Particle Motion

Behavior of individual particles injected into an empty cylinder has been examined under field conditions where analytic solutions are derivable. In three different tests, each of the three field quantities --  $E_z$ ,  $E_r$ , and  $H_\theta$  -- have been specified constant throughout the cavity, with the other two being set to zero. Then particles were injected in such a way that simple analytical expressions could be derived to compare with resultant particle motion. The particles were injected parallel to  $E_z$  and  $E_r$  and along the axis when  $H_\theta$  was non-zero. The particles were found to come to a stop at positions within 5% of the analytic predictions when about 20 time steps from the initial to final positions were taken. The radius of curvature for particles injected perpendicular to the H-field was found to agree very well with the analytical value, slight differences being attributed to finite grid sizes.

Obviously, the abovementioned particle checkouts are limited in scope, but they do provide some confidence in results. More comprehensive tests are reported below.

### 3.4.2 Comparisons of ABORC with Other SGEMP Codes

ABORC has been compared with the computer codes DYNACYL (Refs. 2-4) and SEMP (Refs. 5,6) for the configuration of a cylinder within a cylinder. Both of these codes solve Maxwell's equations employing self-consistent particle motion for describing photo-electron currents. The codes have been applied to varieties of IEMP and SGEMP problems. These comparisons compare the ability of ABORC to treat an object interior to the enclosure and also to treat space-charge-limited situations.

#### Non-Space-Charge-Limited Case - DYNACYL Comparison

The test problem has the following characteristic dimensions.

##### Geometry

Outer cylinder length:	6.0 m
Outer cylinder diameter:	6.0 m
Inner cylinder length:	0.8 m
Inner cylinder diameter:	1.4 m
Inner cylinder position:	center of outer cylinder

##### Emission current

Pulse shape:	triangular (symmetric), 20-nsec FWHM
Peak current:	1 amp
Spatial distribution:	electrons emitted from top of inner cylinder only
Electron velocity	0.2c, axial direction
Angular distribution:	straight-out emission

Space-charge-limiting did not occur here because the fields were not allowed to affect electron motion in this test.

---

<sup>2</sup>T. N. Delmer et al., "SGEMP Phenomenology and Computer Code Development," DNA 3653F, November 11, 1974.

<sup>3</sup>E. P. Wenaas and A. J. Woods, "Comparisons of Quasi-Static and Fully Dynamic Solutions for Electromagnetic Field Calculations in a Cylindrical Cavity," IEEE Trans. Nucl. Sci. NS-21, December 1974, p. 259.

<sup>4</sup>D. C. Osborn et al., "Large-Area Electron-Beam Experiments," INTEL-RT 8101-011, July 15, 1975.

<sup>5</sup>D. L. Mangan and R. A. Perala, "Satellite SGEMP Surface Current Techniques," IEEE Trans. Nucl. Sci. NS-22, No. 6, December 1975, p. 2420.

<sup>6</sup>R. Stettner and H. L. Longley, "Description of the SGEMP Computer Code SEMP," Mission Research Corp. report MRC-R-144, June 1975.

Grid sizes employed in the two codes are listed below. Constant spatial zoning, equal in each direction, was used in both cases.

Number of radial zones:	15
Number of axial zones:	30
Maxwell's equation	0.25 nsec, ABORC
time step	0.33 nsec, DYNACYL

The magnetic field near the edge of the inner cylinder farthest from the emission point is shown for the two codes in Figure 7. This field position is on the inner cylinder wall at a radial position of 0.7 m. The axial position is about 0.2 m from the end of the inner cylinder. The curves show good overall agreement, with differences in the start-up times attributable to emission current pulse start-up time differences between the two cases. These differences were due to initial electron position and time step treatments existing in the two codes at the time of this test, and also to field point position differences due to finite zone sizes.

#### Space-Charge-Limited Case - SEMP Comparison

ABORC has been applied to a space-charge-limited calculation of fields and currents in a double-cylinder geometry and results compared with those obtained by Higgins\* for similar problem conditions. Unfortunately for this comparison, the emission current spectra differed slightly, but all other problem characteristics were approximately the same. The input conditions, while not perfect, do permit comparison of results of testing most facets of the codes, including the ability to perform space-charge-limited calculations.

Problem conditions are listed in Table 1. These and the results are cast in the scaling law forms discussed in Appendix B. These problem conditions result in a peak surface current of about  $1.6 \times 10^{-2}$  times the peak emission current, indicating a highly space-charge-limited situation.

Results for surface currents at two positions on the cylinder are given in Figures 8 and 9 for the two codes. The curves show fairly good agreement, with results becoming more similar as the field point is farther removed from the particle region. SEMP currents appear to be somewhat more space-charge-limited than ABORC results. This is consistent

---

\*D. Higgins, MRC Corp., private communication, March 1976.

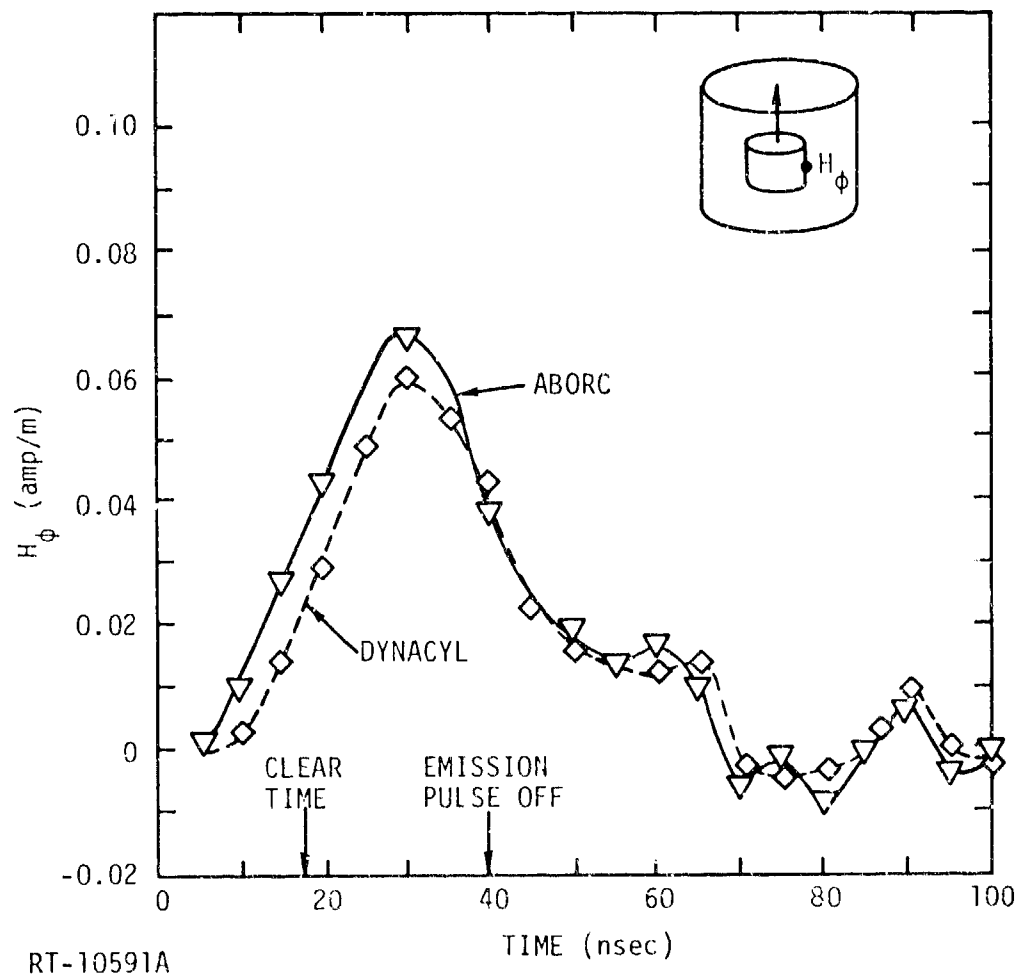


Figure 7. Comparison of ABORC and DYNACYL codes on a double-cylinder SGEMP problem with no space-charge-limiting. Magnetic field versus time near the inner cylinder edge farthest from the emission point of electrons is shown plotted versus time.

Table 1  
ABORC/SEMP COMPARISON PROBLEM

Geometry:	Double cylinders, length = diameter Outer diameter = 3X inner diameter Inner cylinder connected by wire to outer cylinder
Emission Current:	
Pulse shape:	Triangular, symmetric
Pulse rise time:	$\tau = 0.25 \times (2\pi r/c)$ , where $r$ = inner cylinder radius, $\tau$ = pulse rise time $c = 3 \times 10^8$ m/sec
Level:	$5.5 \times 10^4$ amp
Spatial distribution:	Uniform emission over end of inner cylinder away from wire
Angular distribution:	Cos $\theta$ measured from surface normal

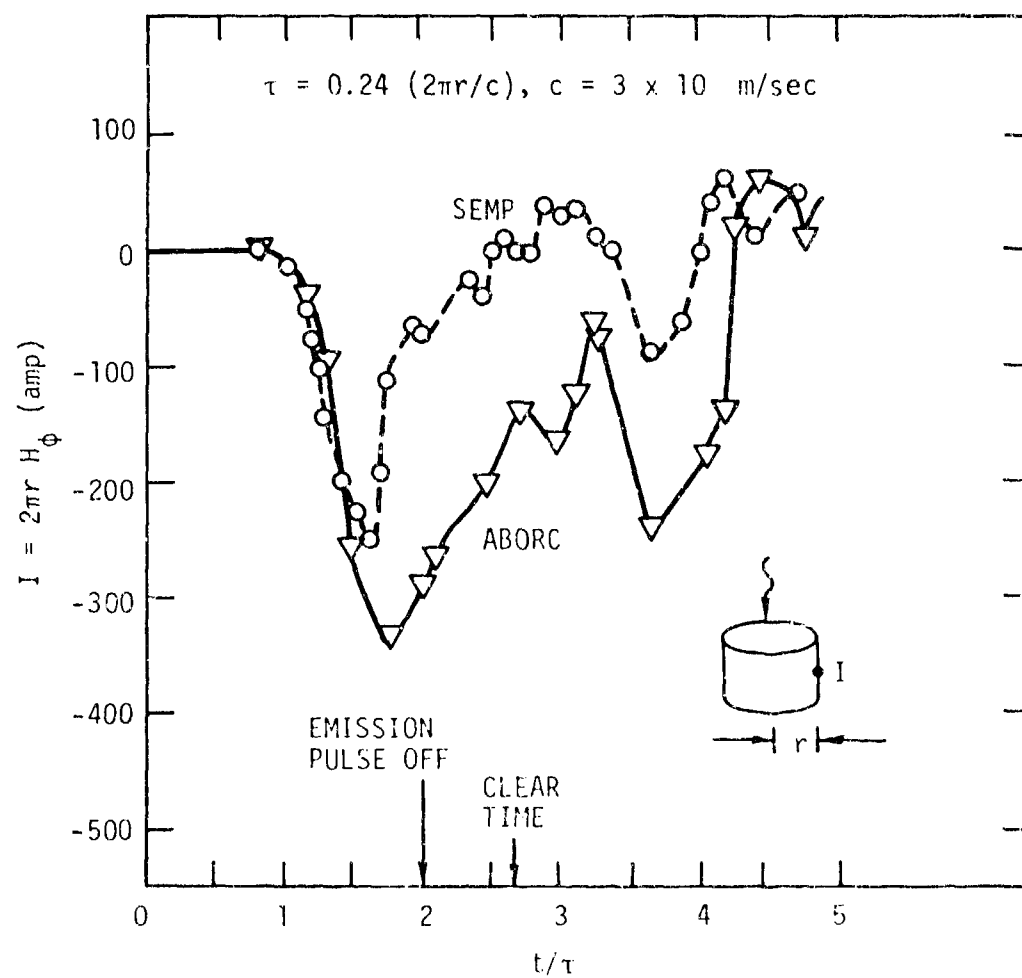


Figure 8. Comparison of ABORC and SEMP surface currents at the midpoint of a cylinder for space-charge-limited conditions

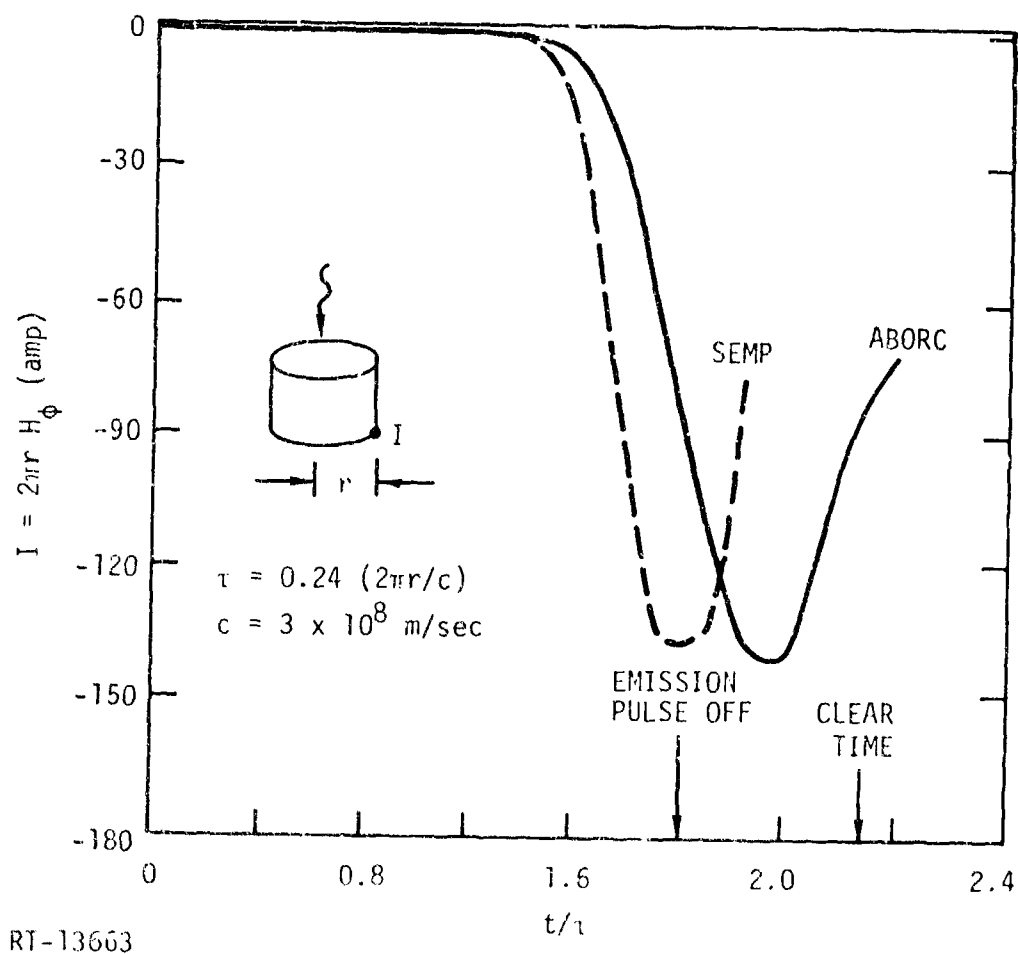


Figure 9. Comparison of ABORC and SEMP surface currents at the back of a cylinder for space-charge-limited conditions.



with observed emission electron spectrum differences where the distribution used in SEMP had slightly lower average energy than that used in ABORC. Response of the object to the reflected wave from the outer walls is seen clearly in Figure 8 in both code results. The clear time is indicated on the graphs. In general, the codes show enough agreement to suggest that both are giving reasonable estimates for space-charge-limited surface currents. Further investigation of the differences between the results would require analyzing the details of the problem numerics and code formulations.

### 3.4.3 Summary of Code Verifications

A summary of the code checkouts is given below.

- Empty-cylinder field solution - analytic
- Double-cylinder field solution - analytic
- Particle-emitter tests - analytic
- Particle motion tests - analytic
- Comparison with DYNACYL - non-SCL
- Comparison with SEMP - SCL

In addition to these checkouts, ABORC results were included in a comparison of data from several computer codes and analytical predictions conducted by dePlomb (Ref. 7). Problem conditions varied slightly between ABORC calculations and the other models, but comparison of the data was still a meaningful exercise. ABORC surface current peak values and times of occurrence were found to be in good general agreement with these other sources over wide ranges of emission currents and spectra including space-charge-limited conditions.

<sup>7</sup>E. P. dePlomb, "Analytical Predictions of SEMP Response and Comparisons with Computer Calculations," Kaman Sciences report to be published April 1976.

#### 4. SUMMARY

The ABORC computer code for the solution of SGEMP/IEMP problems for arbitrary bodies of revolution in two dimensions has been documented in this report. A description of code capabilities and code verifications are given in the main body, while contents of appendices include a detailed description of ABORC physics and modeling, sample calculations, a user's manual, and numerical grid choice considerations.

A brief description summarizing ABORC capabilities, physics, and modeling is given in Table 2. ABORC verification included testing virtually every code capability to some degree, with at least reasonable similarity to other solutions being obtained. Tested code portions include empty-cylinder fields, non-empty-cylinder fields, individual particle trajectories, and both non-SCL and SCL SGEMP calculations in double-cylinder geometries. ABORC has also been compared with DYNASPHERE (Ref. 2) on a spherical geometry under SCL conditions, with reasonable results. Thus, the code appears to have the capability to handle curved surfaces as well. Verification of ABORC on very complicated geometries, including booms, conical surfaces, etc., has been performed only to the extent of checking for reasonable behavior of results and observing numerous computer generated movies of particle trajectories. Direct comparisons of results with another code should probably be made here.

Some investigations conducted using ABORC, in addition to those given in Appendices B and C, are described in References 9 through 11. These present examples of various code capabilities such as the modeling of time-dependent spectra, re-entrant geometries, and current-injection simulation tests of satellites.

<sup>8</sup>E. P. Wenaas et al., "Sensitivity of SGEMP Response to Input Parameters," *IEEE Trans. Nucl. Sci.* NS-22, No. 6, December 1975, p. 2562.

<sup>9</sup>A. J. Woods and R. H. Stahl, "SGEMP Response Sensitivity to Exploding-Wire Source Photon Output Variations," INTEL-RT 8141-002, September 15, 1975.

<sup>10</sup>A. J. Woods and T. N. Delmer, "Skynet Program: Current-Injection Predictions/Solutions to Maxwell's Equations," DNA 3689 1-2, February 7, 1975.

<sup>11</sup>T. N. Delmer, "Response of a Precharge Satellite to a Potential Photon Source," INTEL RT 8141-012, November 21, 1975.

Table 2

SUMMARY OF ABORC CODE CAPABILITIES, PHYSICS, AND MODELING

---

Geometrical Configuration

Arbitrary rotationally symmetric bodies inside arbitrary rotationally symmetric enclosures

Arbitrary energy, angular, and axisymmetric spatial distributions of emission current with arbitrary time histories can be specified; all distributions can be time-dependent

Two-dimensional, axisymmetric electron orbits

Two-dimensional, axisymmetric electric and magnetic fields

Limited External circuits

Physical Phenomena Included

Photocurrent emissions are specified to the code; can be time-dependent in all distributions

Electric and magnetic fields and current densities are calculated

Both perfect and imperfect conductors can be specified

Limited dielectric capability

Fields act on particles of charge via relativistic equations of motion

Time dependence treated by updating Maxwell's equations each time step for new particle positions

Vacuum only

Method of Solution

Emission current broken into particles of charge with velocities; random emission in all variables

Particles of charge are converted into current densities on the spatial grid

Current densities are used to obtain E- and B-fields by finite-differencing and updating Maxwell's equations; variable zone sizes

Electric and magnetic fields act back on the particles via the equations of motion, altering their trajectories

---

## REFERENCES

1. E. P. Wenaas and A. J. Woods, "Electron Backscattering Effects on SGEMP Responses," INTEL-RT 8141-025, March 10, 1976; to be presented at IEEE Conference on Nuclear and Space Radiation Effects, July 1976.
2. T. N. Delmer et al., "SGEMP Phenomenology and Computer Code Development," DNA 3653F, November 11, 1974.
3. E. P. Wenaas and A. J. Woods, "Comparisons of Quasi-Static and Fully Dynamic Solutions for Electromagnetic Field Calculations in a Cylindrical Cavity," IEEE Trans. Nucl. Sci. NS-21, December 1974, p. 259.
4. D. C. Osborn et al., "Large-Area Electron-Beam Experiments," INTEL-RT 8101-011, July 15, 1975.
5. D. L. Mangan and R. A. Perala, "Satellite SGEMP Surface Current Techniques," IEEE Trans. Nucl. Sci. NS-22, No. 6, December 1975, p. 2420.
6. R. Stettner and H. L. Longley, "Description of the SGEMP Computer Code SEMP," Mission Research Corp. report MRC-R-144, June 1975.
7. E. P. dePlomb, "Analytical Predictions of SGEMP Responses and Comparisons with Computer Calculations," Kaman Sciences report to be published April 1976.
8. E. P. Wenaas, S. Rogers, and A. J. Woods, "Sensitivity of SGEMP Response to Input Parameters," IEEE Trans. Nucl. Sci. NS-22, No. 6, December 1975, p. 2362.
9. A. J. Woods and R. H. Stahl, "SGEMP Response Sensitivity to Exploding-Wire Source Photon Output Variations," INTEL-RT 8141-002, September 15, 1975.
10. A. J. Woods and T. N. Delmer, "Skynet Program: Current-Injection Predictions/Solutions to Maxwell's Equations," DNA 3689 T-2, February 7, 1975.
11. T. N. Delmer, "Response of a Precharged Satellite to a Potential Photon Source," INTEL-RT 8141-012, November 21, 1975.

APPENDIX A

DESCRIPTION OF THE PHYSICS AND MODELING  
EMPLOYED IN THE ABGR CODE

## A-1. INTRODUCTION

This appendix contains a mathematical description of the ABORC code, which has been developed to numerically evaluate electron motion and electromagnetic field generation in the vicinity of arbitrary bodies of revolution. The problem characteristics are taken to be rotationally symmetric, reducing the problem to two dimensions. The electromagnetic fields are calculated from Maxwell's equations and are used to influence the electron motion.

Electron emission from the surfaces is the source term(s) for driving the problem. Currents and fields are the quantities which result from the calculation. The electron emission must be specified in space and time. For example, in the case where the emission is due to photon interaction with materials, the photon energy and time spectrum determines the emission characteristics of the electrons. In cases such as this, a separate electron emission code must be used to get the electron spectrum from the photon spectrum. (Particles are used to represent large numbers of electrons.) The quantities calculated directly include the currents in the regions between the conducting surfaces, as well as the electric and magnetic fields in those regions. Applying Maxwell's equations properly at the boundaries gives surface currents and charge densities.

The remainder of this appendix outlines the methods of emitting the particles of charge, calculating particle motion, converting that motion to currents, and solving the field equations. The field equations are written in a generalized coordinate system, so the conversion from the polar coordinates to the general system is also discussed. Polar coordinates are used for the particle motion.

## A-2. ABORC PARTICLE EMITTER

The particle emission sections of ABORC have been designed to allow for relatively easy and flexible descriptions of complex emission characteristics and to simulate "real-world" electron emission with a minimum number of particles. This has been achieved via the use of a free-form input processor which operates upon arbitrarily specified emission descriptions, and by implementation of general Monte Carlo methods to the entire range of emission characteristics — i.e., intensity, energy, angle, space, and time. We describe herein the features of the emission specification method and provide examples of the use of the emitter. A description is included of the operation of the emitter itself, the methods employed, and the benefits derived.

### A-2.1 ABORC Emission Input Description

The problem of describing to the computer code exactly what emission is to be simulated is twofold: (1) description of the particle characteristics and intensity, and (2) the position in the computer model where this emission is to take place. The following describes the essential features which interface the analyst's desires with the ABORC internal arrays, flags, equations, etc.

#### EMISSION CHARACTERISTICS

The above card simply informs the code that emission information follows.

#### EMISSION INTENSITY n = POINT PAIR TABLE

The emission intensity format is used to specify the time history for the emission pulses; n is the intensity number, of which there can be up to 20, and POINT PAIR TABLE is the time history in  $\text{amp/m}^2$  versus time in sec. EI may be used to abbreviate "emission intensity." For example, a 20-nsec FWHM triangular pulse with a peak of  $0.1 \text{ amp/m}^2$  would be input:

EMISSION INTENSITY 5 = 0,0,20E-9,.1,40E-9,0  
(or E15)

The table may contain up to 50 point pairs, allowing high resolution to fairly complex emission time histories, and may be continued on as many cards as desired.

ENERGY DISTRIBUTION n (BINS = i) = POINT PAIR TABLE

Similarly, the energy distribution card allows for the arbitrary specification of the emission energy spectrum; n is the distribution number, and again, up to 20 are allowed at present. ED may be used to abbreviate "energy distribution." (BINS = 1) is optional. i specifies that there shall be i particles emitted per particle time step per emission zone for the distribution. If the (BINS = i) input is omitted, the default value of i is 4. The POINT PAIR TABLE is as before, with relative frequency [number/unit energy versus energy (eV)] as the parameters. For example, the spectrum of Figure A-1 might be input:

ENERGY DISTRIBUTION 7 = 4K,0,5K,.4,6K,.8,7K,1,  
(or ED7) 9K,.8,12K,.4,15K,.15,20K,0

Mono-energetic emission is specified simply by EDn = energy.

Note the use of the "K," which is interpreted as  $10^3$ . Various other letters may be used with floating point numbers in the emission section; they are listed in Table A-1. The example spectrum is given normalized to a peak of 1; however, the emitter normalizes all distribution functions, so the emission current density has the value specified by the "TIMES" factor described below under "EMISSION ZONES," and multiplied by the "FLUENC" factor discussed in Appendix E. Desired relative height for all distributions is all the user need consider.

ANGLE DISTRIBUTION n = POINT PAIR TABLE

The angle distribution card is shown above. AD may be used to abbreviate "angle distribution." The parameters for the point pair table in this instance are the number of particles per unit angle versus angle in radians. For example, the distribution of Figure A-2 is given by:

ANGLE DISTRIBUTION 3 = 0,0,.6,.75,1.1,.45,1.57,0  
(or AD3)



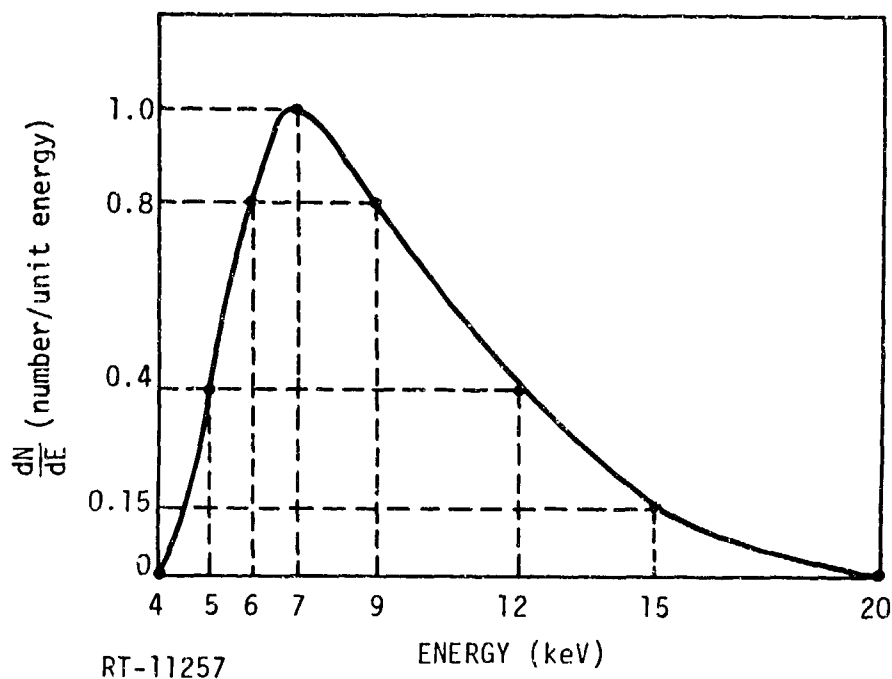


Figure A-1. Sample energy spectrum input to ABORC

Table A-1  
FLOATING POINT MULTIPLIERS FOR ABBREVIATED ABORC INPUTS

Letter Factor	Power of 10
P	-12
N	-9
U	-6
K	+3
M	+6

The letter factor can be used to replace the power of 10 desired on input cards.

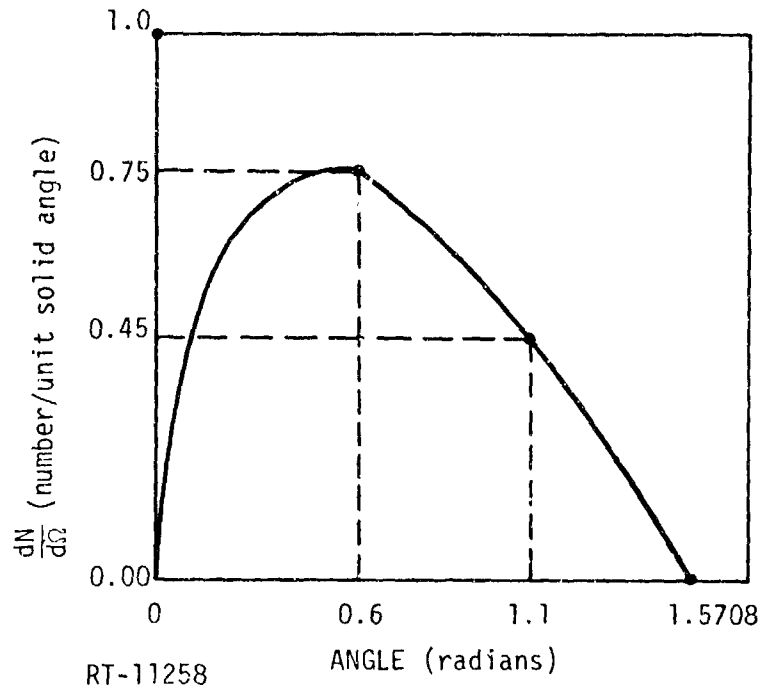


Figure A-2. Sample angle distribution input to ABORC

Polar angles are employed in the coding for emission specification. The angle on the given sample is the angle from the emitting surface normal. The azimuthal angle distribution is specified uniform from 0 to  $2\pi$  for two-dimensional calculations. Straight-out emission is specified simply by  $ADn = 0$ .

#### EMISSION ZONES

The emission zones card simply specifies that emission zone information follows. The emission zones, then, are indicated by:

$(z_1, r_1)$  TO  $(z_2, r_2)$  INT  $i$  DELAY  $\times$  TIMES  $y$ , ED  $j$ , AD  $k$ , ADQ3  $\ell$

$z_1$ ,  $r_1$ ,  $z_2$ ,  $r_2$  give, of course, the coordinates of the zone.  $i$  is the emission intensity time history number reference to be used for the zone, delayed by  $x$  seconds and multiplied by  $y$ . The DELAY and TIMES factors are optional.  $j$  is the energy distribution number to be used for the zone,  $k$  is the angle distribution to be used for determining the direction of each particle relative to the surface normal, and  $\ell$  is the angle distribution reference for the emission electron direction azimuthal

angle about the surface normal. Particles are always emitted to the left of the line segment running from  $(z_1, r_1)$  to  $(z_2, r_2)$ . Therefore, care must be taken to specify zones in proper order.

As an example, suppose we desire an emission zone position on the top of a cylinder, from the axis to 0.2-m radius and at vertical position 0.5 m. We shall reference the previous distributions and input:

```
(.5,0) TO (.5,.2) INT 5 TIMES 10, ED7, AD3, ADQ3 2
```

where we have multiplied the current density by 10. We may also want to emit from the side of the cylinder (e.g., radius = 0.2 m) but with reduced intensity and delayed by a couple of nanoseconds:

```
TO (.3,.2) INT 5 DELAY 2E-9 TIMES .1, ED7, AD3, ADQ3 2
```

where  $z_1$  and  $r_1$  for this emission zone are obtained from the previous zone's  $z_2$  and  $r_2$ .

```
END OF INPUT
```

terminates the emission input processing.

#### A-2.2 ABORC Emitter Operation

The emitter operation is outlined here. Generally, the idea has been to randomize the entire emission process instead of emitting from discrete points in space, angle, energy, and time, as has been done in the past. This randomization reduces the systematic excitation of high-frequency modes, and represents physically continuous distributions more accurately than discrete points for the same number of particles. This treatment of emission currents is particularly beneficial under high SCL conditions, where a small fraction of the emitted charge may be causing dominant response.

The emitter, then, based upon the amount of charge to be emitted at a given time step, sets up particles with randomly determined energies from the given energy spectrum, randomly determined angles (velocity components) consistent with the given angular distribution, randomly determined position in the emission zone (taken to be uniform over the zone area), and randomly determined emission time (taken to be uniform over the particle time step).

The energy characteristics of the emitted charges are taken to be crucial to effective simulation. For coding purposes, this translates to allowing very precise definition of the desired spectrum (discussed in the input section) and effectively sampling values from this spectrum without generation of too many particles (which could result in excessive running times). We achieve these objectives via the use of the "stratified sampling" scheme.\* Given a spectrum such as that presented in Figure A-1, we transform (via integration/normalization) to a distribution function of the form shown in Figure A-3.

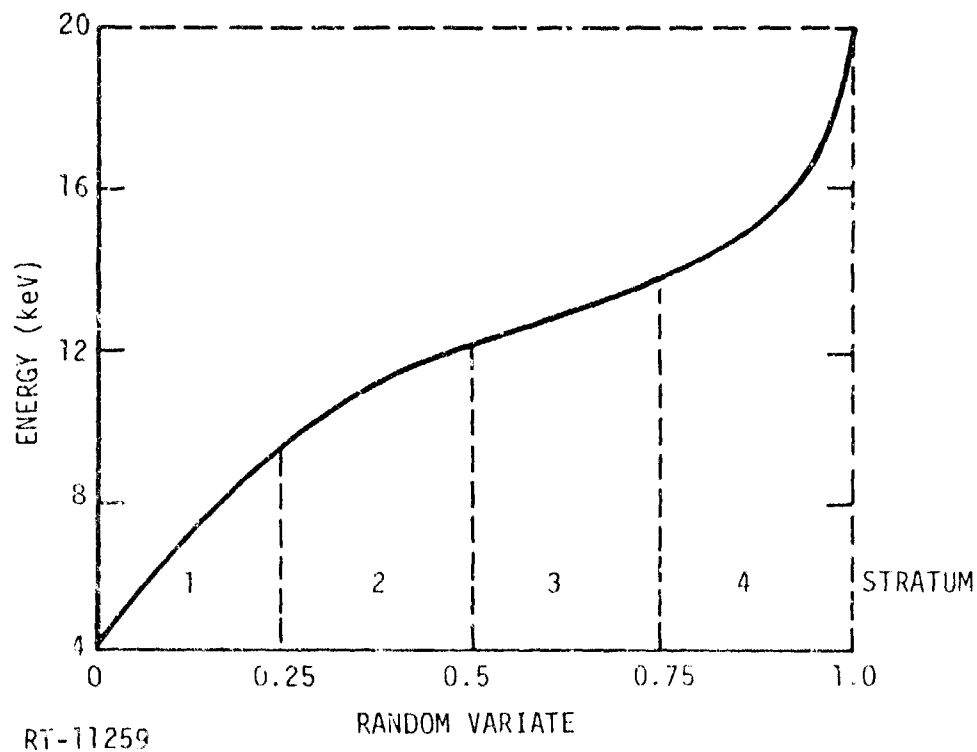


Figure A-3. Sample distribution function employed by ABORC

A comparison of "stratified" sampling with "straight" sampling — i.e., sampling from the entire distribution instead of from ranges within the distribution — will illustrate the benefits of stratification. Straight Monte Carlo sampling applied to this distribution (i.e., generation of a

\*J. Hammersby and D. Handscomb, Monte Carlo Methods, J. Wiley & Sons, New York (1965).

random variate between 0 and 1 and interpolating the function for the corresponding energy) yields a standard sampling error  $s$ :

$$s^2 = \frac{1}{n-1} \sum_{i=1}^n (e_i - \mu)^2 ,$$

where

$\mu$  = mean,  
 $e_i$  =  $i$ th sampled energy,  
 $n$  = number of samples taken.

The sampling error, then, goes inversely with the square root of the number of samples, or four times as many samples must be taken to increase the accuracy of  $s$  by a factor of 2.

The use of stratified sampling (i.e., dividing the 0-to-1 interval into  $k$  strata and sampling from within each stratum) gives a standard error:

$$s^2 = \sum_{j=1}^k \frac{(\Delta\alpha_j)^2}{n_j(n_j-1)} \sum_{i=1}^{n_j} (e_{ij} - \mu)^2 ,$$

where

$k$  = number of strata,  
 $\Delta\alpha_j$  = random variate range for the  $j$ th interval,  
 $n_j$  = number of samples taken in the  $j$ th interval,  
 $e_{ij}$  = energies selected.

It is seen that the error goes inversely with the number of samples taken; i.e., doubling the number of samples roughly halves the standard error. This translates to better statistics for fewer particles.

The directional characteristics of the emitted charge are important also. Experience indicates that the angle distribution is not as critically important as the proper energy distribution, particularly at higher fluence conditions. We allow, then, the specification of angular characteristics and apply standard Monte Carlo sampling to these distributions instead of the more sophisticated stratified variety.

With regard to the space and time characteristics, we take the emission to be uniform over the emission zone area and over the emission time

step. Since the intent is to simply spray the emitted charge from the zone at random positions in the space interval and at random times in the time step interval, we find that the standard Monte Carlo is adequate here also.

In summary, the emitter calculates, from the specified current density time history, the charge to be emitted at each emission time step in each emission zone. The energy characteristics are randomly and accurately selected using the stratified energy distribution sampling. The particles are then assigned directional characteristics, emission time, and position via standard Monte Carlo sampling.

An outstanding capability of this particle emitter, aside from the ease of inputs and specification of complicated characteristics, is its ability to model time-dependent energy spectra. This capability, necessary for complete modeling of photo-electron emission results obtained from photon-generating machines, is available by using the existing coding and simply specifying different energy distributions with different time histories for emission from a common spatial zone. As many as 20 energy distributions and 20 time histories can be specified to model the complete time-dependent spectrum, if necessary.

### A-3. ABORC PARTICLE-PUSHER

The finite "particles" of charge emerging from the emitter portion of the code, discussed in the previous section, are picked up and propagated through the spatial zones with forces acting on them due to the E- and H-fields in the space. The particle trajectories are determined by the equations of motion, which are updated each particle time step. The old and new particle positions are then employed to generate currents. The currents are used to update the E- and H-fields. A description of the determination of particle trajectories in ABORC is given here.

The particle has rest mass  $m$  and charge  $q$ , and is in an electric field  $E = (E_z, E_r, 0)$  and magnetic field  $B = (0, 0, B_0)$ . The equation of motion can be numerically integrated in two steps:

1. Find the new magnitude of the velocity  $v$  from the energy equations.
2. Find the direction of the velocity from momentum equations.

The equations were originally updated by differencing the momentum equations in cylindrical coordinates. This had the effect of introducing a singularity at the axis of the coordinate system. To eliminate this singularity, the particle motion is now described in Cartesian coordinates. This was a simple and expeditious means of solving the problem.

The force is calculated from the nearest field points of the grid in the following manner. The magnetic field is equal to the field at the nearest point. Since in SGEMP problems the magnetic force is small, this is sufficiently accurate. For the electric fields — say, in the Z direction — the two nearest fields in that direction are found to have the same coordinates in that direction. These two are averaged to get the field acting on the particle. This has the advantage of giving forces on emitted particles which are given by the normal forces just outside the emission surface even though in free space there are self-forces on the particles. (This latter fact may be significant for bodies with booms, where a long distance must be traversed by the electrons.)

For motion of the particles, some confusion exists due to the time centering of the problem. A primary cause of this is the fact that, as a particle is injected into the problem, the first time step is important since violent motion occurs in this step for low-particle energies. We use a random time step for the injection so that low-energy particles do not systematically leave the problem in one step; therefore, the centering is not strictly defined. Still, we have found the following scheme adequate.

Let the superscript "+" denote new values and  $\vec{x}$  the position and  $\vec{v}$  the velocity of the particle. The particle is treated as being in three dimensions and rotated about the axis of symmetry back to a coordinate system, where one of the coordinates is zero to save storage.

Using the notation

$$\gamma = \frac{1}{\sqrt{1 - \frac{v^2}{c^2}}},$$

where  $c$  is the velocity of light,

$$\vec{v}^{++} = \vec{v} + \frac{q\Delta t}{m\gamma} (\vec{E} + \vec{v} \times \vec{B})$$

and

$$\gamma^{++} = \gamma + \frac{q\Delta t}{2mc^2} \vec{E} \cdot (\vec{v}^{++} + \vec{v}) .$$

Making one iteration,

$$\vec{v}^{+++} = \frac{\vec{v}\gamma}{\gamma^{++}} + \frac{q\Delta t}{m\gamma^{++}} [E + 0.5(\vec{v}^{++} + \vec{v}) \times \vec{B}] ,$$

$$\gamma^{+++} = \gamma + \frac{q\Delta t}{2mc^2} [E \cdot (\vec{v}^{+++} + \vec{v})] ,$$

and

$$\vec{x}^{++} = \vec{x} + \vec{v}^{++} \Delta t ,$$

where  $q$  and  $m$  are the charge and mass of the electron and  $\Delta t$  is the time step. This operation is followed by the abovementioned rotation which involves taking a square root and is, therefore, not ideal.

#### A-4. DESCRIPTION OF CHARGED-PARTICLE MOTION BY CURRENTS

In the numerical solution of Maxwell's equations, currents are evaluated at discrete points in space and time. Particles, representing electrons, move in a generalized coordinate system in time. An interpolation scheme must be constructed to translate the continuous motion of the particles into a set of discrete currents. The scheme chosen is such that the residual charge, as calculated from the time integral of the divergence of the current is zero after a particle has passed into and then out of a region. (This does not hold for boundary zones since currents outside the region of interest are not considered.)

In the present zoning, currents are evaluated at zone centers in their own direction and zone boundaries in perpendicular directions. The current is time-centered. Accordingly, as forced by the continuity equation, the charge densities are at zone boundaries in space and time.

The present objective is, then, to take a particle from point

$$(q_1^a, q_2^a, q_3^a, t^a)$$



to the point

$$(q_1^b, q_2^b, q_3^b, t^b)$$

where  $t^b = t^a + \Delta t$ . That is, the currents representing such a translation must be generated.

Since the grid spacing is uniform in the  $q$ 's, linear interpolation can be performed in the transverse coordinates. This can be seen from the formulation

$$J_1(i+\frac{1}{2}, j, k, t^a + \frac{\Delta t}{2}) = Q_p \left[ \frac{q_1^b - q_1^a}{\Delta t} Q_1(i+\frac{1}{2}, j, k) \right]$$

$$Q_1(i+\frac{1}{2}, j, k) \Delta q_1 Q_2(i+\frac{1}{2}, j, k) \Delta q_2 Q_3(i+\frac{1}{2}, j, k) \Delta q_3$$

$$\int_{t_1}^{t_2} \left[ 1 - \left| \frac{q_2^a - q_2(j) + (q_2^b - q_2^a)(t - t^a)/\Delta t}{\Delta q_2} \right| \right]$$

$$\left[ 1 - \left| \frac{q_3^a - Q_3(k) + (q_3^b - q_3^a)(t - t^a)/\Delta t}{\Delta q_3} \right| \right] \frac{dt}{\Delta t}$$

for point  $(q_1, q_2, q_3) = [(i+\frac{1}{2})\Delta q_1, j\Delta q_2, k\Delta q_3]$ , particle of charge  $Q_p$ . Here,  $J_1$  is the current in the  $q_1$  direction.

The first bracket contains the real-space particle velocity in the  $q_1$  direction. The second bracket contains the real-space volume element. The integral represents the time-average fractional distance from the point of interest in the transverse directions. It can be seen that the particle is treated as a volume element in  $q$  space of dimensions  $\Delta q_1, \Delta q_2, \Delta q_3$ , and the integral represents the transverse area overlapping the zone of interest.

The time limits are such that they are within the range of interest,  $t^b, t^a$ , and the particle is within one zone of the point of interest in its linear traversal:

$$q_1 = \left[ q_1^a + (q_1^b - q_1^a) \frac{(t - t^a)}{\Delta t} \right],$$

$$q_2 = \dots,$$

$$q_3 = \dots,$$

from point a to point b.

In practice, a particle is tracked from point a to point b in intervals of zone crossings so that the appropriate values of  $i$ ,  $j$ , and  $k$  are easily established. The treatment for  $J_2$  and  $J_3$  is related to that of  $J_1$  by the same symmetry as mentioned in the discussion of the field calculation below.

#### A-5. SOLUTION OF THE FIELD EQUATIONS

The numerical solution of Maxwell's equations is straightforward. The initial conditions are that all fields and charge densities are zero. The currents, as calculated from the motion of the charged particles injected into the region (see below), are the quantities which drive the time evolution of the fields. Thus, for a medium with the permittivity ( $\epsilon_0$ ) and permeability ( $\mu_0$ ) of free space, Maxwell's equations reduce to

$$\epsilon_0 \frac{\partial \vec{E}}{\partial t} = -\vec{J} + \vec{\nabla} \times \vec{H}$$

and

$$\mu_0 \frac{\partial \vec{H}}{\partial t} = -\vec{\nabla} \times \vec{E},$$

with the initial conditions

$$\vec{E} = 0 \quad \text{at } t = 0,$$

$$\vec{H} = 0 \quad \text{at } t = 0,$$

$$\vec{E} \times \vec{n} = 0 \quad \text{where } \vec{n} \text{ is the normal to the bounding surface.}$$

Putting these equations into numerical form for solution is also straightforward, and may be done directly in two dimensions. However, by performing the task in three dimensions, one is forced into a symmetry which is very convenient and not obvious in the two-dimensional case.

To complete the geometrical generality (and permit a simple method of varying zone spacing), the space under consideration is taken to be metrized by the generalized orthogonal coordinates ( $q_1, q_2, q_3$ ) where the order is such that the coordinate system is right-handed. Using the

notation of Margenau and Murphy,<sup>\*</sup> displacements in real space,  $ds$ , may be related to displacements in  $q$  space by the functions  $Q$ , where

$$ds = Q_1 dq_1.$$

Using this definition and the definition of the curl,  $\nabla \times$ , as the path integral of a quantity in the left-hand direction (Cauchy rule) around a closed path divided by the area of the enclosed surface, Maxwell's equations in finite-difference form can be represented by

$$\begin{aligned} E_1^{n+1}(i+\frac{1}{2}, j, k) &= E_1^n(i+\frac{1}{2}, j, k) - \frac{\Delta t^{n+\frac{1}{2}}}{\varepsilon_0} J_1^{n+\frac{1}{2}}(i+\frac{1}{2}, j, k) \\ &+ \left\{ \frac{\Delta t^{n+\frac{1}{2}}}{\varepsilon_0 Q_2(i+\frac{1}{2}, j, k) \Delta q_2 Q_3(i+\frac{1}{2}, j, k) \Delta q_3} \right\} \\ &\times \left\{ \left[ H_3^{n+\frac{1}{2}}(i+\frac{1}{2}, j+\frac{1}{2}, k) Q_3(i+\frac{1}{2}, j+\frac{1}{2}, k) \Delta q_3 - H_3^{n+\frac{1}{2}}(i+\frac{1}{2}, j-\frac{1}{2}, k) Q_3(i+\frac{1}{2}, j-\frac{1}{2}, k) \Delta q_3 \right] \right. \\ &\left. - \left[ H_2^{n+\frac{1}{2}}(i+\frac{1}{2}, j, k+\frac{1}{2}) Q_2(i+\frac{1}{2}, j, k+\frac{1}{2}) \Delta q_2 - H_2^{n+\frac{1}{2}}(i+\frac{1}{2}, j, k-\frac{1}{2}) Q_2(i+\frac{1}{2}, j, k-\frac{1}{2}) \Delta q_2 \right] \right\} \end{aligned}$$

and

$$\begin{aligned} H_1^{n+3/2}(i, j+\frac{1}{2}, k+\frac{1}{2}) &= H_1^{n+\frac{1}{2}}(i, j+\frac{1}{2}, k+\frac{1}{2}) \\ &- \left\{ \frac{\Delta t^{n+1}}{\mu_0 Q_2(k, j+\frac{1}{2}, k+\frac{1}{2}) \Delta q_2 Q_3(i, j+\frac{1}{2}, k+\frac{1}{2}) \Delta q_3} \right\} \\ &\times \left\{ \left[ E_3^{n+1}(i, j+\frac{1}{2}, k+\frac{1}{2}) Q_3(i, j+\frac{1}{2}, k+\frac{1}{2}) \Delta q_3 - E_3^{n+1}(i, j, k+\frac{1}{2}) Q_3(i, j, k+\frac{1}{2}) \Delta q_3 \right] \right. \\ &\left. - \left[ E_2^{n+1}(i, j+\frac{1}{2}, k+1) Q_2(i, j+\frac{1}{2}, k+1) \Delta q_2 - E_2^{n+1}(i, j+\frac{1}{2}, k) Q_2(i, j+\frac{1}{2}, k) \Delta q_2 \right] \right\} \end{aligned}$$

with the continuity equation (not essential to determining the fields, but of interest for itself and for converting particle motion into equivalent currents) represented by

<sup>\*</sup>H. Margenau and G. M. Murphy, The Mathematics of Physics and Chemistry, Princeton, D. van Nostrand Company, Inc. (1956).

$$\rho^{n+1}(i,j,k) = \rho^n(i,j,k)$$

$$\begin{aligned} & - \left\{ \frac{\Delta t^{n+1/2}}{C_1(i,j,k) \Delta q_1 Q_2(i,j,k) \Delta q_2 Q_3(i,j,k) \Delta q_3} \right\} \\ & \times \left\{ \left[ J_1^{n+1/2}(i+1/2, j, k) Q_2(i+1/2, j, k) \Delta q_2 Q_3(i+1/2, j, k) \Delta q_3 \right. \right. \\ & \quad \left. \left. - J_1^{n+1/2}(i-1/2, j, k) Q_2(i-1/2, j, k) \Delta q_2 Q_3(i-1/2, j, k) \Delta q_3 \right] \right. \\ & + \left[ J_2^{n+1/2}(i, j+1/2, k) Q_1(i, j+1/2, k) \Delta q_1 Q_3(i, j+1/2, k) \Delta q_3 \right. \\ & \quad \left. - J_2^{n+1/2}(i, j-1/2, k) Q_1(i, j-1/2, k) \Delta q_1 Q_3(i, j-1/2, k) \Delta q_3 \right] \\ & + \left[ J_3^{n+1/2}(i, j, k+1/2) Q_1(i, j, k+1/2) \Delta q_1 Q_2(i, j, k+1/2) \Delta q_2 \right. \\ & \quad \left. - J_3^{n+1/2}(i, j, k-1/2) Q_1(i, j, k-1/2) \Delta q_1 Q_2(i, j, k-1/2) \Delta q_2 \right] \left. \right\} . \end{aligned}$$

The notation used in these equations requires some comment. The superscript refers to the time step. Thus, some quantities are centered in time and some are at boundaries in time. Corresponding to this, there are two time steps: the time step connecting quantities centered in time  $\Delta t^n$ , and the time step connecting quantities at boundaries in time,  $\Delta t^{n+1/2}$ .

Subscripts refer to directions in the generalized coordinate space. Thus,  $E_1$  is the component of the electric field along the direction of a displacement in space given by a displacement in  $q_1$  at the spatial point in question. Quantities in parentheses refer to the position in space. Thus,  $E_1(\alpha, \beta, \gamma)$  is evaluated at the point in space determined by the coordinates

$$\begin{aligned} q_1 &= \alpha \Delta q_1 + q_1(\text{MIN}) , \\ q_2 &= \beta \Delta q_2 + q_2(\text{MIN}) , \\ q_3 &= \gamma \Delta q_3 + q_3(\text{MIN}) , \end{aligned}$$

where the minimum value of the coordinate is specified for convenience, allowing the spatial boundaries to be other than zero in the  $q$  space.

It will be noted that the grid spacing in  $q$  space is uniform. Further, if one of the  $Q$ 's is zero at a point of interest, the procedure fails. In fact, at such points the coordinate system does not metrize real space. The failure is that many points in  $q$  space correspond to one point in real space. Such cases must be treated specially.

The equations for the other components of the electric and magnetic fields are obtained by cyclically permuting the integer subscripts and the corresponding coordinates  $\alpha$ ,  $\beta$ , and  $\gamma$ .

APPENDIX B

SAMPLE ABOVE CALCULATIONS:  
SCALING LAWS FOR SGEMP

## ABSTRACT

General scaling laws have been previously derived and used for numerous applications in electromagnetic theory. The purpose of this appendix is to report investigations of the scaling laws specifically for the nonlinear system-generated electromagnetic pulse (SGEMP) problem, and to use the scaling laws to present parametric SGEMP calculations applicable to a wide range of pertinent excitation parameters including pulse width, fluence, energy spectrum, and object dimensions.

According to the scaling laws, if the pulse time history and object dimensions are scaled by a factor  $\alpha$ , the incident photon fluence is scaled as  $1/\alpha$ , and the emitted electron energy distribution is unchanged, the resulting electromagnetic response of a perfectly conducting body will scale as shown in Table B-1.

Results of specific SGEMP calculations are presented, using the ABORC code in such a format as to make possible structural response estimates for a wide variety of conditions. Interesting trends in the response of simple objects as a function of excitation parameters are observed and discussed.

## B-1. INTRODUCTION

General scaling laws have been previously derived (Refs. 1,2) and used for numerous applications in electromagnetic theory. This appendix investigates the scaling laws specifically for the nonlinear system-generated electromagnetic pulse (SGEMP) problem and, using the scaling laws, presents parametric calculations applicable to a wide range of

<sup>1</sup>George Sinclair, "Theory of Models of Electromagnetic Systems, Proc. IRE, Vol. 36 (1948), p. 1364-1370.

<sup>2</sup>T. N. Delmer et al., "SGEMP Phenomenology and Computer Code Development," DNA 3653F, November 11, 1974.

<sup>3</sup>E. P. Wenaas, S. Rogers, and A. J. Woods, "Sensitivity of SGEMP Response to Input Parameters," IEEE Trans. Nucl. Sci. NS-22, December 1975.

pertinent excitation parameters (Ref. 3) including pulse width, fluence, energy spectrum, and object dimensions. Interesting trends in the response of a simple object to variations in the excitation parameters are noted and discussed.

## B-2. SCALING LAWS

The quantities most readily scaled are time  $t$ , object dimension  $r$ , incident photon fluence  $\Phi$ , and electron energy or velocity  $v$ . To determine how electromagnetic quantities of interest scale with  $t$ ,  $r$ ,  $\Phi$ , and  $v$ , one need only substitute the scaled quantities shown below in the applicable equations describing the electromagnetic response.

$$\begin{aligned} t' &= t/\tau & \Phi' &= \Gamma\Phi \\ r' &= r/R & v' &= \beta v \end{aligned}$$

For the linear regime where the electron motion is unaffected by the electric and magnetic field forces, the set of Maxwell's equations is sufficient to describe the electromagnetic response of a perfectly conducting body. Substituting the scaled quantities into Maxwell's equations results in the requirement that the nondimensional quantities  $\tau$  and  $R$  be equal and that the quantity  $\beta$  be unity. The resulting scaled electromagnetic quantities for the linear regime are shown in Table B-1, where  $R = \tau \triangleq \alpha$ .

If the electron trajectories are affected by the electric or magnetic fields (nonlinear regime), then Newton's first law describing electron motion under the influence of electric and magnetic field forces must also be considered. The additional requirement resulting from the scaling substitution into Newton's law is that the nondimensional parameters  $\Gamma$  and  $\alpha$  must be equal. The resulting scaled electromagnetic quantities applicable to the nonlinear regime are also shown in Table B-1.



Table B-1  
SCALING LAWS

Quantities	Scaled Quantities (Linear Regime)	Scaled Quantities (Nonlinear Regime)
Current density, J	$J' = \alpha \Gamma J$	$J' = \alpha^2 J$
Charge density, $\rho$	$\rho' = \alpha \Gamma \rho$	$\rho' = \alpha^2 \rho$
Electric field, E	$E' = \Gamma E$	$E' = \alpha E$
Magnetic field, H	$H' = \Gamma H$	$H' = \alpha H$
Potential difference, $\Delta V$	$\Delta V' = \Gamma / \alpha \Delta V$	$\Delta V' = \Delta V$
Current, I	$I' = \Gamma / \alpha I$	$I' = I$

### B-3. RESULTS

SGEMP response calculations using the ABORC computer code (Ref. 4) were performed parametrically as a function of the various excitation parameters. Responses resulting from a wide range of excitation parameter values can be displayed by utilizing the scaling laws. As an example, calculations have been performed for the response of a right circular cylinder of radius R exposed to a photon pulse of fluence  $\Phi$  having a Planck radiation spectrum characterized by an energy  $\mathcal{E}$ . The pulse time history is proportional to  $\sin^2 [(\pi t/2)/\tau]$ . Note that because of the scaling laws, one need not select specific values for all the various excitation parameters to display the results; they may be displayed parametrically as functions of  $\tau/2\pi R/c$ ,  $\Phi R$ , and  $\mathcal{E}$ . The nondimensional quantity  $\tau/(2\pi R/c)$  is simply the ratio of pulse rise time to the time required for light to travel around the object. The quantity  $\Phi R$  is the product of fluence and object dimension which we define as the "fluence-product," having dimensions of cal/m in the mks system.

For purposes of this summary, the surface current at midpoint on the side of the cylinder is the quantity chosen to characterize SGEMP response. Results of the computer calculations are shown in Figures B1 and B2.

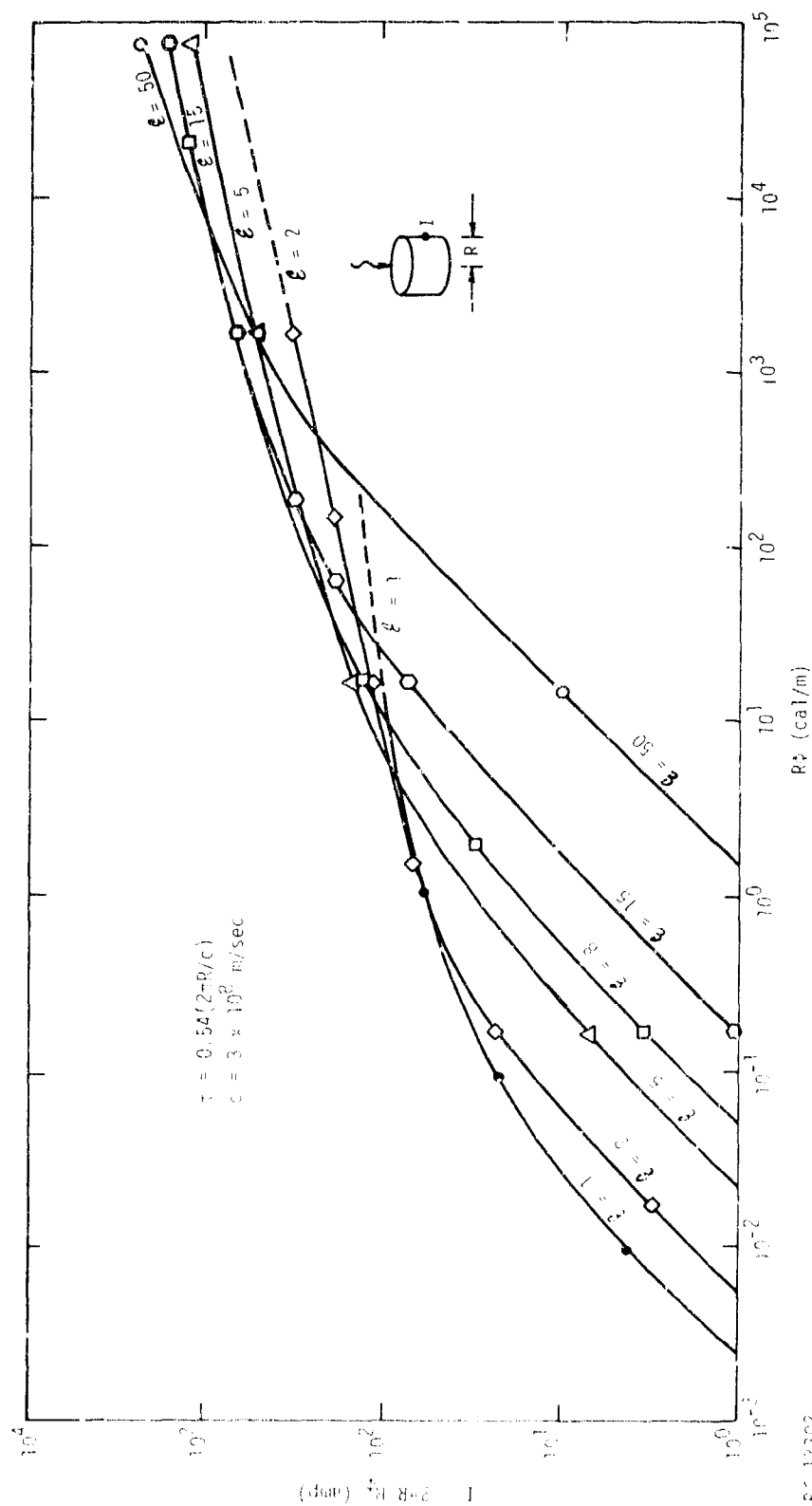


Figure B-1. Surface current versus fluence product for different spectra characterized by energy  $\bar{\epsilon}$  in kev

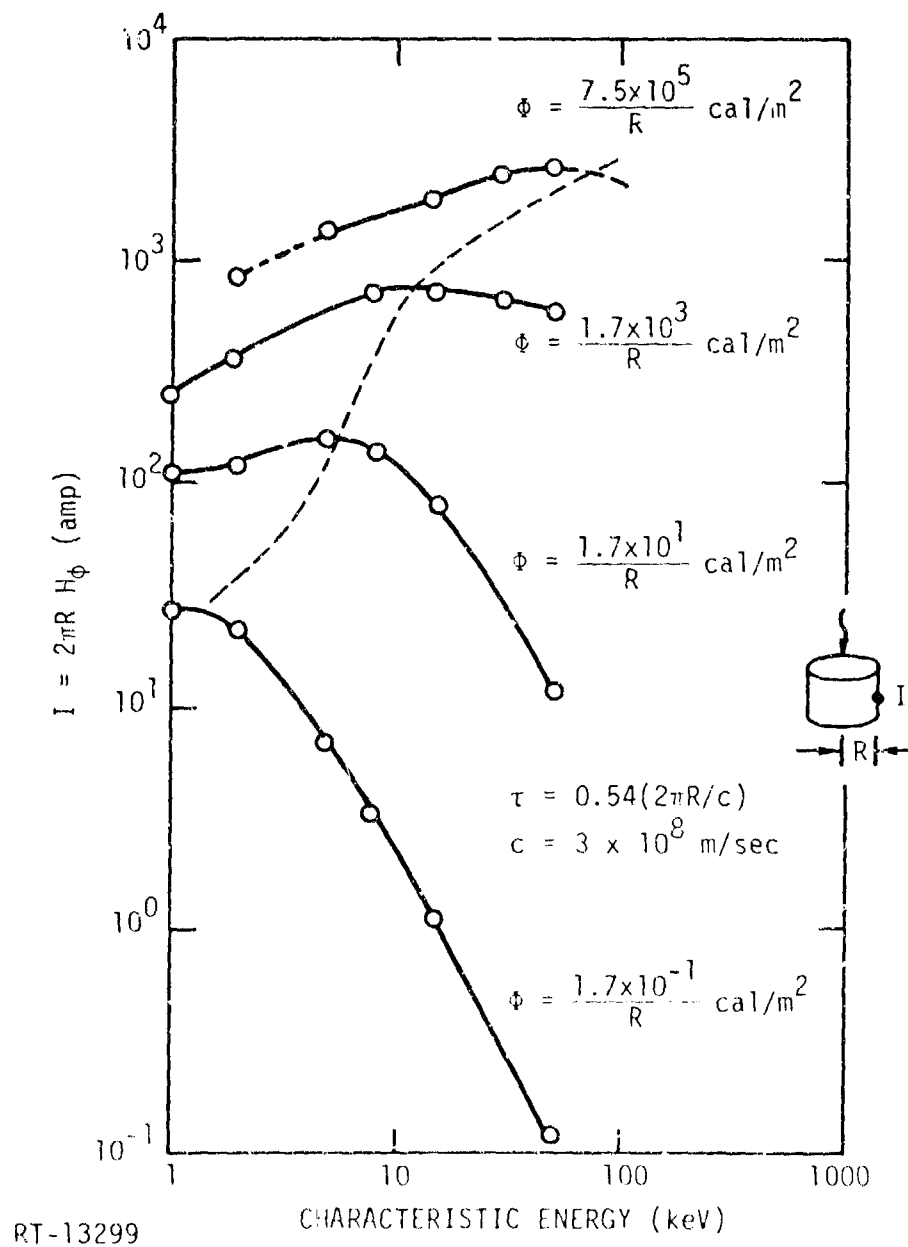


Figure B-2. Surface current versus spectrum energy for different fluences. Dashed line shows locus of worst-case response energy spectra for different fluences.

In Figure B-1, the total current flowing on the cylinder across the midpoint is shown as a function of the fluence product for various photon spectra. The following observations are drawn from Figure B-1.

- For characteristic energy in the range of 1 to 100 keV, the response is essentially linear for fluence-products ( $R\Phi$ ) less than  $10^{-2}$  cal/m. In this range, the softest spectrum yields the largest emission current and, therefore, the largest response.
- The responses became nonlinear with increasing fluence products, and the harder spectra yield higher responses because the more energetic electrons in these spectra are less space-charge-limited.

In Figure B-2, the total current is shown as a function of characteristic energy for various fluence levels. The following observations can be made.

- At the lower fluences in the linear regime, the response falls off as  $1/E^2$ , which corresponds roughly to the fall-off in emission current density with increasing photon energy.
- At higher fluences, there is a definite peak in the maximum response as a function of energy. Thus, for a given fluence, there is a defined energy range which produces a worst-case response.

The previous results have been obtained for a constant ratio of pulse width to object dimension.

#### B-4. SUMMARY

Scaling laws for SGEMP excitation are defined.

SGEMP calculations have been performed and displayed in a compact format using the scaling laws. Results are useful for making order-of-magnitude external SGEMP response estimates for a wide variety of excitation parameters.

## APPENDIX C

### SAMPLE ABORC CALCULATIONS: SGEMP GEOMETRY EFFECTS

## ABSTRACT

Self-consistent, fully dynamic computer calculations were performed using the recently developed arbitrary body-of-revolution code ABORC for complex geometries in SCEMP environments to test the validity of simplifying geometry assumptions previously made in the solutions of these problems. Assumptions such as simple geometry representations of complex bodies and separability of inside and outside problems are tested. Effects of gaps, interior electrical paths, and booms protruding from bodies are discussed. High space-charge-limited results are emphasized.

The response of simple bodies such as cylinders and spheres was found to be similar to more complex geometries in terms of peak currents and response rise times, although much of the detail in terms of resonant frequencies, internal responses, and responses around reentrant bodies is lost. The inside and outside responses of an object can be separated in many cases even though both solutions by themselves are highly nonlinear and the leakage currents are relatively large. The external response of a highly segmented body is similar to the response of a smoothly connected body of revolution. The internal response can be considerably different when a conducting path exists between the segments.

## C-1. INTRODUCTION

The problems associated with computing the SGEMP response of a complex structure can be conveniently divided into two categories: the choice of structural configuration that best represents the complex object, and the choice of various input excitation parameters for a given geometry. Problems associated with the response of different structural configurations are tested in this paper, while problems associated with differences in excitation parameters for a given configuration are treated in a companion paper (Ref. 1).

The structural detail that can be treated by the SGEMP codes has increased from simple spheres and cylinders (Refs. 2,3) to two-dimensional arbitrary bodies of revolution (Ref. 4), and techniques are being developed to treat fully self-consistent problems in three dimensions. The increase in modeling detail has been pursued to gain a better understanding of the SGEMP response of complex structures, to determine how well the SGEMP response of complex structures are represented by simple bodies, and to determine how much structural detail must be included in the model to represent well defined but quite complex geometries. The purpose of this paper is to report ongoing investigations in this area, and in particular to address (1) representation of complex bodies by simple spheres and cylinders, (2) separability of the internal response from the external response, (3) representation of segmented bodies by continuous bodies, and (4) response characteristics of dumbbell objects consisting of two large bodies separated by a boom.

## C-2. COMPUTATIONAL TECHNIQUE

The ABORC (arbitrary body-of-revolution) code (Ref. 4) used in this study solves the complete set of Maxwell's equations with self-consistent electron motion for axisymmetric geometries. Direct finite-differencing of the field equations is done employing generalized coordinates, and finite "particles" of charge are followed through the spatial mesh of zones to obtain currents. Emission of arbitrary energy, angular, spatial, and time distributions of currents can be specified. Randomizing techniques for the emission are employed for efficient representation of emission distributions. Finite conductivities can be specified representing imperfect conductors, and dielectric structures may be treated by specifying proper dielectric constants.

<sup>1</sup>E. P. Wenaas, S. H. Rogers, and A. J. Woods, "Sensitivity of SGEMP response to Input Parameters," IEEE Conference on Nuclear and Space Radiation Effects, July 14-17, 1975.

<sup>2</sup>T. N. Delmer et al., "SGEMP Phenomenology and Computer Code Development," DNA 3653F, November 11, 1974.

<sup>3</sup>E. P. Wenaas et al., "Topics in SGEMP Analysis," IRT document INTEL-RT 0001-080, February 25, 1974.

<sup>4</sup>T. A. Tumolillo et al., "Skynet Program: Current-Injection Predictions," 3 volumes, IRT document INTEL-RT 8121-007, February 1975.



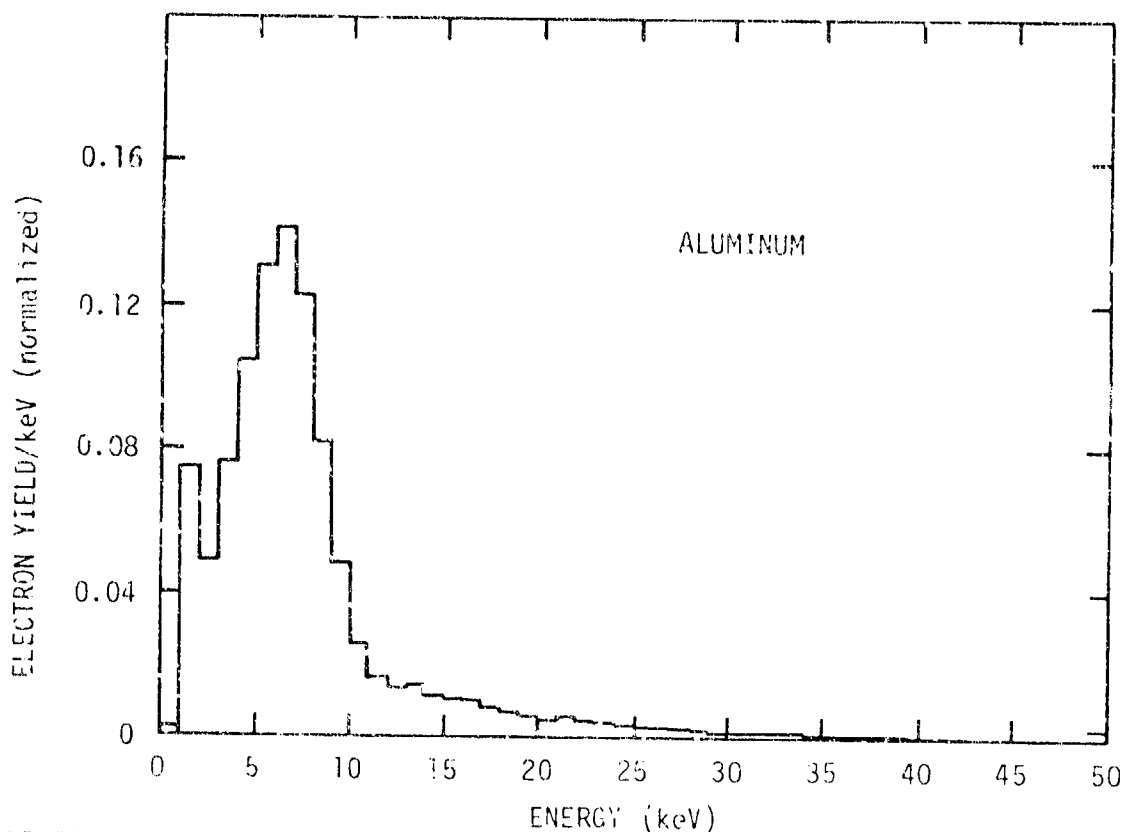
The free-space boundary condition is treated by enclosing the entire problem in a second outer conducting body of revolution rather than by utilizing a radiative boundary condition. Free-space solutions can be obtained by moving the outer boundary out so the clear time (the time at which reflections from the outer wall return to the structure) is larger than the problem time of interest.

### C-3. MODELING OF EXCITATION PARAMETERS

All geometries have been placed inside a cylindrical outer enclosure of 30 m length and diameter. This provides for a clear time of about 100 nsec. Thus, free-space conditions for the satellite models are simulated for a period of time long compared to the assumed incident photon pulse, modeled as a symmetric triangle with a 10-nsec rise and fall and a 10-nsec full width at half maximum (FWHM). The 10-nsec pulse used in these studies was chosen because it is approximately equal to the transit time for light around the skynet satellite, thus allowing for the possibility of exciting resonances on the structures. Results obtained here may be scaled to other object dimensions and pulse lengths using appropriate scaling laws (Ref. 2). All geometry models are rotationally symmetric, and all surfaces are perfect conductors.

Electron emission currents are specified from the various surfaces of the bodies representing photo-electron emission. The emitted electron energy spectrum employed in all cases is shown in Figure C-1. The angular distribution of emitted electrons is assumed to be proportional to  $\cos \theta$  in all cases. Uniform spatial distributions of emission currents are assumed in all cases except the Skynet model, although measurements indicate a weak dependence on the yield with the angle of incidence of the photons relative to the surface (Ref. 5).

<sup>5</sup>M. J. Bernstein and K. W. Paschen, "Forward and Backward Photoemission Yields from Metals at Various X-ray Angles of Incidence," IEEE Trans. Nucl. Sci. NS-20 (1973).



RT-11254

Figure C-1. The electron energy spectrum used in all photo-emissions here is the reverse emission from A as computed by the POEM code. The photon spectrum is a 50-keV bremsstrahlung spectrum with a 5-mil Mylar filter; the preponderance of photons lie in the energy range from 7 to 50 keV (Refs. 6,7).

All emissions of currents are time-phased according to the time required for the photons to reach the emission point. The calculations have been performed for two fluence conditions which, for the spectrum indicated, result in peak emission currents of 1.5 and 1500 amp/m<sup>2</sup>. The lower fluence corresponds to levels at which the fields are small enough that no significant electron trajectory perturbations occur and the problem is essentially linear, while high fluence indicates significant modification of electron trajectories by the fields. Results presented here are primarily for the high-fluence regime where responses are nonlinear and effective excitations are shorter, causing higher-frequency response.

<sup>6</sup>J. N. Bradford, "X-Ray-Induced Electron Emission II," IEEE Trans. Nucl. Sci. NS-20 (1973).

<sup>7</sup>J. N. Bradford, IEEE Trans. Nucl. Sci. NS-19 (1972).

All data for which time histories are presented are averaged over 1 nsec unless otherwise noted. This step is helpful in some cases for interpreting results due to numerical hash which is caused by the particle nature of the code.

The validity of some of the assumptions made here for photo-emission specifications with respect to practical considerations can certainly be questioned. To assume the same spectrum for forward-emitted electrons as for backward-emitted electrons may not be unrealistic for surfaces such as Mylar thermal blankets, but it is certainly not realistic for thick surfaces or where significantly different materials are present. To use the same peak intensity and angular distribution from the sides of a cylinder as from the top could also be questioned. However, as stated before, the purpose of this paper is to investigate geometry effects, and we have endeavored to keep the studies and results uncluttered with effects and numerous parameter variations which may cloud the geometry effects themselves. Sensitivities of these excitation parameters are treated in the companion paper (Ref. 1).

#### C-4. RESPONSE CHARACTERIZATION

Ways to characterize the response of an object include electric and magnetic fields, surface currents, charge densities, potentials, etc. Inasmuch as we are interested in the response of the structure, the fields at the surface of the structure are particularly useful, and in fact, the normal electric field and tangential magnetic field at the surface of a perfectly conducting body are sufficient to specify charge densities and surface currents. In this paper, the magnetic fields are used primarily to characterize the response, although it must be remembered that the electric fields are just as important in many cases.

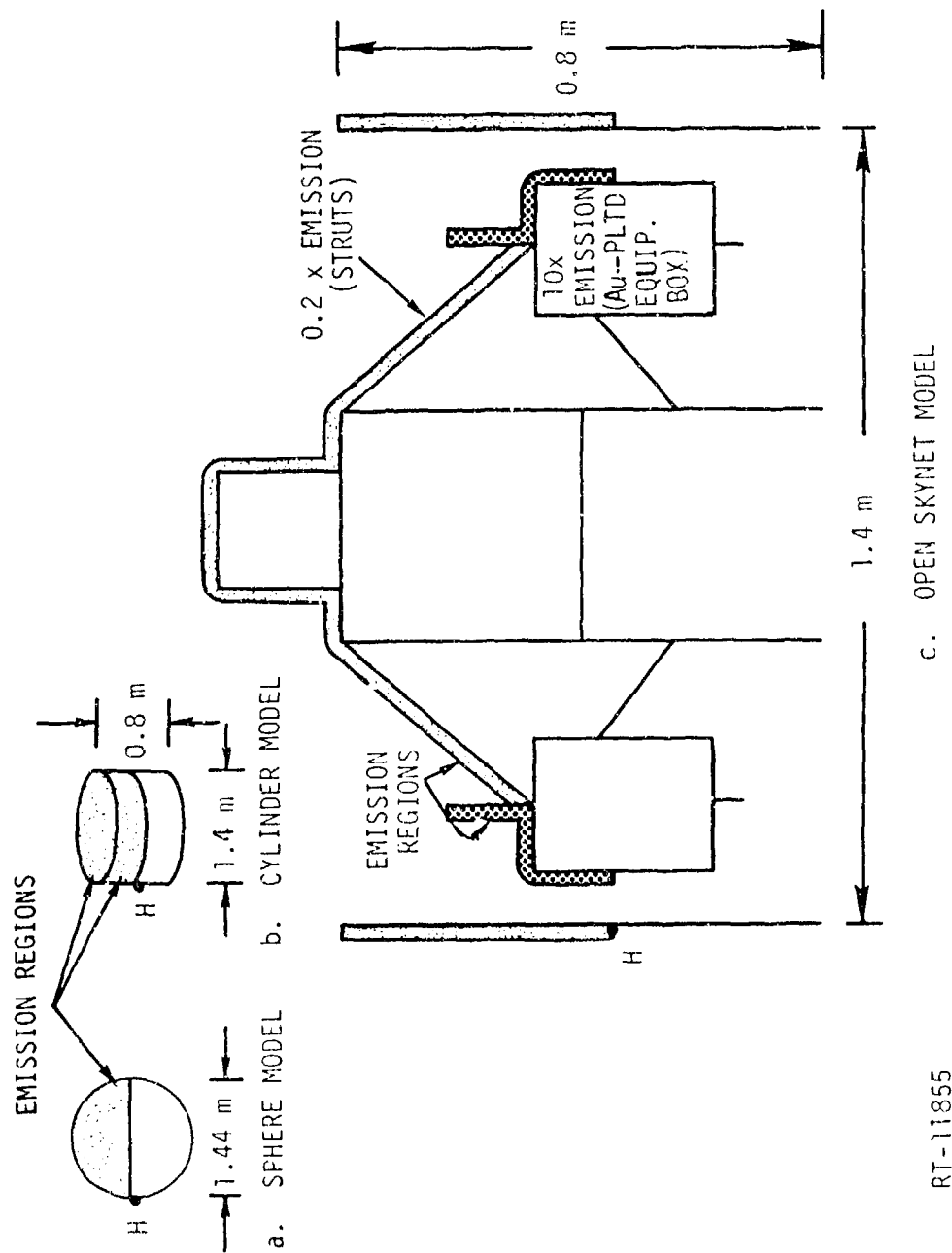
#### C-5. REPRESENTATIONS OF COMPLEX BODIES BY SIMPLE BODIES

The first issue to be addressed is how well complicated satellite structures can be represented by rather simple bodies of revolution such

as a cylinder or sphere. This question is particularly relevant because much of the previous modeling of the SGEMP response of structures has been performed with these simple bodies (Ref. 2). For purposes of this study, we compare the response of the Skynet satellite (Ref. 4) of that of a cylinder and sphere. A simplified representation of the satellite is shown in Figure C-2, along with a simple cylinder of the same basic dimensions and a sphere of radius 0.72 m having a surface area equal to that of the cylinder. The regions of emission on all three structures are represented by the shaded areas on the surfaces. Higher electron emission from regions of the satellite plated with gold are indicated by 10X, while regions of the satellite with lower emission are indicated by 0.2X. No emission is assumed from the inside of the outer wall because this surface is coated with low-Z material which emits fewer electrons. The outer wall is modeled as an electrically isolated surface to represent its being held in place by dielectric braces. In reality, the outer structure is electrically connected by means of solar cell cables, but these cables cannot be modeled by a body of revolution without disastrous results for the structural response. The problem of two bodies connected by a cable or thin rod is treated in subsequent sections.

The regions of emission on the outer surface for the three bodies are chosen so that the emission surface areas are approximately equal. Half-sphere emission is chosen for the sphere to generate worst-case surface currents for the spherical model. This constraint, along with that of equal emission surface areas, requires an unrealistic emission pattern from the cylindrical object in which emission occurs over the top half of the structure only. Thus, it is evident that the sphere has at least one shortcoming in modeling a cylindrical structure.

Results in terms of the magnetic fields at the center of the side surfaces of the three models for the high-fluence case are shown in Figure C-3. The predicted peak currents for the three structures are similar, although the simple models fail to reproduce the resonant behavior exhibited by the more complicated body. In general, the modeling of the exterior surface currents by simple bodies appears to be reasonable.



RT-11855

c. OPEN SKYNET MODEL

Figure C-2. Geometry models investigated with ABORC for determination of validity of representing satellite structures with simple cylindrical and spherical objects

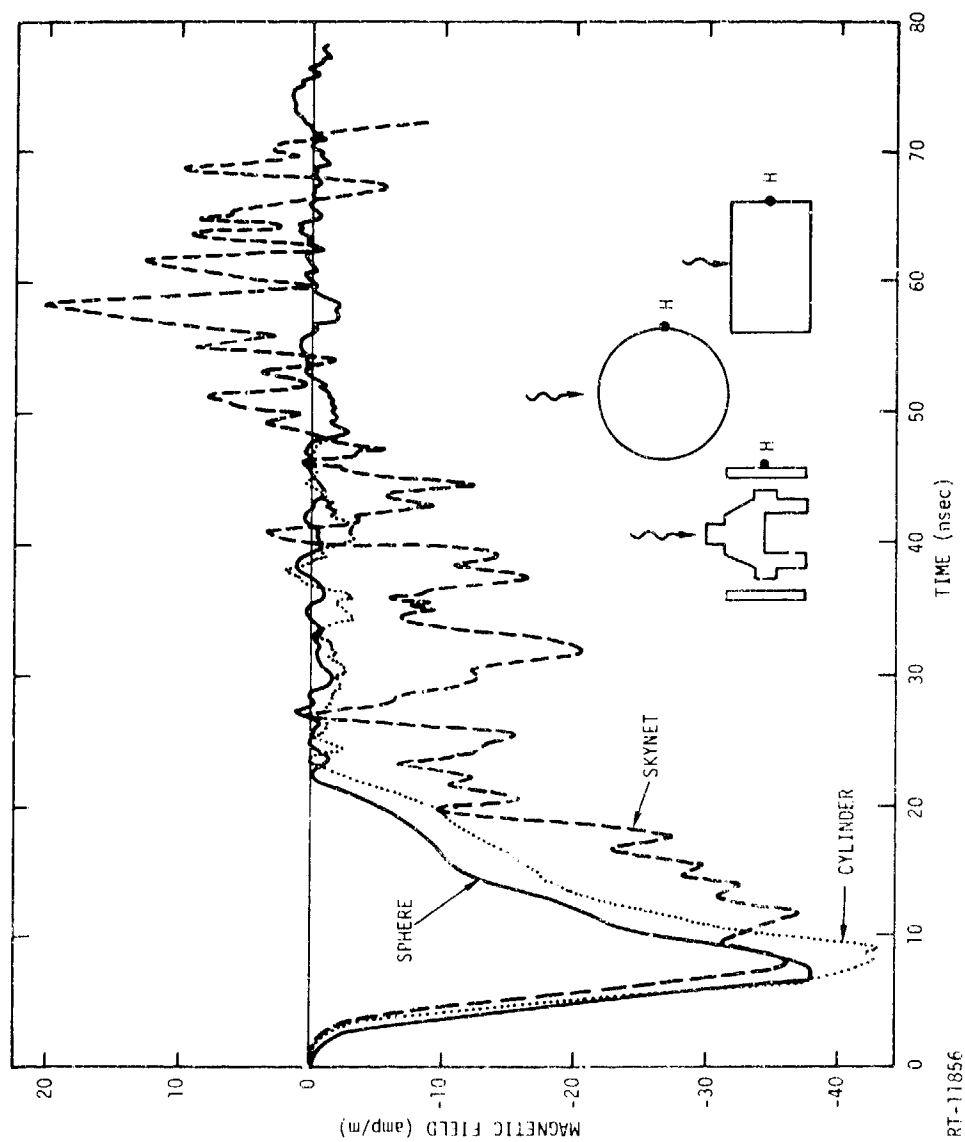
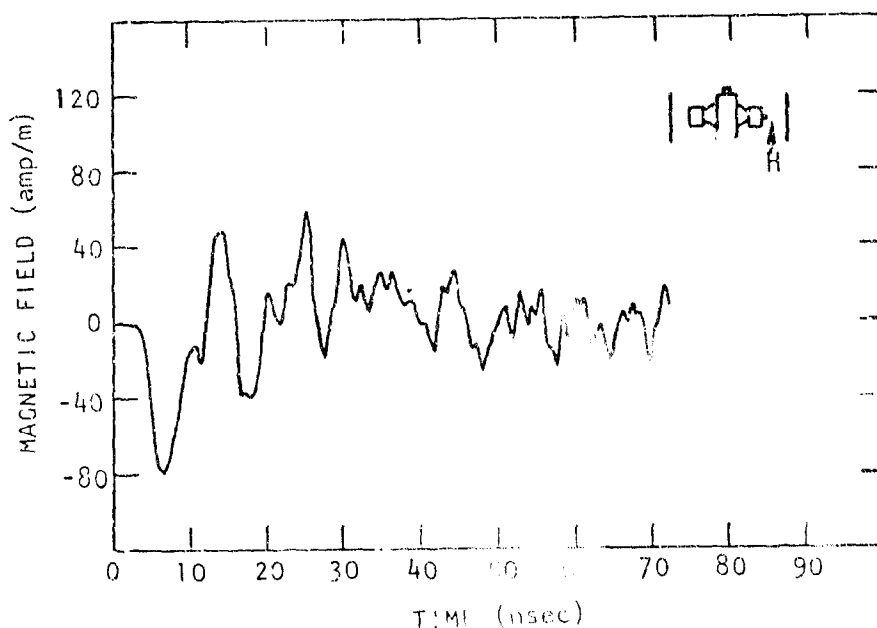


Figure C-3. Comparison of magnetic fields at the sides of a sphere, cylinder, and Skynet model. The peak emission current is 1500 amp/m<sup>2</sup>, corresponding to a highly space-charge-limited solution.

The response of the complex body is shown in Figure C-4 at a second point within the reentrant portion of the structure which has no parallel on the simple bodies. The response at this point is quite different from the responses exhibited by the simple bodies. Thus, we conclude that simple bodies can reasonably model the external response at least in terms of peak currents, but that they cannot model features introduced by complex structures such as reentrant bodies.



RT-11857

Figure C-4. Magnetic field between equipment box and outer wall for Skynet satellite model. The peak emission current is 1500 amp/m<sup>2</sup>, corresponding to a high space-charge-limited solution.

#### C-6. SEPARABILITY OF INTERNAL AND EXTERNAL RESPONSE

The modeling of the SCVP response of complex bodies is usually performed by separating the response of the internal portion of the problem from that of the external portion. Thus, the details of the internal nonlinear response are assumed to be unperturbed by external emission and vice versa. Leakage currents between the interior and exterior are considered although they are assumed to represent a small perturbation, and

the two solutions are assumed to be additive. Obviously, this assumption is valid in the low-level linear regime where field coupling, even if significant, will not affect the electron motion. Thus the separability issue is treated here for the high-fluence, nonlinear response only.

The geometry of Figure C-5 has been chosen because such a configuration, with the relatively large 9-cm gap, was thought to maximize the coupling between the external and internal response, thus tending to represent a worst case. In fact, it will be shown in the following section that the coupling of the two responses is much less severe for a similar object without the center rod. A gap of 9 cm is larger than most gaps in actual satellites, and this again tends to be worst-case.

The electric and magnetic fields were computed at the four points shown in Figure C-5 for emission from the surfaces indicated by the shaded and dashed lines.

Three cases were considered, including (1) external emission only, (2) internal emission only, and (3) simultaneous internal and external emission. The resulting exterior magnetic field at point 1 is shown in Figure C-6 for exterior emission only and interior emission only. The resulting interior magnetic field at point 2 is shown in Figure C-7, again for exterior emission only and interior emission only. It is evident from these results that emission from the external surfaces causes currents to flow on the interior which are on the same order as those produced by internal emission, but that the converse is not true. That is, currents produced by emission on the inside do not cause large structural currents on the outside.

The magnetic fields are not the entire story, however. Perturbations in the nonlinear response arise from perturbations in the electric field rather than the magnetic field (e.g., the nonlinearity in electron trajectories is caused primarily by the electric field, not the magnetic field). Thus, the strong coupling of the outside current to the inside does not necessarily mean that nonlinear internal response cannot be computed separately from the external response. The peak fields are summarized in Table 1, and the fields at two points in time in Table 2, where it is evident that the electric field coupling from the inside to outside is



Table C-1

PEAK FIELDS AT POINTS INDICATED IN FIGURE C-5 FOR (1) INSIDE EMISSION ONLY, (2) OUTSIDE EMISSION ONLY, (3) SUMMATION OF INSIDE ALONE AND OUTSIDE ALONE, AND (4) SIMULTANEOUS EMISSION (UNITS ARE amp/m OR V/m)

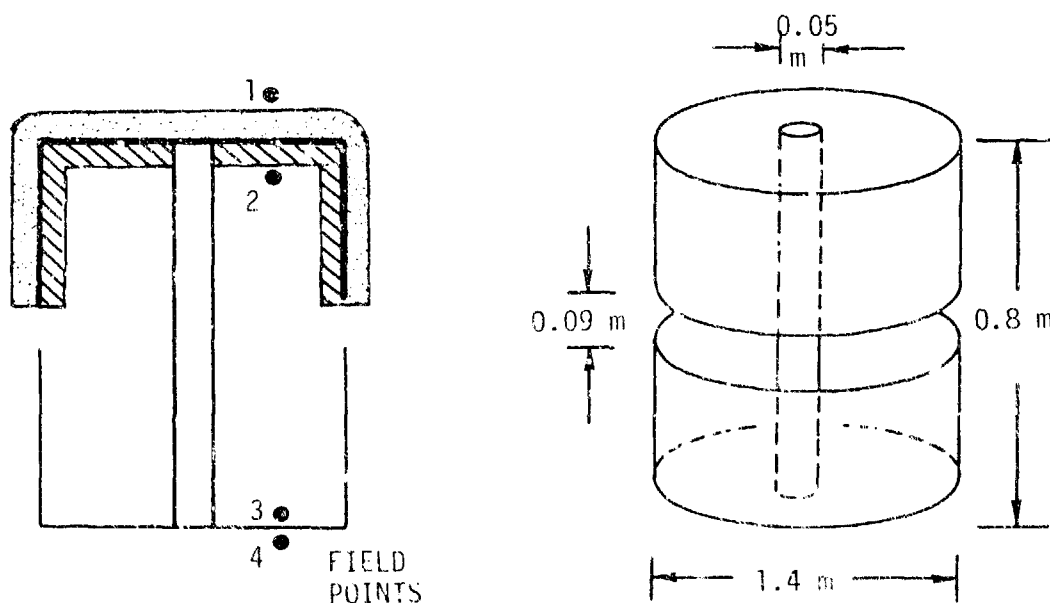
Field Points	Inside Emission Only	Outside Emission Only	Superposition of Inside-Only and Outside-Only Solutions	Simultaneous Emission
H <sub>1</sub>	3.1	15	18	20
H <sub>2</sub>	-104	-80	-184	-128
H <sub>3</sub>	-116	-75	-191	-136
H <sub>4</sub>	-3.7	-3.2	-6.7	-4.2
E <sub>1</sub>	$2.0 \times 10^4$	$1.1 \times 10^5$	$1.3 \times 10^5$	$1.1 \times 10^5$
E <sub>2</sub>	$-1.1 \times 10^5$	$-2.0 \times 10^4$	$-1.3 \times 10^5$	$-1.1 \times 10^5$
E <sub>3</sub>	$2.0 \times 10^4$	$2.0 \times 10^4$	$4.0 \times 10^4$	$2.6 \times 10^4$
E <sub>4</sub>	$-2.2 \times 10^4$	$-3.1 \times 10^4$	$-5.3 \times 10^4$	$-3.4 \times 10^4$

Table C-2

FIELD VALUES AT POSITIONS INDICATED FOR (1) INSIDE EMISSION ONLY, (2) OUTSIDE EMISSION ONLY, (3) SUMMATION OF INSIDE ALONE AND OUTSIDE ALONE, AND (4) SIMULTANEOUS EMISSION; FIELDS INDICATED AT 10 nsec, THE APPROXIMATE TIME OF PEAK OF INTERNAL RESPONSE (UNITS ARE V/m)

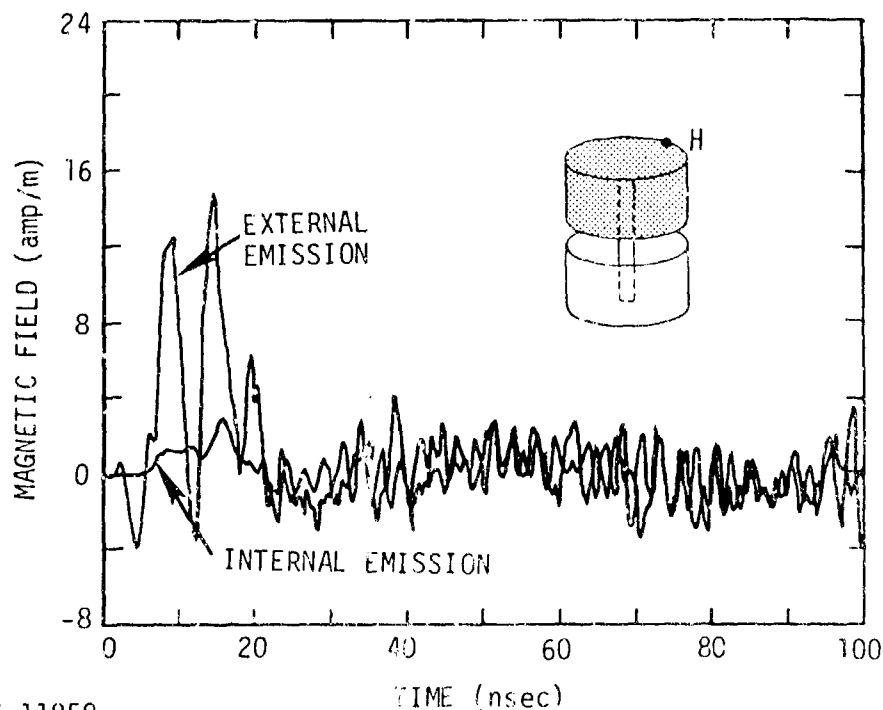
Field Points	Inside Emission Only	Outside Emission Only	Superposition of Inside-Only and Outside-Only Solutions	Simultaneous Emission
<u>Time = 10 nsec</u>				
E <sub>1</sub> (outside)		$1.1 \times 10^5$	$1.1 \times 10^5$	$1.1 \times 10^5$
E <sub>2</sub> (inside)	$-1.1 \times 10^5$	$-7.7 \times 10^3$	$-1.2 \times 10^5$	$-1.1 \times 10^5$
E <sub>3</sub> (inside)	$1.4 \times 10^4$	$-7.7 \times 10^3$	$6.3 \times 10^3$	$6.5 \times 10^3$
E <sub>4</sub> (outside)	$2.6 \times 10^3$	$-6.9 \times 10^3$	$-4.3 \times 10^3$	$-4.5 \times 10^3$
<u>Time = 30 nsec</u>				
E <sub>1</sub> (outside)	$5.7 \times 10^3$	$2.9 \times 10^4$	$3.5 \times 10^4$	$2.7 \times 10^4$
E <sub>2</sub> (inside)	$-7.5 \times 10^3$	$-2.3 \times 10^3$	$-9.8 \times 10^3$	$-5.3 \times 10^3$
E <sub>3</sub> (inside)	$1.5 \times 10^4$	$1.7 \times 10^4$	$3.2 \times 10^4$	$1.9 \times 10^4$
E <sub>4</sub> (outside)	$-1.2 \times 10^4$	$-2.4 \times 10^4$	$-3.6 \times 10^4$	$-2.4 \times 10^4$

weak, and vice versa. Thus, there is every reason to believe that the two nonlinear solutions can be computed separately. This conclusion is demonstrated in Figures C-8 and C-9, where the solutions obtained by adding the response due to external emission alone to the response from internal emission alone are compared to the response with simultaneous emission from the inside and outside. Thus, the internal and external responses appear to be separable in that the nonlinear responses may be computed independently. However, the external response is in general not isolated from the internal response, and the field leakage must be considered.



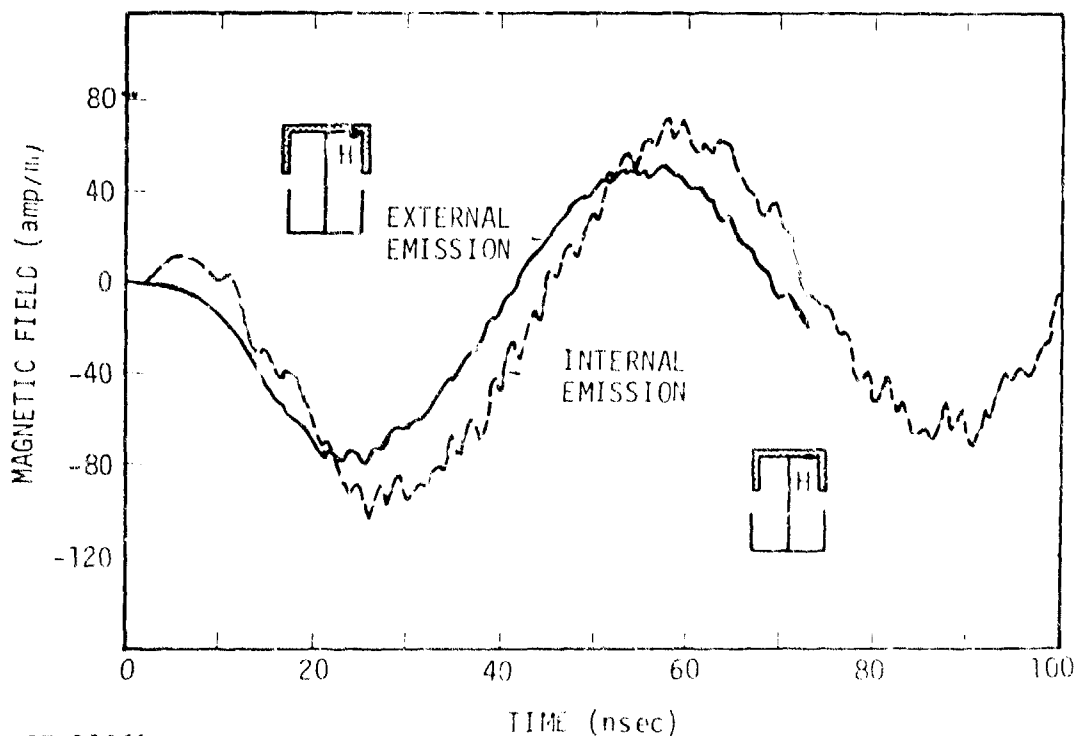
RT-11858

Figure C-5. Geometry utilized in separability study. Four field points are considered as indicated. The radial position for H-fields is 0.34 m and for E-fields 0.41 m.



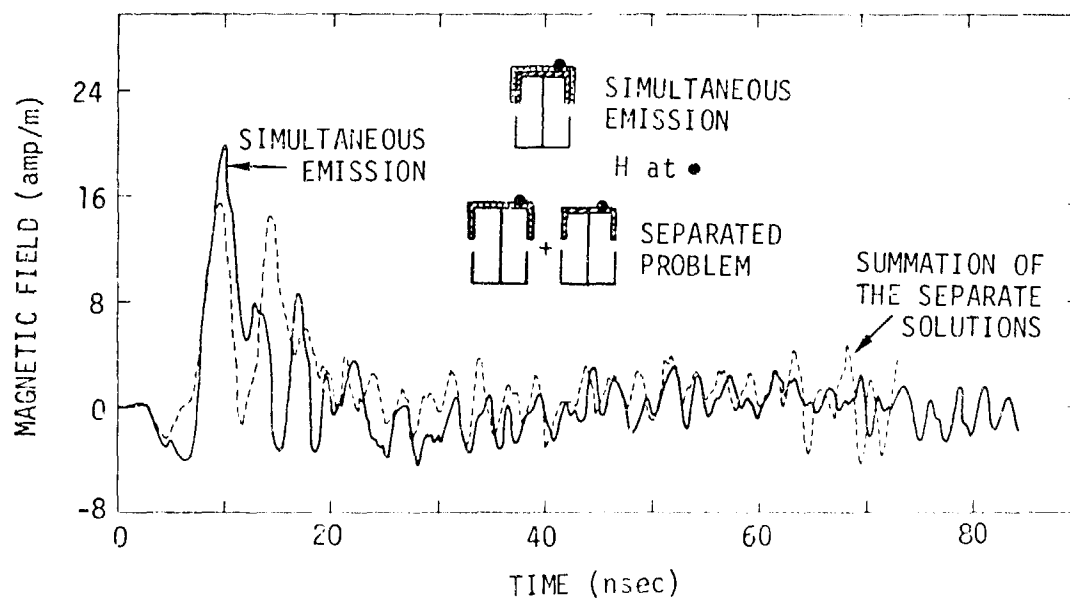
RT-11859

Figure C-6. Magnetic field at point 1 outside the cylinder obtained with exterior emission alone compared with the response at the same point produced by interior emission alone



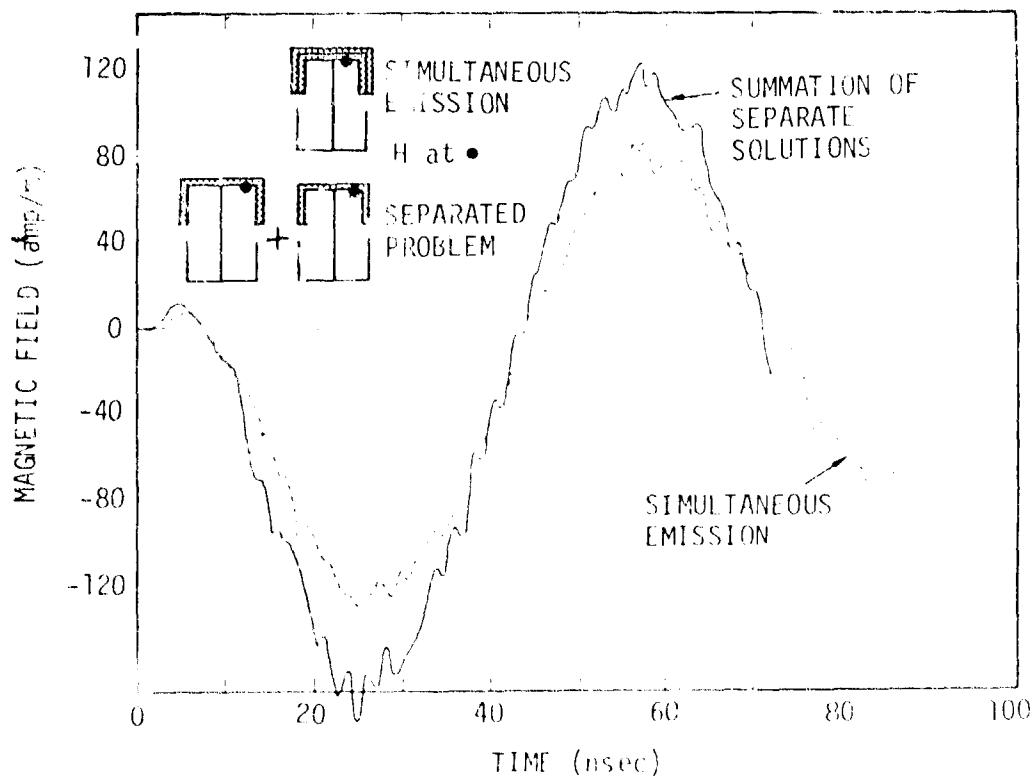
RT-11860

Figure C-7. Magnetic field at point 2 inside cylinder obtained with internal emission alone compared with response at same point produced by external emission alone



RT-11861

Figure C-8. Magnetic field at point 1 outside the cylinder obtained by adding the response from inside emission alone to the response from outside emission alone compared to the response at the same point obtained by simultaneous emission from the inside and outside



RT-11862

Figure C-9. Magnetic field at point 2 inside the cylinder obtained by adding the response from inside emission alone to the response from outside emission alone compared to the response at the same point obtained by simultaneous emission from the inside and outside.

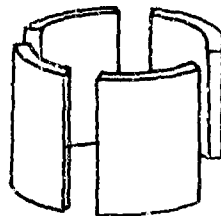
## C-7. SEGMENTED-BODY EFFECTS

Satellite bodies have generally been represented by continuous bodies of revolution for purposes of SGEMP calculations, although many of the spacecraft manufacturers have designed these systems with segmented panels, as shown in Figure C-10a. Although this type of segmentation cannot be modeled with codes limited to rotational symmetry, we can gain insight into the response of segmented bodies by considering segmentation in the axial direction, as shown in Figure C-10b. The figure without a connecting rod simulates truly isolated panels, while the configuration with a connecting rod simulates an internal connection between panels such as a solar cell cable.

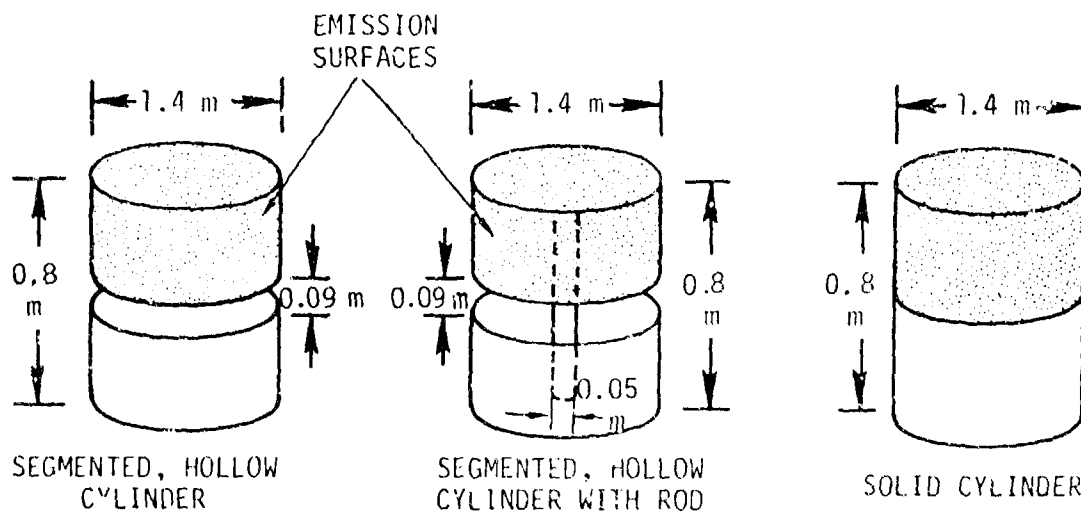
Computations were performed with the three bodies shown in Figure C-10b with equal emission from the top half of each cylinder. Peak field values are shown in Table C-3 for the three geometries. The table reveals very small differences between outside peak field values due to segmenting or interior return paths. The slight difference in the peak electric field at the back in the separated cylinder case is due to the lack of charge transfer to the bottom half of the cylinder in that case. A very significant effect on the interior magnetic field is seen, due to large currents on the interior of the body flowing through the rod.

The external magnetic field near the top of the cylinder is shown in Figure C-11 for the case of high space-charge-limiting. It is quite evident that the response is essentially the same for these objects. Similar results also hold for the magnetic fields at other points on the external surfaces.

Differences in electric fields on the lower half of the cylinder should be evident in the isolated cylinder as compared to the conducting cylinder due to the difference in charge transfer. (The late-time electric field on the lower half of the solid body should be larger than on the isolated body because transferred charge can be redistributed on the solid body while it cannot redistribute in the isolated case except by capacitive coupling.) Expected differences in the late-time electric fields at the bottom of the cylinder are evident in Figure C-12.



a. TYPICAL SATELLITE SEGMENTATION



b. SEGMENTED BODIES UTILIZED FOR EXAMINING SEGMENTED BODY EFFECTS. THE SAMPLE CYLINDER AT RIGHT IS COMPARED WITH RESULTS.

RT-11863

Figure C-10(a),(b). Typical and presently calculable segmented bodies in nonlinear SGEMP

Table C-3

PEAK FIELD VALUES AT POSITIONS INDICATED<sup>a</sup>  
ON A SIMPLE CYLINDER AND SEGMENTED CYLINDERS OBTAINED  
AT HIGH FLUENCE (UNITS ARE amp/m OR V/m)

Field	EMISSION SURFACES		
	Solid Cylinder	Hollow Cylinder Segmented	Segmented Hollow Cylinder Connected by Rod
$H_1$	13	14	14
$H_2$	0	5	-80
$H_3$	0	6	-75
$H_4$	-4.9	-3.2	-3.2
$E_1$	$1.1 \times 10^5$	$1.1 \times 10^5$	$1.1 \times 10^5$
$E_2$	0	$-2.8 \times 10^4$	$-1.8 \times 10^4$
$E_3$	0	$-1.2 \times 10^4$	$2.0 \times 10^4$
$E_4$	$-3.1 \times 10^4$	$-1.5 \times 10^4$	$-3.1 \times 10^4$

<sup>a</sup>Points 2 and 3 are inside the top and bottom walls of the cylinders, respectively. Radial position for H values is 0.34 m, for E values 0.41 m.

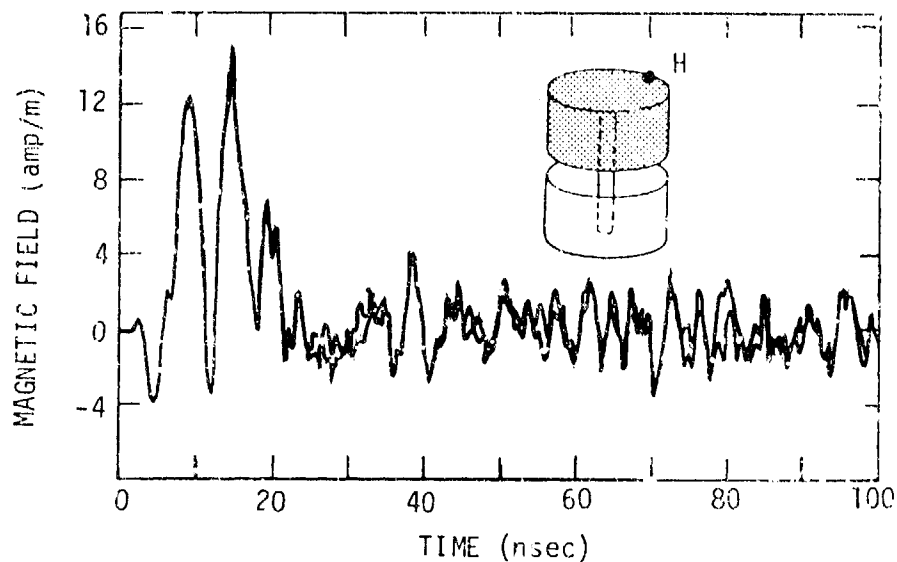


Figure C-11. Exterior magnetic fields at top surface (radius 0.34 m) versus time for simple and segmented cylinders shown in Figure C-10

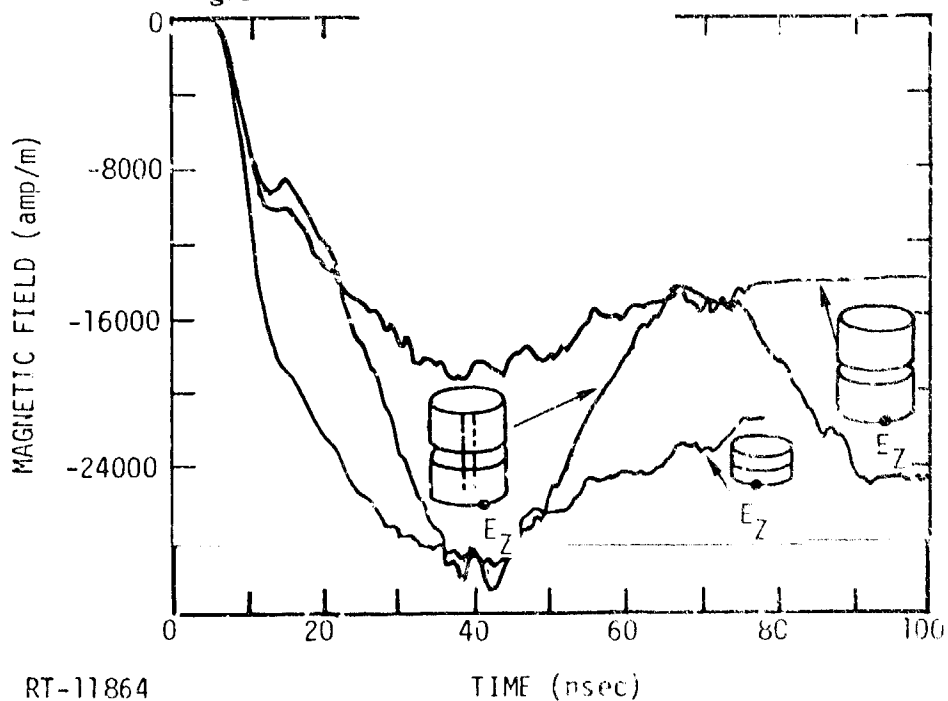


Figure C-12. Exterior electric field at point 4 (radius 0.41 m) outside the cylinder at bottom for simple and segmented cylinders. Peak emission current of 1500 amp/m<sup>2</sup>, corresponding to high space-charge-limiting, was used.



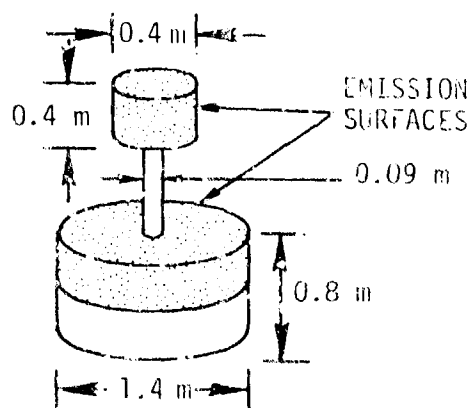
The internal response of the isolated cylinder is markedly different from the response of the cylinder with the rod, however. This is not surprising in as much as current is driven internally because of the transfer of charge between segments. Large low-frequency oscillations are evident, representative of an LC circuit consisting of the inductance of the rod and capacity of the segments.

In summary, the modeling of the gross external currents of a segmented body can be well represented by a body of revolution, but in general, the response within the object is lost by such simple modeling.

#### C-8. DUMBBELL GEOMETRY

Another facet of modeling which has been explored is a geometrical configuration consisting of two relatively large bodies separated by a thin rod or boom. Such a configuration might correspond to the case of solar paddles extending from a satellite body.

The dumbbell geometry shown in Figure C-13 was chosen for this study. The dimensions of the main body are the same as those of the isolated cylinders treated previously. Boom lengths of 1 and 2 m were considered, with a smaller body attached to the end. The boom radius was held constant.



RT-11865

Figure C-13. Dumbbell geometry calculated with ABORG for study of separate bodies connected by booms. Boom lengths of 1 and 2 m are considered.

Calculations were performed for emission from the top and side of the small cylinder and from the top half of the large cylinder, as shown in the figure. Thus, the emission from the larger cylinder is identical to that used in the isolated-cylinder studies.

Figure C-14 shows the magnetic field responses at the midpoint of the larger cylinder of the dumbbell compared to results obtained by treating the larger cylinder separately. The responses at this point are strikingly similar, indicating that the boom and small attached object do not significantly perturb these fields on the side surface of the large cylinder at this high-fluence level.

The response of the boom is shown in Figure C-15 for boom lengths of 1 and 2 m. It is evident that the response on the boom is significantly different from the response on the body. The large resonances appear to be characteristic of an LC circuit consisting of the inductance of the dumbbell and the capacity of the two bodies. The resonant frequency decreases with increasing boom length, as expected.

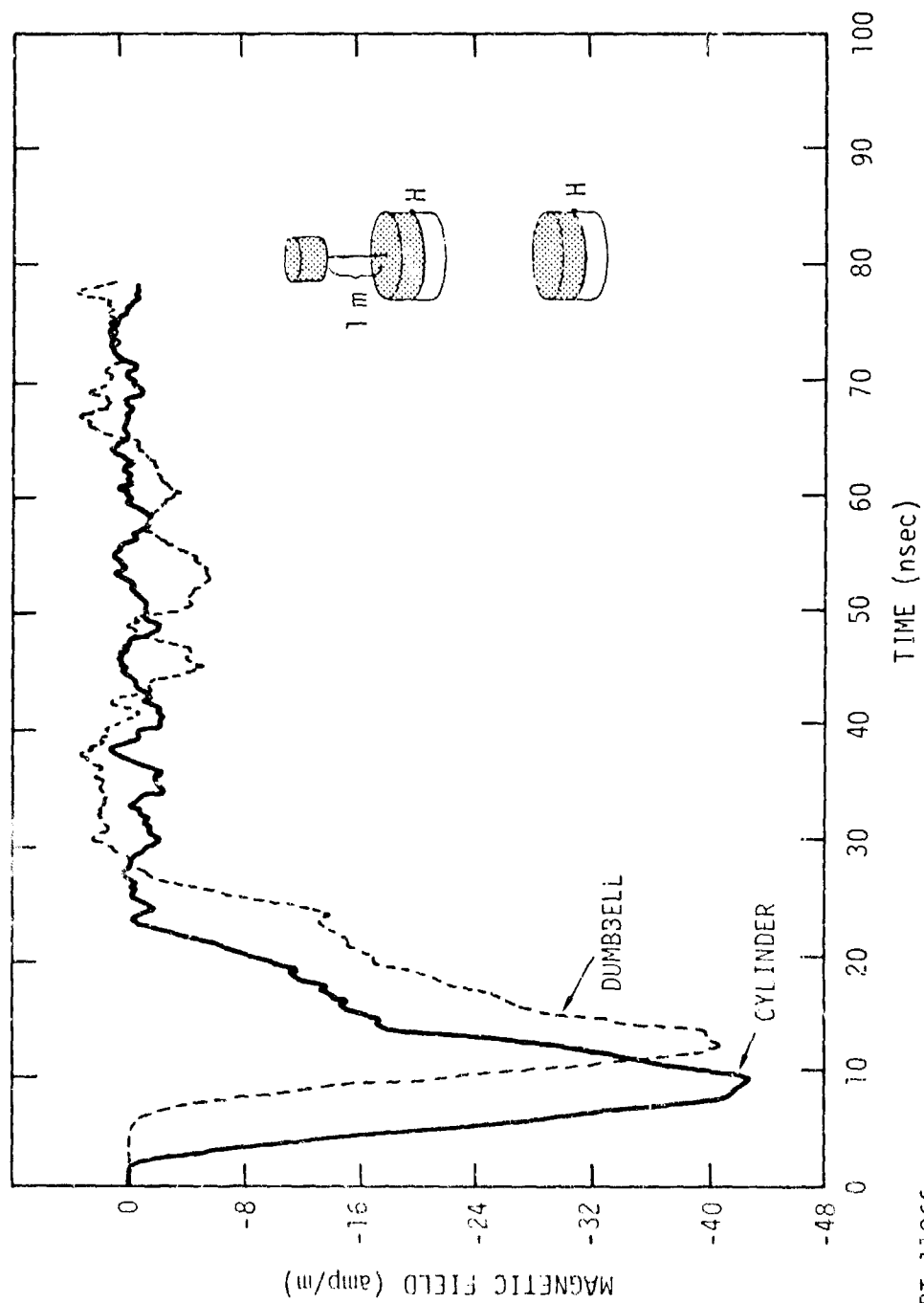
Peak H-fields in the boom are significantly higher than on the sides of the body, but the total peak currents flowing on the boom are less than on the large body:

$$I_{\text{boom}} \approx H \times 2\pi r \approx 135 \times 2\pi(0.07) \approx 57 \text{ amps} ,$$

$$I_{\text{boom}} \approx 42 \times 4\pi(0.7) \approx 180 \text{ amps} .$$

Thus, it is evident why the presence of the boom does not significantly perturb the response of the larger cylinder. The currents on the boom are lower than on the surface of the body due to effective cancellation from currents emitted to infinity from each body.

At the higher fluence levels treated here, the space-charge-limited responses of each body appear to be somewhat decoupled. As indicated in Table C-4, the peak magnetic fields do not change significantly as the two bodies are moved further apart, indicating that the trajectories of electrons emitted from the two bodies are not altered by the presence of each other. In the case of lower space-charge-limiting, where a large number of electron trajectories would reach out to distances on the order of the separation of bodies, however, we would expect much more coupling.



RT-11866

Figure C-14. Segmented body effect; magnetic fields versus time for a simple cylinder and a dumbbell at high space-charge-limiting. The field point is at the center of the large cylinder, as indicated by the dot in the figure.

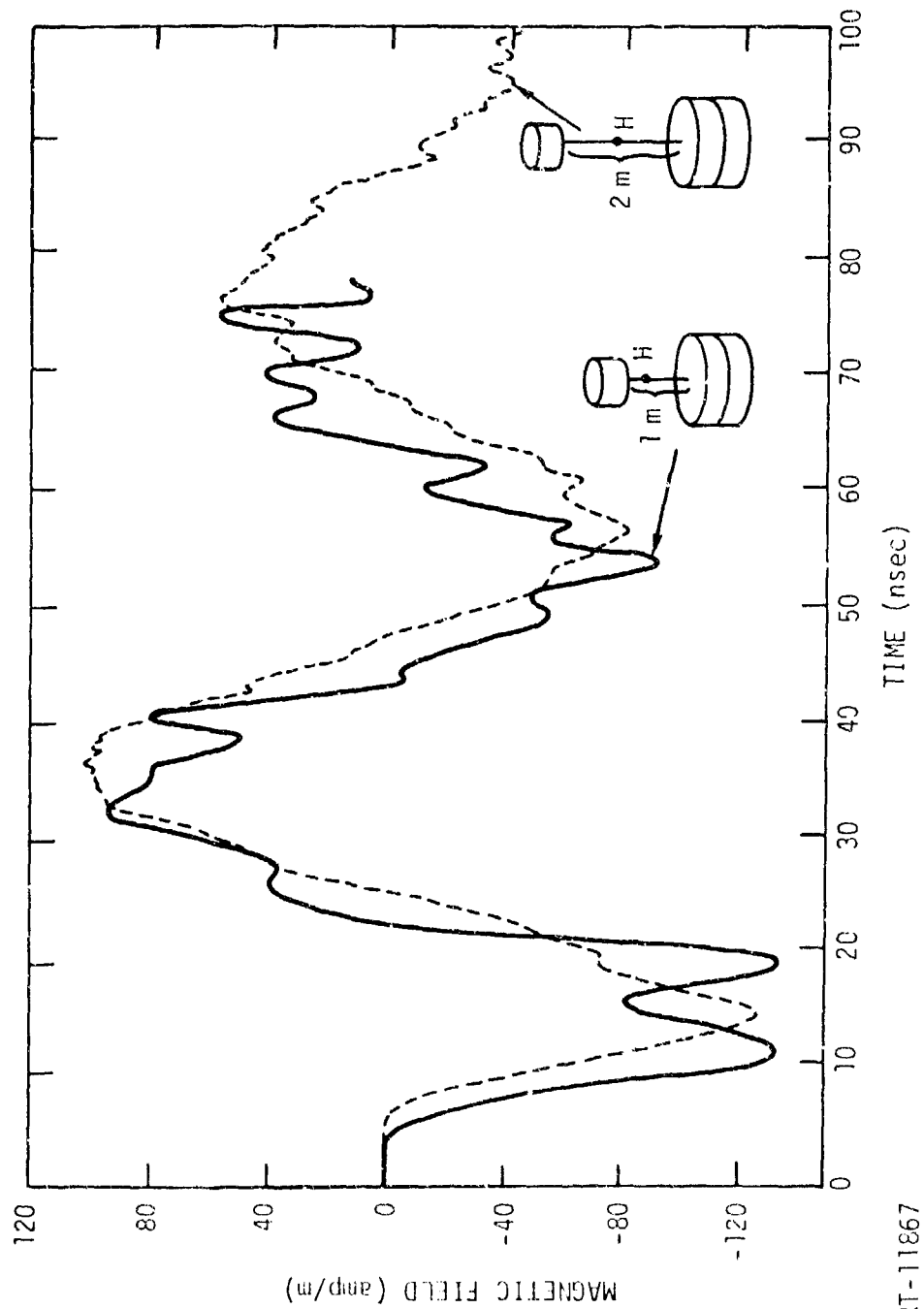
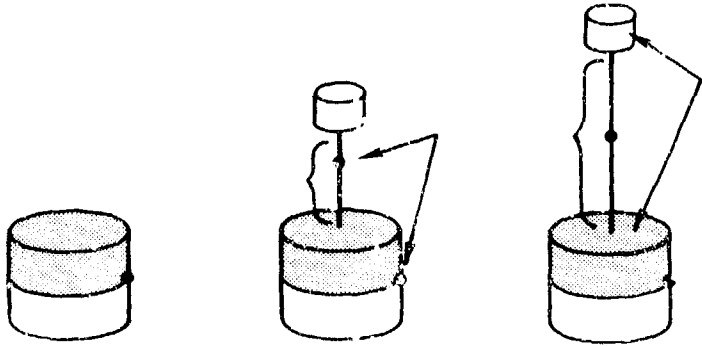


Figure C-15. Segmented-body effect; magnetic field near the boom at radius 0.07 m versus time for dumbbell geometry at high fluence with different boom lengths

Table C-4

SEGMENTED-BODY EFFECT; PEAK MAGNETIC FIELD VALUES  
AT POINTS INDICATED AND OSCILLATION PERIODS FOR A CYLINDER  
COMPARED TO A DUMBBELL CONFIGURATION AT HIGH FLUENCE

---

			
$H_1$ (amp/m)	$\sim 2$	-135	-127
$H_2$ (amp/m)	-43	-41	-44
$t_{osc}$ (nsec)	10	$\sim 35$	$\sim 41$

---

#### C-9. SUMMARY AND CONCLUSIONS

The self-consistent, fully dynamic ABORC code for rotationally symmetric bodies has been employed on a number of bodies to investigate the effects of approximations of geometries in analyzing the SGEMP response of a system. We arrive at the following tentative conclusions based on this relatively small number of geometrical studies.

1. The response of simple bodies such as cylinders and spheres is similar to more complex geometries in terms of peak currents and response times.
2. The inside and outside responses of an object can be separated to first order in many cases, even though both solutions by themselves are highly nonlinear and the leakage currents are relatively large. Some interaction of the

internal and external responses was seen, and that is undoubtedly geometry-dependent.

3. The external response of a highly segmented conducting body is similar to the response of a smoothly connected body of revolution. The internal response can be considerably different when a conducting path exists between the segments. The response then contains a long low-frequency oscillation similar to the response of an LC circuit consisting of the inductance of the interconnecting rod and the capacity of the segments.
4. The space-charge-limiting characteristics of two large objects separated by a distance large compared to the dimension of the space-charge barrier are relatively unperturbed by the presence of each other.

APPENDIX D

NUMERICAL SENSITIVITY CONSIDERATIONS IN ABORC CALCULATIONS

## D-1. INTRODUCTION

A question which must be considered with every calculation made by a finite-difference/particle-mover code is how sensitive the results are to the numerical grids and particle statistics employed in the problem. This issue is particularly important when calculations are being compared where only minor changes in input are being considered to determine effects on response. In this appendix, some results of various grid sensitivity investigations carried out during the course of several projects are presented. The goal is to demonstrate how to evaluate ABORC calculations for numerical grid sensitivity. Some example calculations are shown, and parameters useful in measuring calculational quality are discussed.

This discussion is an outgrowth of several projects, and therefore, the examples may be mildly disjointed. The principles discussed apply to a broad spectrum of conditions, however.

## D-2. ABORC GRIDS

Grids which must be specified in ABORC calculations are:

- Spatial zoning,
- Time steps,
- Energy bins,
- Angular distributions,
- Emission spatial zones.

The first three grid types are considered here. Results of variations of the last two inputs on SGEMP-IEMP calculations can be found in References 1 and 2.

---

<sup>1</sup>E. P. Wenaas, S. Rogers, and A. J. Woods, "Sensitivity of SGEMP Response to Input Parameters," IEEE Trans. Nuc. Sci., Vol. NS-22, Dec. 1975, p. 2362.

<sup>2</sup>E. P. deFlomb and A. J. Woods, "TEDIEM-RZ and R0: Two-Dimensional Time-Dependent IEMP Computer Codes," DNA 3140F, Mar. 10, 1973.



Considerations which must be made in choosing ABORC grids are summarized below.

- Resolution of object
- Resolution of time response
- Pulse shape
- Electron velocity
- Clear time
- Field gradients
- Statistical noise
- Computer run time
- Computer memory

Object resolution can require fine grids if effects of re-entrant bodies are being considered, or if body shapes are unnatural for the cylindrical coordinates employed in ABORC, or if pulse lengths are short compared to object dimensions. For simple cylinders, however, body resolution is usually not a restriction. Time response resolution requirements also must be considered, particularly if the problem is very dynamic. At least 5 or 6 grid points are required for accurate transmission of wavelengths. Shorter wavelengths are distorted or do not propagate through the grid at all (Ref. 3). Obviously, the pulse shape must be considered in choosing time steps and spatial grids if it is short or has fine structure which should be resolved. Electron velocity is important in that the distance travelled by the electrons in a time step should be roughly compatible with grid spacing and field gradient distances. Clear-time requirements, or time for radiation to be reflected back to the inner object from the outer tank walls, generally determine the outer cylinder size because ABORC does not have a free-space boundary condition. A large clear time results in large outer zone and charge zone size changes, especially if small object detail or space-charge barriers are being resolved.

Distances over which fields change significantly should also be considered in choosing space and time zones. Any gross discrepancy in

---

<sup>3</sup>J. P. Boris, "Relativistic Plasma Simulation-Optimization of a Hybrid Code," Proc. Fourth Conference on Numerical Simulation of Plasmas, NRL, 1970.

which resolution of a space-charge barrier much smaller than the minimum spatial zone size is attempted, for example, is bound to result in grid-dependent results. Computer memory available limits the code to 100 by 100 spatial zones at present.

Statistical noise, due to finite particles of charge crashing through the spatial mesh, decreases with the number of particles. Computer run time usually limits the number of particles, however. The time required for both particles and fields is shown below in 7600 central processor (CP) seconds.

Particles:  $3 \times 10^{-4}$  sec/particle step

Fields:  $10^{-5}$  sec/zone step

These numbers translate into about 5 minutes of CP time for a calculation with an average of 3000 particles followed for 300 steps through a spatial mesh of 70 by 40 axial and radial zones. The present cost for such a calculation at a government installation is about \$100. While the field solution portion of the code is programmed very efficiently, very little optimization of the particle-pusher coding has been performed to date. Present run times could be reduced considerably through efficiency measures.

Obviously, the large number of considerations in choosing grids prohibits writing down an exact formula for grids which always work without resulting in unreasonable computer time requirements. Also, to even suggest that all of the above are important in producing grid-independent results is somewhat speculative. For example, the requirement of limiting the distances over which particles travel in each time step to dimensions small or comparable to distances over which fields acting on them change considerably seems intuitively very reasonable. The problem is so complicated in a case with many particles at different energies that results might smooth out and give correct responses even though trajectories of individual particles might be grossly different from reality. The best way to know for certain is to vary grids while holding physical properties of a calculation constant, and compare responses. In the following sections, results of some of these grid variations are shown, and discussion of some of the parameters which determine numerical quality of the calculations is given.

Table D-2  
NUMERICAL GRID SPECIFICATIONS FOR MEDIUM- AND HIGH-FLUENCE ZONING STUDIES

	Medium-Fluence		High-Fluence	
	A	B	A	B
Minimum zone size (m)	0.005	0.02	0.002	0.005
Number of emission zones	3	3	4	4
Energy bins	15	15	10	10
Time step (sec)				
Particles	$1.00 \times 10^{-10}$	$1.00 \times 10^{-10}$	$2.5 \times 10^{-11}$	$2.5 \times 10^{-11}$
Light	$1.11 \times 10^{-11}$	$3.33 \times 10^{-10}$	$4.17 \times 10^{-12}$	$8.33 \times 10^{-12}$
Number of particles in system at 10 nsec	2214	2273	1258	1320
Total CPU time to 10 nsec (sec)	47	36	229	160

Exact axial zones above the emission surface can be seen in Figures D-2 and D-3 (similar variations in radial zones were undertaken simultaneously), along with effects on normal electric fields in the space-charge barrier when zone sizes are varied. Figure D-2 is for moderate SCL, while Figure D-3 is for very high SCL. Notice the much steeper gradients and higher fields in the high-SCL case. It is obvious that the particles will see a considerably higher electric field right near the emission face with the fine zoning than with the coarser zoning. This is also true in the medium-SCL case, only much less pronounced. It would be reasonable, therefore, to expect zone size sensitivity in the high-SCL case to be more pronounced than in the moderate-SCL case. Also notice that much coarser zones can be employed at lower fluences without resultant unreasonable changes in fields from grid point to grid point.

Time histories of fields at several positions around the object are found in Figures D-4 and D-5. Figure D-4 is for medium fluence and D-5 for high fluence. The curves are smoothed with a 0.5-nsec time constant in the medium-fluence case and 0.2-nsec in the high-fluence case. The

### D-3. RESULTS OF GRID STUDIES

#### Fluence Dependence of Grid Requirements

Of the considerations mentioned above for choosing grid sizes in ABORC calculations, the resolution of field gradients has been one of the most consistent problems in producing grid-independent responses. Gradients are not generally a problem for low-fluence conditions in SCMP.

As fluence is increased and the electrons are turned back by fields, very large charge densities can build up close to the object's emitting surfaces. The distance over which the electric field changes by a factor of 10 can be as little as 2 or 3 cm for fluences and spectra of interest, while the object may be 3 m long. Such large differences in zone requirements to describe both the space-charge barrier and the object cause concern over the spatial zone dependences of results.

To investigate spatial zone sensitivities, calculations were performed in which spatial grids were changed while holding all other parameters constant. The comparisons were made at intermediate and high SCL. Physical problem conditions are listed in Table D-1 and numerical grids in Table D-2. Electron emission results were obtained from QUICKE2.

Table D-1

#### TEST PROBLEM DESCRIPTIONS FOR ZONING STUDIES

---

Problem Geometry	Cylinder with length = diameter = 3 m
Clear Time	Greater than simulation time
Electron Emission	
Emission Surface:	top + half side uniform
Spectrum:	see Figure D-1
Angular distribution:	$\cos \theta$
Time history:	medium fluence: 10-nsec rise, 40-nsec fall
	high fluence: $\sin^2$ pulse with 17-nsec rise

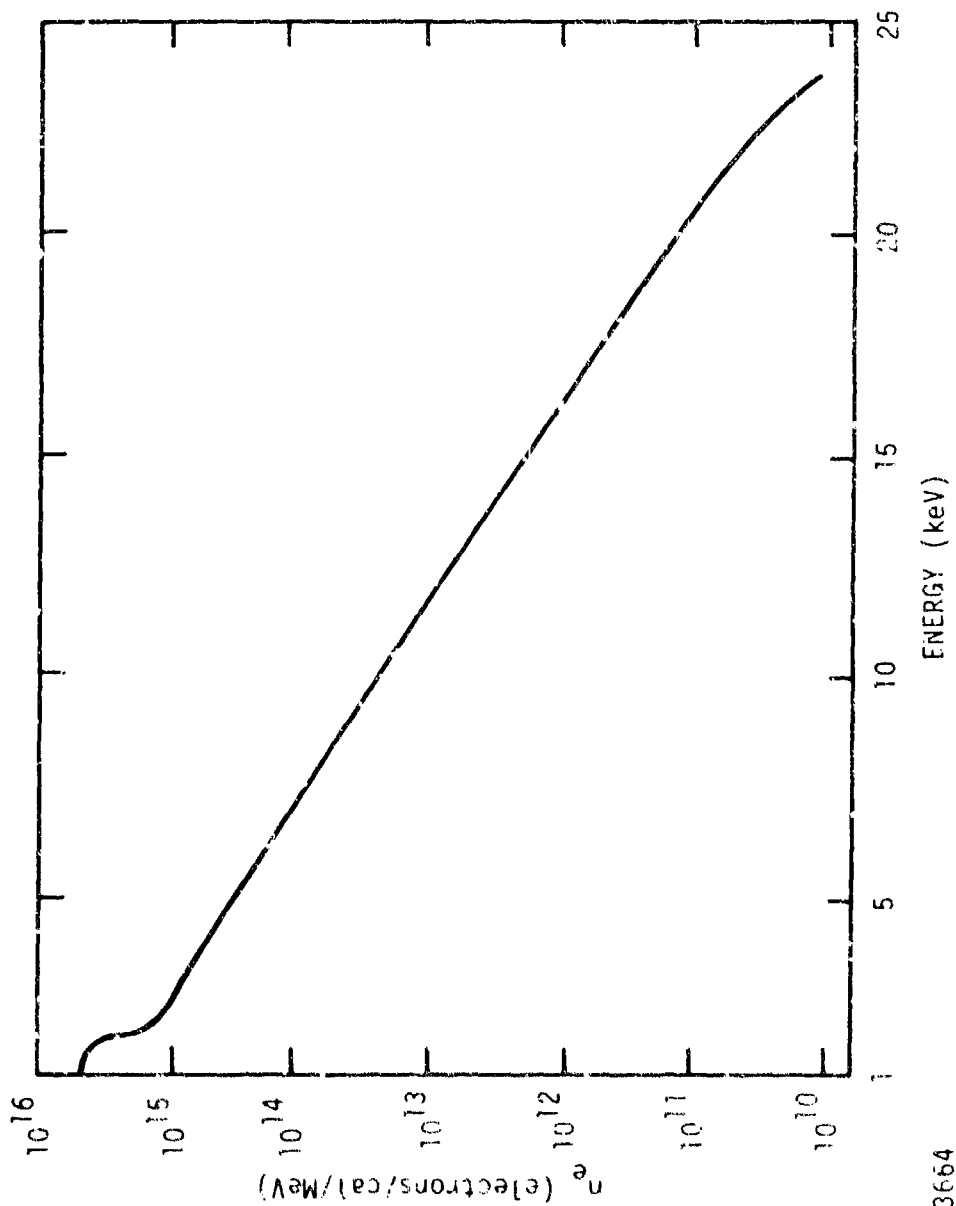
---

medium-fluence curves show almost complete independence of the grid change, whereas substantial differences are seen in the high-level case, especially for field quantities evaluated in regions where many particles are present. The curves permit several conclusions to be drawn regarding spatial zone requirements in ABORC calculations:

- Spatial grid requirements are fluence-dependent.
- Time histories of fields near the object are virtually spatial-zone-independent for zoning in which electric fields fall off less than a factor of two for each zone (see Figures D-2 and D-4).
- Spatial zone dependence of results is observed for electric fields falling off by a factor of three in one zone (Figures D-3 and D-5).
- Sensitivity of response to spatial zoning is greatest in regions close to the space-charge barriers (Figure D-5a versus Figure D-5d) — i.e., where many particles of charge are present.

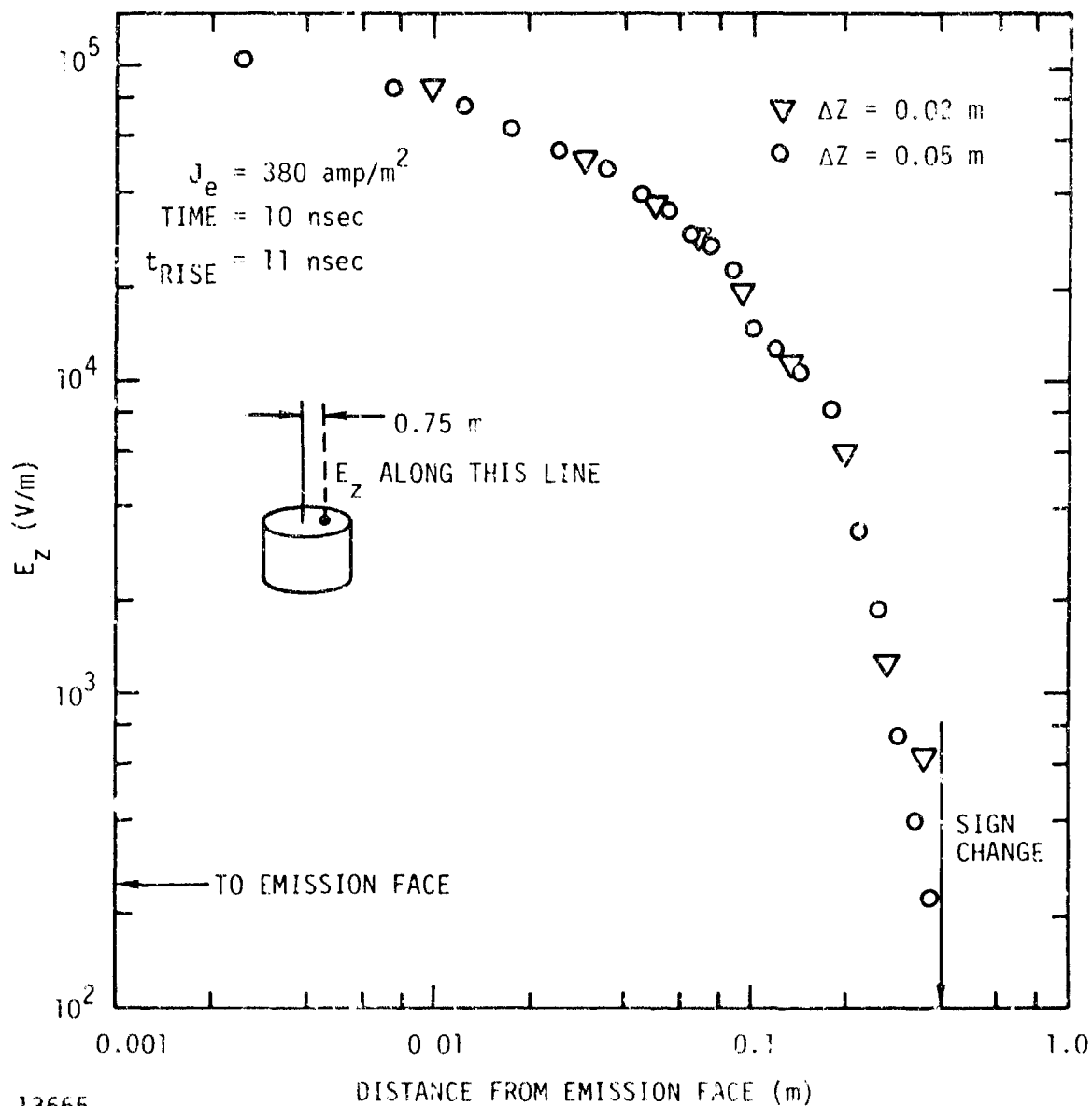
#### REFERENCES

1. E. P. Wenaas, S. Rogers, and A. J. Woods, "Sensitivity of SGEMP Response to Input Parameters," IEEE Trans. Nucl. Sci. NS-22, December 1975.
2. E. P. dePlomb and A. J. Woods, "TEDIEM-RZ and RD: Two-Dimensional Time-Dependent IEMP Computer Code," DNA 3140F, March 10, 1973.
3. J. P. Boris, "Relativistic Plasma Simulation-Optimization of a Hybrid Code," Proc. Fourth Conf. Numerical Simulation of Plasmas, NRL (1970).



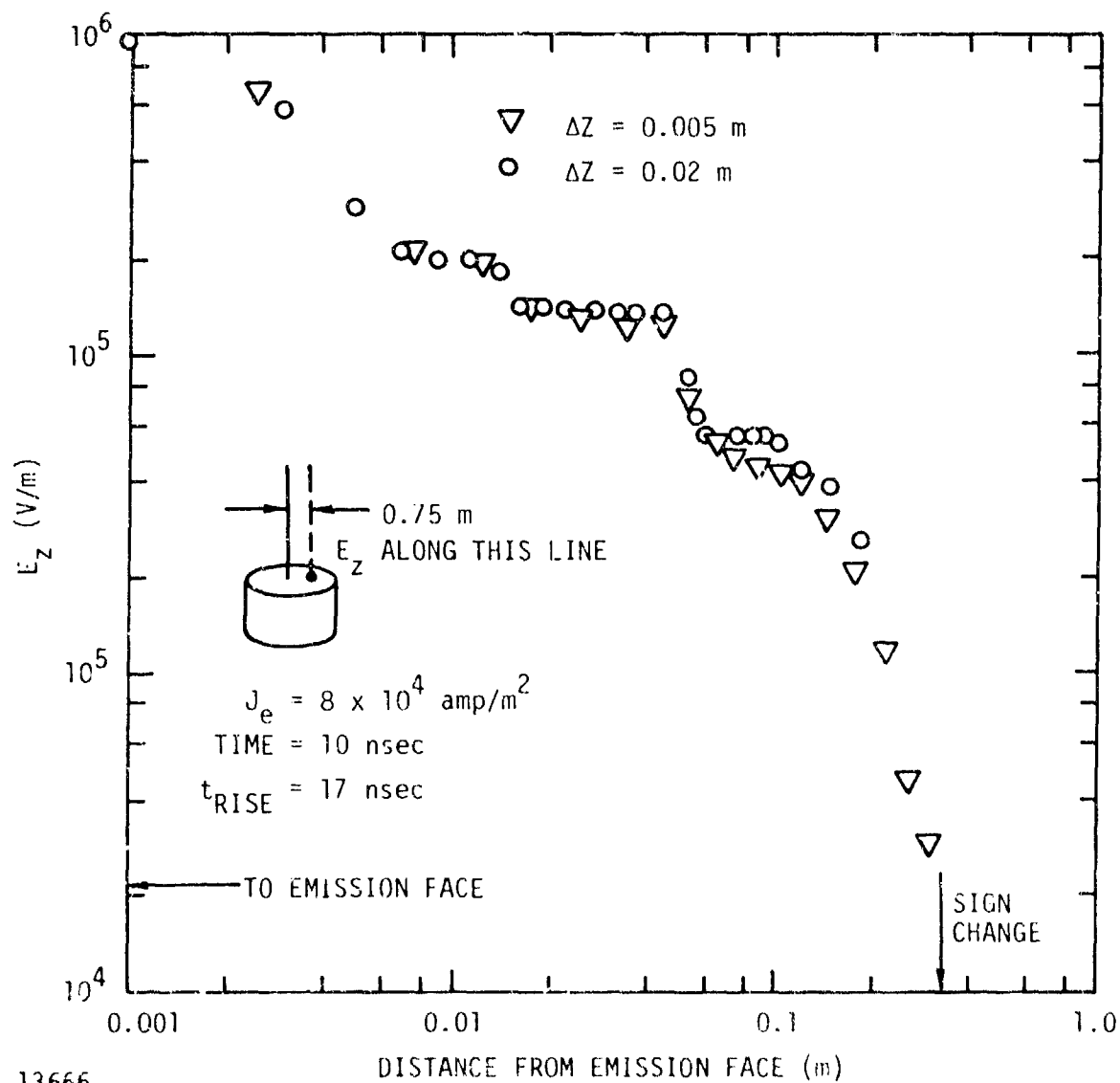
RT-13664

Figure D-1. Electron energy spectrum employed in zone-size effect study



RT-13665

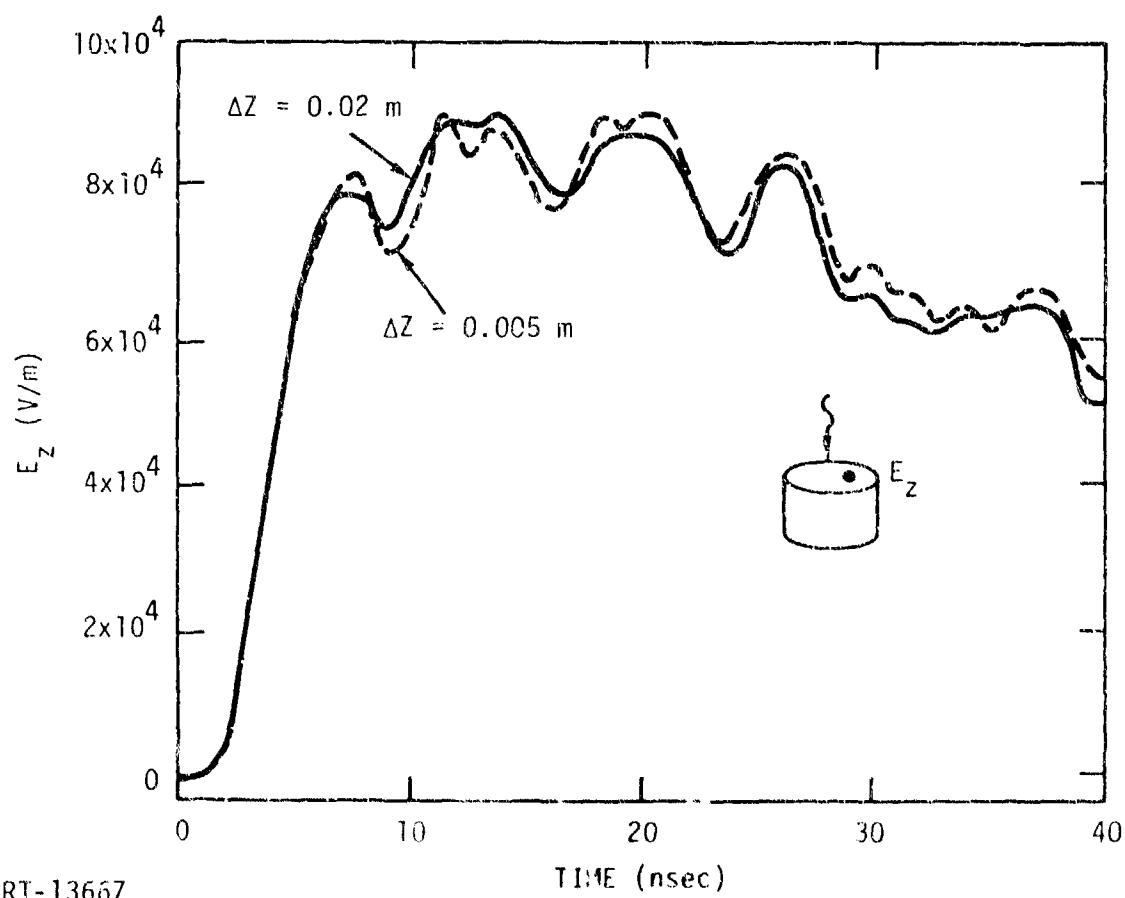
Figure D-2 Distributions of normal electric field near peak of emission current pulse for different spatial zonings. All field points near the emission face are plotted.



RT-13666

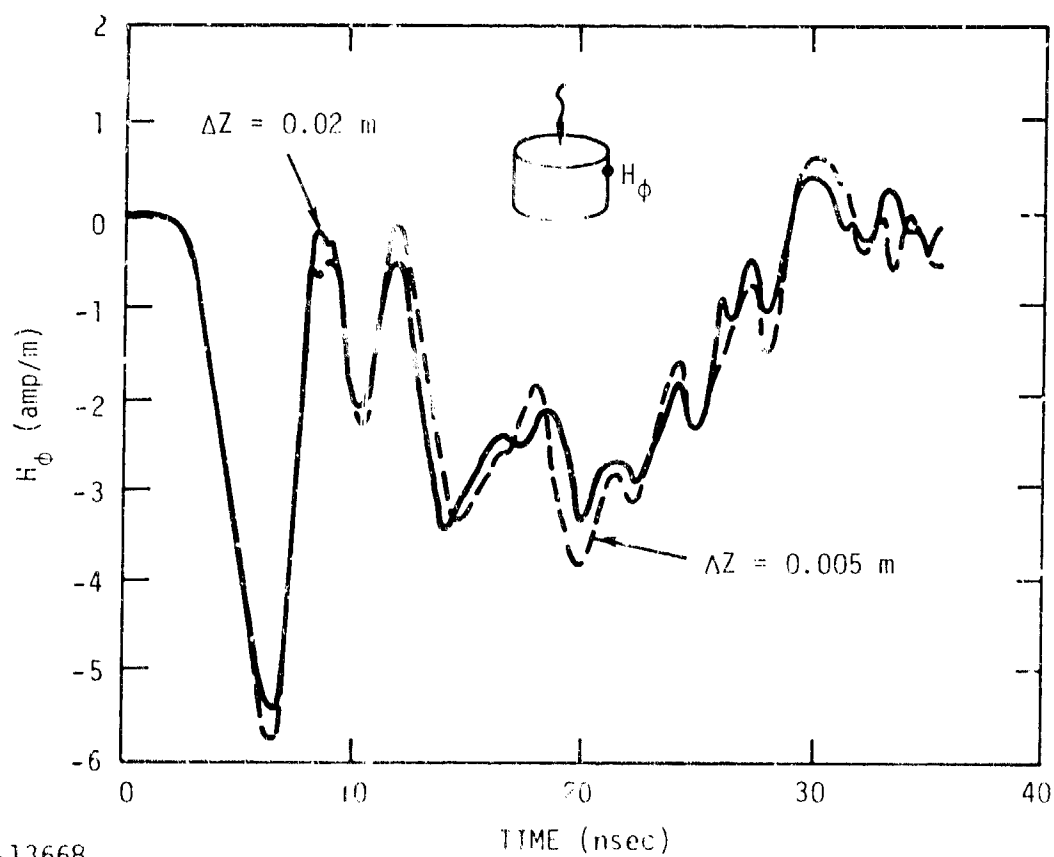
Figure D-3. Distributions of normal electric field near peak of emission current pulse for different spatial zonings. All field points are plotted.





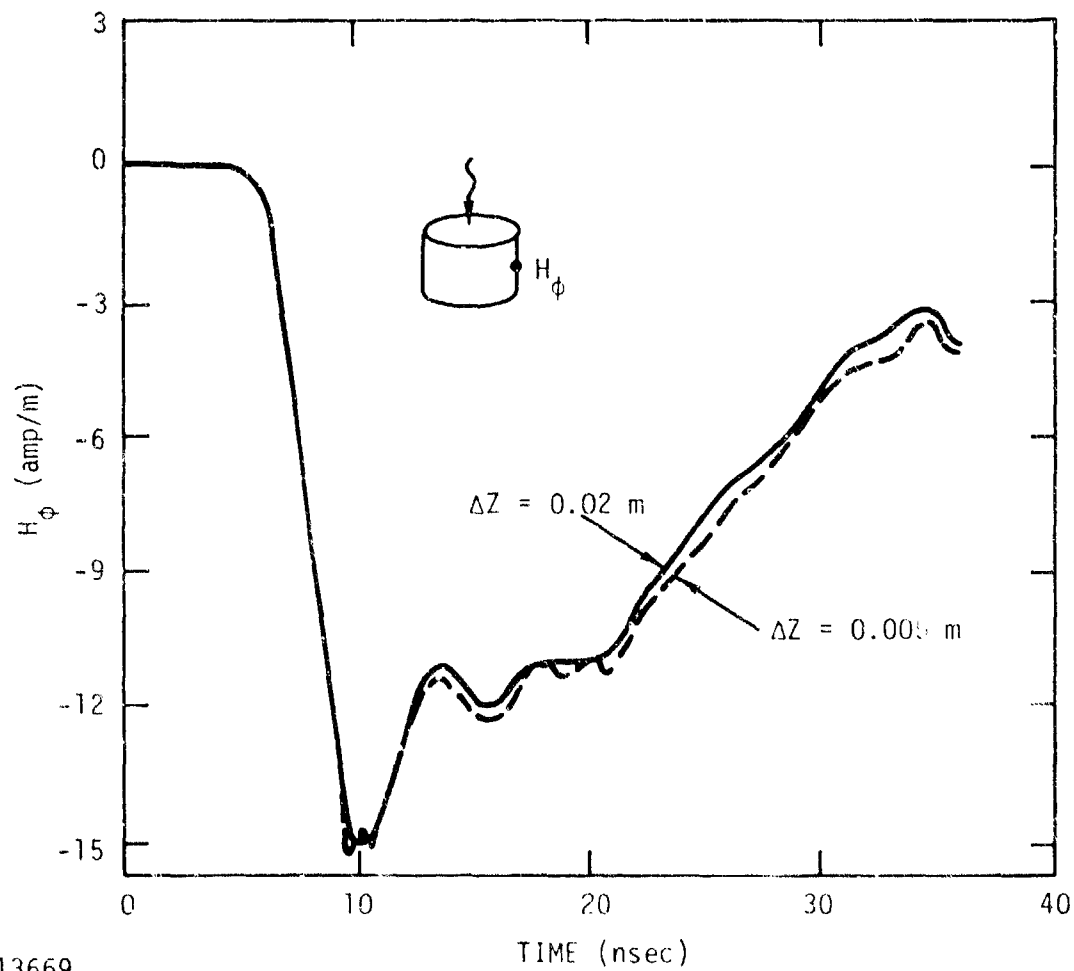
RT-13667

Figure D-4a. Electric field time histories at top of cylinder at radius 0.75 m for medium SCL, obtained with minimum spatial zonings of 0.02 and 0.005 m



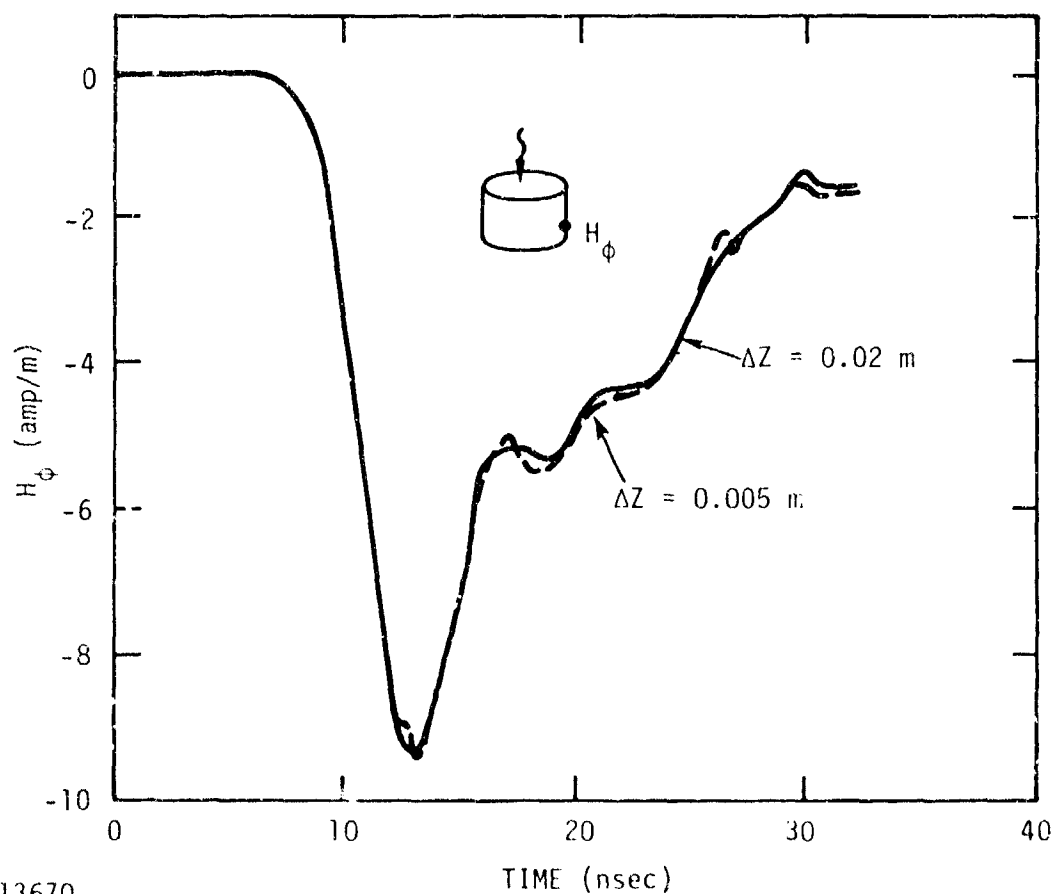
RT-13668

Figure D-4b. Magnetic field time histories at side of cylinder 0.425 m from top for medium SCL, obtained with minimum spatial zonings of 0.02 and 0.005 m



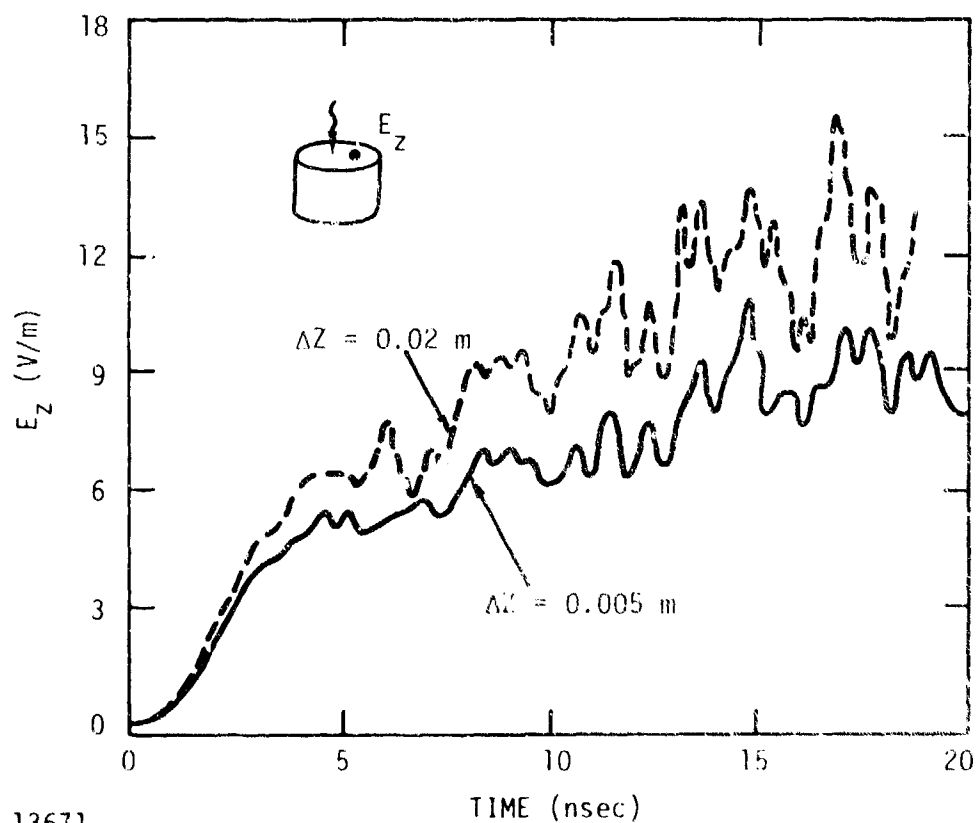
RT-13669

Figure D-4c. Magnetic field time histories at side of cylinder 1.6 m from top for medium SCL, obtained with minimum spatial zonings of 0.02 and 0.005 m



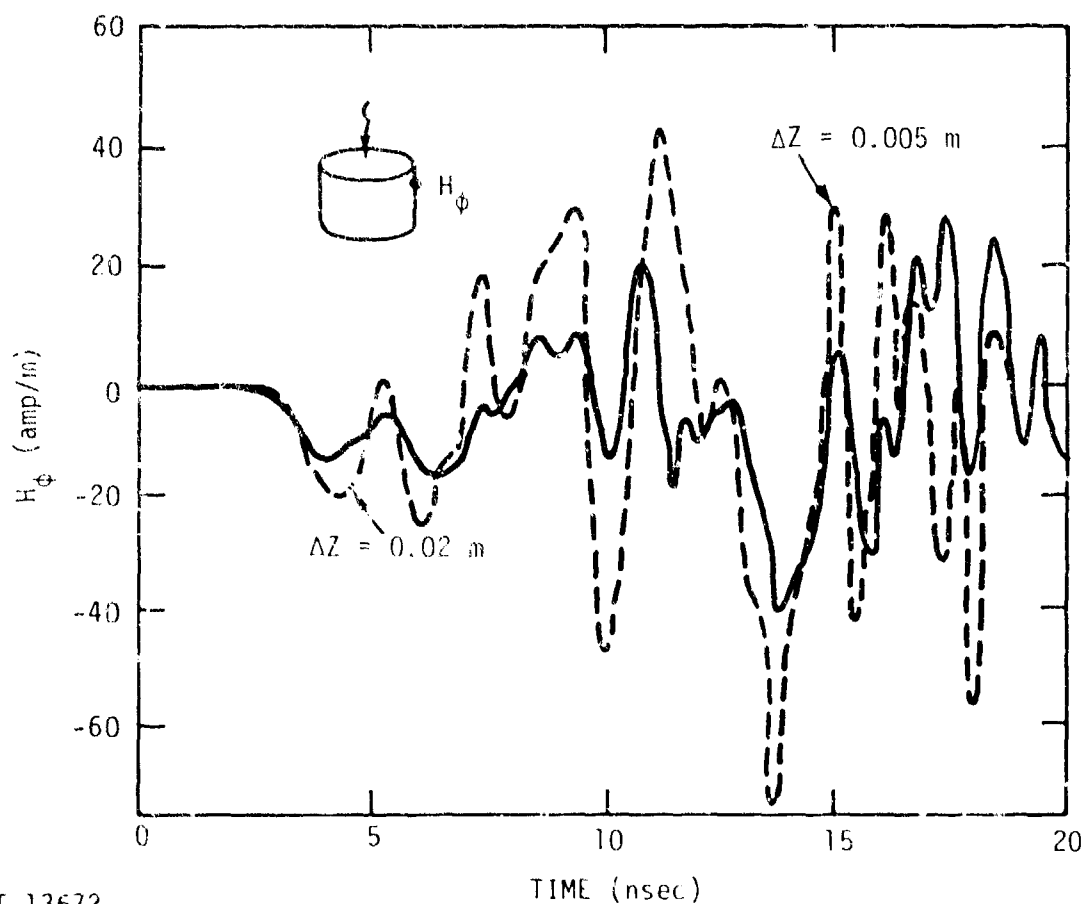
RT-13670

Figure D-4d. Magnetic field time histories at side of cylinder 2.4 m from top for medium SCL, obtained with minimum spatial zonings of 0.02 and 0.005 m



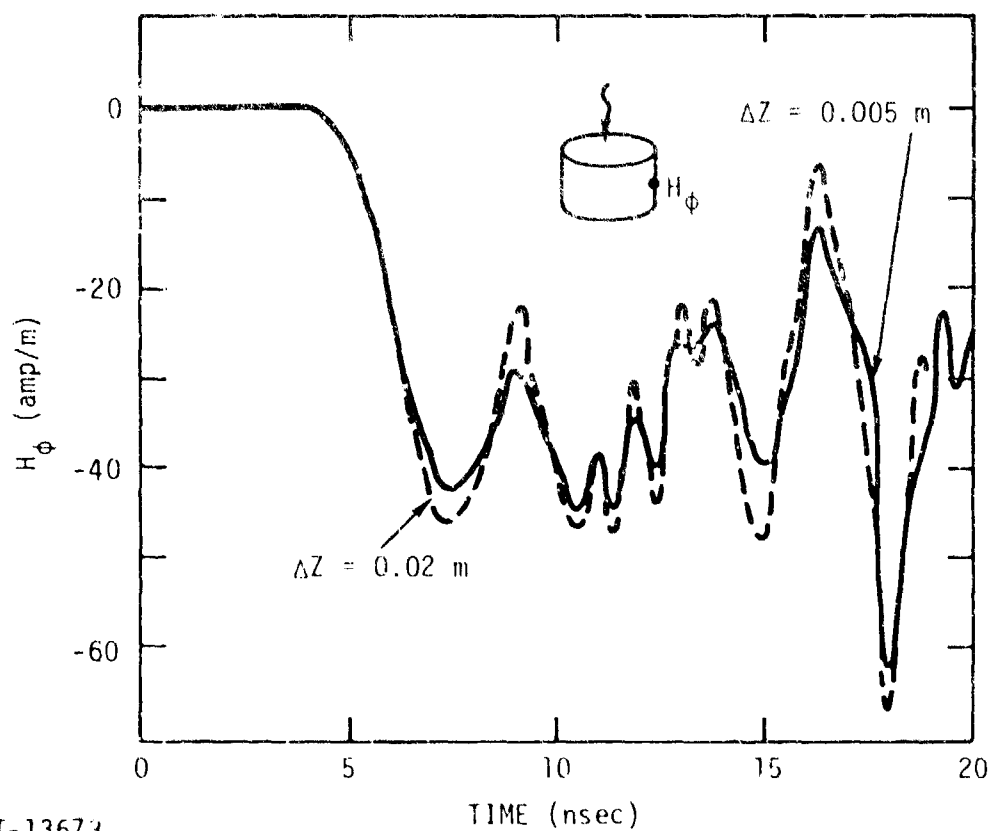
RT-13671

Figure D-5a. Electric field time histories at top of cylinder at radius 0.75 m for high SCL, obtained with minimum spatial zonings of 0.02 and 0.005 m. The fields are evaluated at the first axial grid position above the emitting surface. See Figure D-3 for electric field comparison at same positions for the two cases.



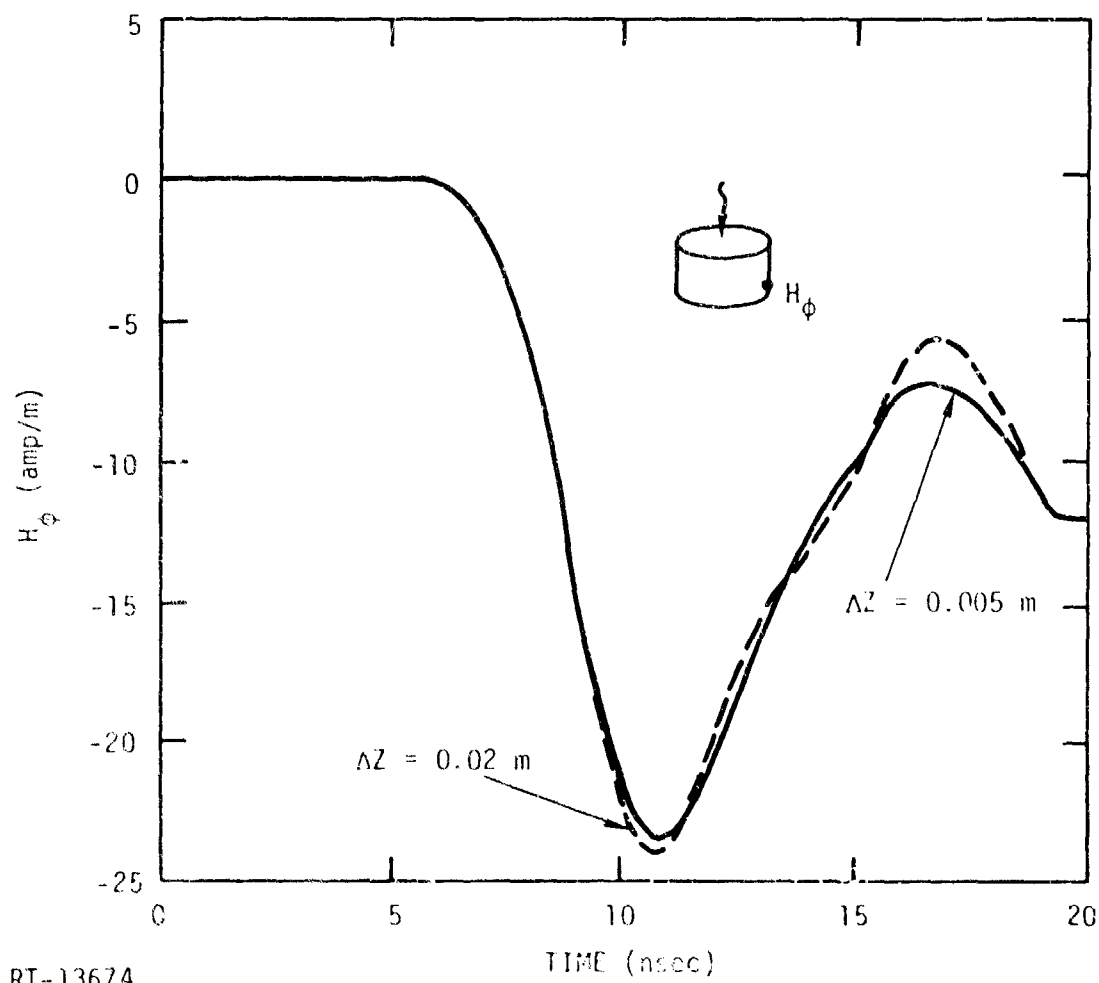
RT-13672

Figure D-5b. Magnetic field time histories at side of cylinder 0.425 m from top for high SCL, obtained with minimum spatial zonings of 0.02 and 0.005 m



RT-13673

Figure D-5c. Magnetic field time histories at side of cylinder 1.6 m from top for high SCL, obtained with minimum spatial zonings of 0.02 and 0.005 m



RT-13674

Figure D-5d. Magnetic field time histories at side of cylinder 2.4 m from top for high SCL, obtained with minimum spatial zonings of 0.02 and 0.005 m



## APPENDIX E

### USER'S MANUAL FOR ABORC AND PERIPHERAL COMPUTER CODES

## E-1. INTRODUCTION

This appendix contains a user's manual for ABORC and for peripheral codes PLOTALL and MOVIE. Information relating to specific computer requirements for the system is given, a flow chart is presented, inputs are described, and a sample calculation is illustrated. The particulars of generating overlaid plots and creating computer MOVIES are also spelled out in "cookbook" fashion, with examples provided. The PLOTALL and MOVIE codes are described in some detail because they can be used to operate on data from other electron emission and SGEMP, and because they are documented in no other place.

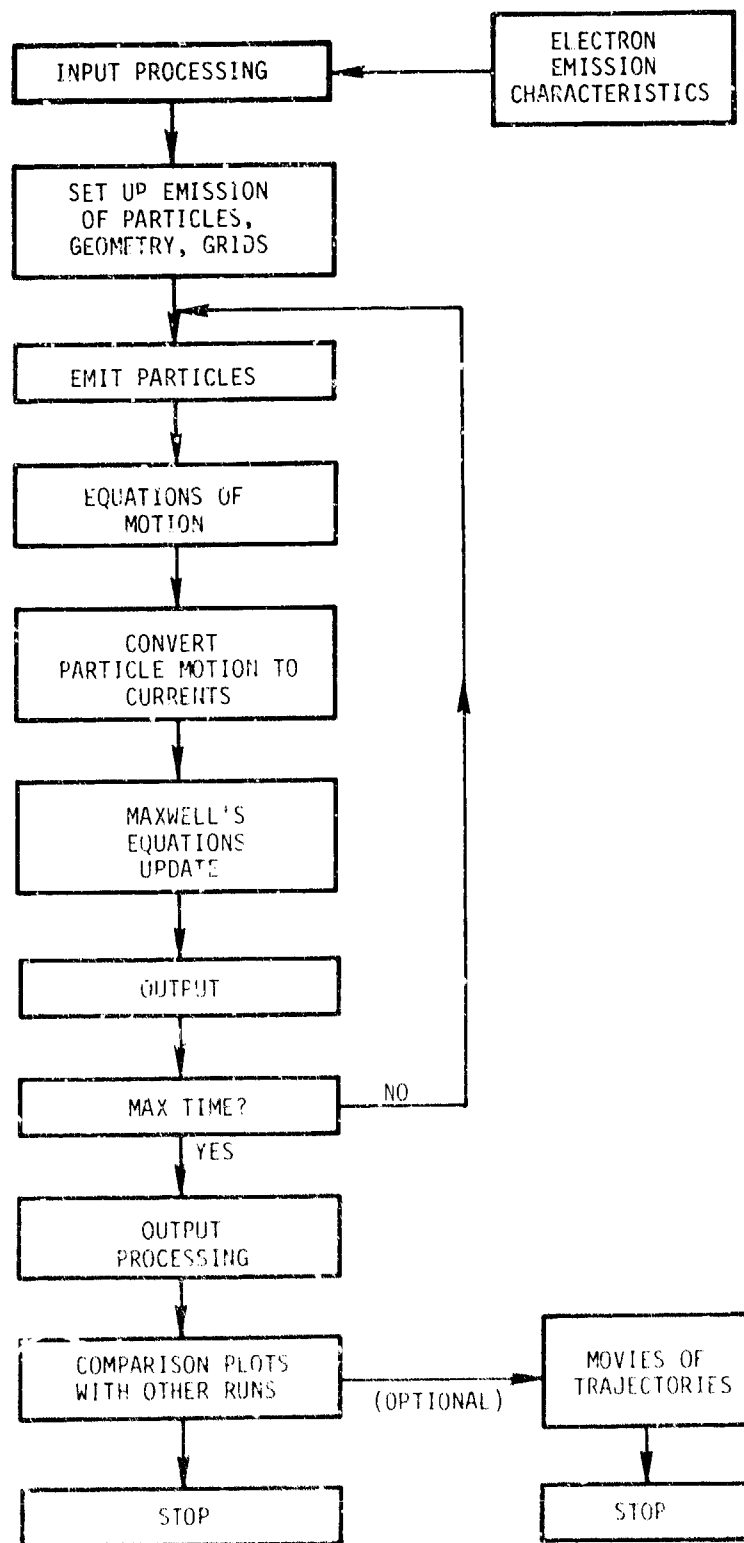
## E-2. ABORC COMPUTER REQUIREMENTS

ABORC is a FORTRAN IV computer program operational on the CDC 7600 system. The code consists of about 3500 cards, including all FORTRAN programs used. No machine language routines are employed. The code currently is dimensioned for about 160,000 (octal) words of fast memory storage and about 720,000 (octal) words of large-core storage. One fast-access file is required during execution, although two are used if the movie option is invoked by the programmer. Run time of the code varies from 1 to 30 CPU minutes on the CDC 7600 computer, depending on problem conditions.

An automatic warn time is programmed into ABORC so that sufficient time is allowed to save plot files and perform graphics functions even if the computer run time exceeds the maximum amount requested. The FTN compiler is used with extended and preset-to-zero core options.

## E-3. ABORC FLOW CHART

A brief flow chart of the code system is shown in Figure E-1. Note that the electron emission information must come from a source external to ABORC.



RT-13675

Figure E-1. ABORC flow chart

#### E-4. ABORC INPUT DESCRIPTIONS

The problem being considered is defined by geometry, emission characteristics, and conductivity characteristics. The two-dimensional geometry is defined by specifying annular conductivity zones which are described by minimum and maximum axial and radial coordinates. The total geometry considered by the problem is the sum of all defined annular zones. The electrons emitted from the body give the driving function for the problem. Emission characteristics include axial and radial bounds of each emission zone, energy spectra, angular distributions, and emission intensities.

The method of describing these physical properties to the code is outlined below in the input card description. Variable names and their meanings are given. Data formats are provided if required. Name-list variables are input in free form according to the variable type (real or integer), with commas separating them. Column 1 must remain blank, and the list begins with b\$DEFINE and ends with b\$END (where b indicates a blank space).

The word DEBUG is used at the beginning of the description of those variables whose primary function is use in debugging problems. Under normal circumstances, the default values of these inputs are adequate and the variables can be ignored. The word EDIT at the beginning of a variable description means that this variable is used in editing results of the calculations.

The names in parentheses are the variable names used internally in the code in cases where the internal variable name differs from the input variable name. If no default is given for a variable, that variable must be input. If a variable has a maximum value or number of values, the designation MAX = or MAX NO. + is given. A convenient summary of the minimum and maximum values is found in Table E-1.

Table E-1  
MINIMUM AND MAXIMUM VALUES OF ABORC VARIABLES

	Min No.	Min No.	Max No.
<u>Input Variables</u>			
Zone number (each direction)		3	100
Time steps		-	-
Emission zones		1	20
Energy distributions		1	20
Time histories		1	20
Angular distributions		1	20
Conducting annuli		0	100
2-D prints		0	30
Mini-prints		-	-
Plot quantities		1	40
<u>Calculational Variables</u>			
Total number of particles emitted in a given time step		0	1000
Number of particles being followed in a given time step		0	17,300
Number of point pairs per distribution		1	50
Total allowed values in all point pair tables for emission		-	≤2000
Total allowed point pairs in time history plots (counting all curves which are overlaid)		2	4000

Certain terms peculiar to this code are used in the input card descriptions repeatedly. Definitions of the terms are listed below.

Mini-print      A short printout of certain problem parameters plus requested plot quantities can be requested at times independent of large "2-D prints" (see below). Automatically printed at 2-D print times.

2-D print      Spatial distribution printouts of fields, currents, and charge densities (very large).

c      Speed of light ( $3 \times 10^8$  m/sec).

$\Delta x$       Used to designate both  $\Delta r$  and  $\Delta z$ , the spatial zone increments.

Card 1 (8A10)

TITLE

Card 2 (40I2)

IOPT(1)=0      The driver of the problem is the particle emitter.  
          =1      The driver is an analytic current specification up the axis (see subroutine TESTJ); used for debug purposes.  
                  Default: IOPT(1) = 0

IOPT(2)      DEBUG. Particle motion printout. Print first and last IOPT(2) particles.  
                  Default: IOPT(2) = 0

IOPT(3)=+1      Plot all input distributions.  
          =-1      Suppress input distributions.  
                  Default: IOPT(3) = 1

IOPT(4)=0      Random emission.  
          =1      Analytical emission (see subroutine TESTJ); used for debug purposes.  
                  Default: IOPT(4) = 0

IOPT(4)=0      Random emission  
          =1      Analytical emission (see subroutine TESTJ); used for debug purposes.  
                  Default: IOPT(4) = 0

IOPT(5)      DEBUG. Print first and last IOPT(5) emission particles every emission step.



IOPT(33) EDIT. Print every IOPT(33) axial zones outside region with axial zone indices IOPT(34) to IOPT(35) in 2-D prints.  
Default: IOPT(33) = 1

IOPT(34) EDIT. Print every axial zone with index between IOPT(34) and IOPT(35), inclusive, in 2-D prints.  
Default: IOPT(34) = 1

IOPT(35) See IOPT(33), IOPT(34)  
Default: Number of axial zone boundaries

IOPT(36-38) Like IOPT(33-35) only for radial zones.

IOPT(39) EDIT. Number of significant figures desired in 2-D prints for all quantities except electric fields. Also gives the range of the variable to be printed out — i.e., from peak value down to  $10^{-[\text{IOPT}(39)]}$  times peak value. Useful in limiting printout size. Use -1 for E10 format.  
Range:  $1 \leq \text{IOPT}(39) \leq 7$ .  
Default: IOPT(39) = 4

All of the following variables are in NAMELIST DEFINE:

DTN Light time step (sec). Code adjusts to meet stability criterion if necessary.  
Default:  $\text{DTN} = \Delta x_{\min} / \sqrt{2} c \times 0.95$ , but then DTN is decreased to the nearest integer divider of the particle time step.

DTPART Particle time step (sec).

TMAX Maximum simulation time (sec).

DTPRNT Time increment for mini-prints (sec).  
Default is DTPR values.

DTPR Times at which to print 2-D prints (sec).  
MAX NO = 20.  
2-D print at last time step is automatic.

DTMOVE Time increment for plotting particle positions on the printer-plotter (sec). If zero, no plots.

FLUENC Multiplier of all emission current levels from all zones.  
Dimensionless.  
Default: 1



PG            Axial zone boundaries read in in ascending order (m).  
               MIN NO = 3  
               MAX NO = 100

RG            Radial zone boundaries read in in ascending order (m).  
               MIN NO = 3  
               MAX NO = 100

The variables from here to the end of the NAMELIST DEFINE are read in only if electron backscattering is being included in the calculation.

REFQ          Fraction of charge on particles reflected off conductor walls each collision. Dimensionless.  
               Default: 0

EFRAC        Kinetic energy per unit charge contained by backscattered electrons as a fraction of incident energy. Dimensionless.  
               Default: 0.9

ZBOT          Bottom position of cylindrical region from which to backscatter electrons (m).\*

RSIDE        Outer radius of cylindrical region from which to backscatter electrons (m).\*

QABTF        Fraction defining range of charge particles which are continued in the calculation. All particles with charge less than QABTF times maximum particle charge are eliminated.  
               Default: 0

\$END NAMELIST DEFINE

---

\* Particles will backscatter only upon striking conduction regions in such a way that no grid point is having a contribution to its current density due to that particle and if the particle is entering the region defined by ZBOT, ZTOP, and RSIDE.

Card Type 1	Col.
After DEFINE	1-80 Comment Card
Card Type 2	
After DEFINE	<p>Specification of conduction regions. E10 format.</p> <p>MAX NO = 100</p> <p>MIN NO = 0 (i.e., no conduction regions are necessary)</p> <p>1-10 SIG1M Lower axial position of conducting annulus (m)</p> <p>11-20 SIG1P Upper axial position of conducting annulus (m)</p> <p>21-30 SIG2M Inner radial position of conducting annulus</p> <p>31-40 SIG2P Outer radial position of conducting annulus.</p> <p>41-50 SIG Conductivity value assigned (mho/m)</p> <p>          DEFAULT: <math>1.0E+9 * \epsilon_0 / \Delta t</math>.</p> <p>51-60 FD Read in non-zero value if another annulus is to follow; otherwise, blank.</p> <p>61-80 Comment field</p>

Card Type 3	
After DEFINE	1-80 Comment card

NOTE: The rest of the code inputs are free-form. Columns 1-80 may be used and blanks are unnecessary. Quantities may be listed in any order within the division labeled EMISSION CHARACTERISTICS.

Card Type 4	
After DEFINE	<p><math>H(Z_1, R_1), ER(Z_2, R_2), EZ(Z_2, R_2), \dots</math></p> <p>This card sets quantities which are to be written onto the plot file for use by the plot routines. The quantities that may be written to the file are:</p>

Plot Type

1	H	Magnetic field (amp/m)
2	EZ	Axial electric field (volt/m)
3	ER	Radial electric field (volt/m)
4	JZ	Axial current density ( $\text{amp}/\text{m}^2$ )
5	JR	Radial current density ( $\text{amp}/\text{m}^2$ )
6	KZ	Axial surface current density (amp/m)
7	KR	Radial surface current density (amp/m)
8	IEMIT	Total emission current (amp)
9	WEMIT	Total cumulative emission energy (joule)

### Plot Type

10	WKINETIC	Total kinetic energy of electrons (joule)
11	WFIELDS	Total energy in fields (joules)
12	WLEAVE	Total cumulative kinetic energy leaving system (joule)
13	VMAX	Maximum potential anywhere along axis (volt)
14	VMIN	Minimum potential anywhere along axis (volt)
15	ILEAVE	Total current leaving system (amp)

- Plots 1-7 are input as H(z,r), etc.
- Plots 8-15 are input as IEMIT, etc., with no position specification.
- To finish the list, put END after the last plot.
- Commas are not necessary at the end of a card.
- At least one plot quantity must be specified.
- As many cards can be used as needed up to the specification of 40 plot quantities.

The rest of the inputs specify the electron emission parameters of the problem.

### Card Type 5

After DEFINE EMISSION CHARACTERISTICS

This card simply informs the code that emission information follows. Cards within this group are not numbered because the individual distributions can be input in any order within the group.

### E-4.1 Emission Intensity n = Point Pair Table

The emission intensity format is used to specify the time history for the emission pulses; n is the intensity number, of which up to 20 are allowable, and POINT PAIR TABLE is the time history in  $\text{amp/m}^2$  versus time in sec. EI may be used to abbreviate emission intensity.

For example, a 20-nsec FWHM triangular pulse with a peak of  $0.1 \text{ amp/m}^2$  would be input:

EMISSION INTENSITY 5 .0, 0, 20E-9, .1, 40E-9, 0

The table may contain up to 50 point pairs, allowing high resolution to fairly complex emission time histories, and may be continued on as many cards as desired.

An abbreviated form is available for specifying emission pulse shapes of the form  $f(t) = \sin^2[(\pi/2)(t/\tau)]$ , where  $\tau$  is the rise time and FWHM of the pulse. Simply specify  $EIn = \text{SIN2}(T)$  where  $n$  is the distribution number set by the user and  $T$  is the rise time in seconds. Note: Abbreviations listed in Table E-2 may be used here.

Table E-2  
FLOATING POINT MULTIPLIERS FOR  
ABBREVIATED ABORC INPUTS

Letter Factor	Power of 10
P	-12
N	-9
U	-6
K	+3
M	+6

The letter factor can be used to replace the power of 10 desired on input cards.

#### E-4.2 Energy Distribution $n$ (bins = $i$ ) = Point Pair Table

Similarly, the energy distribution card allows for arbitrary specification of the emission energy spectrum. Again,  $n$  is the distribution number, and up to 20 are allowed. (BINS =  $i$ ) is optional. ED may be used to abbreviate energy distribution.  $i$  specifies that there shall be  $i$  particles emitted per particle time step per emission zone for the distribution. If the (BINS =  $i$ ) input is omitted, the default value of  $i$  is 4. The POINT PAIR TABLE is as before, with relative frequency [number/unit energy versus energy (eV)] as the parameters. For example, the spectrum of Figure E-1 might be input:

ENERGY DISTRIBUTION / = 40, 0.50, .4, 0.38, 71, 1,  
90, .28, 1.0, .4, 116, .15, 20, 0

Note the use of the "K" which is interpreted as  $10^3$ . Various other letters may be used with floating point numbers in the emission section; they are enumerated in Table E-2. The example spectrum is given normalized to a

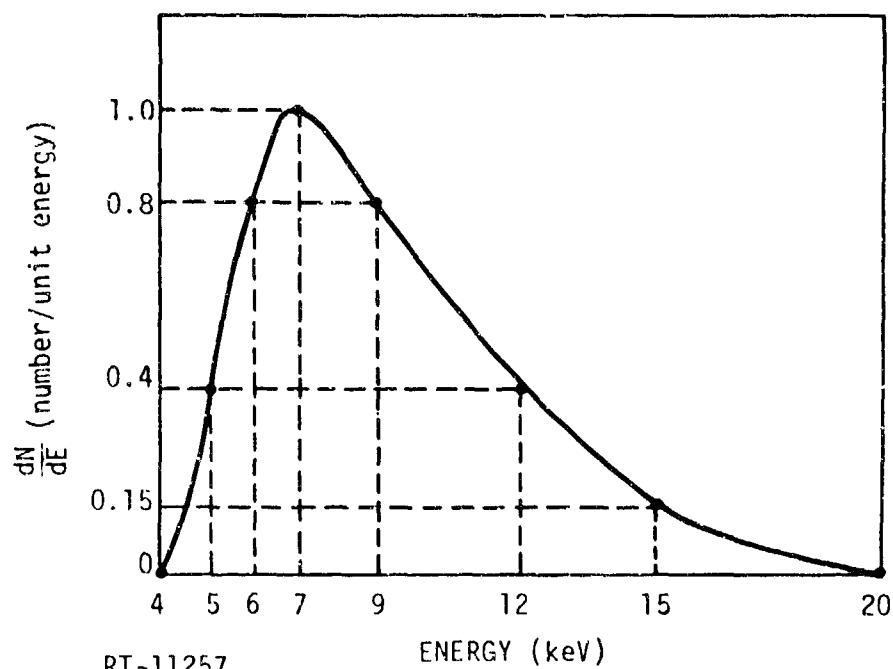


Figure E-1. Sample energy spectrum input to ABORC

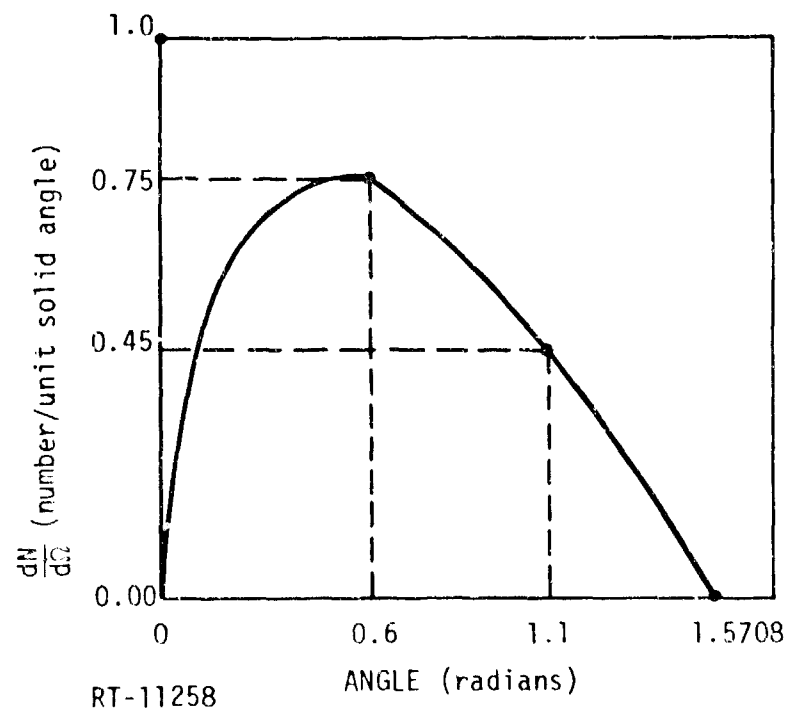


Figure E-2. Sample angle distribution input to ABORC

peak of 1; however, the emitter normalizes all distribution functions, so the emission current density has the value specified by the emission intensity versus time curve multiplied by the FLUENCE and TIMES factors. The FLUENCE parameter has already been discussed; the TIMES factor is discussed below. Desired relative height for all distributions is all the user need consider.

#### ANGLE DISTRIBUTION n = POINT PAIR TABLE

The angle distribution card is shown above. AD may be used to abbreviate angle distribution. The parameters for the point pair table in this instance are the number of particles per unit solid angle versus angle in radians. For example, the distribution of Figure E-2 is given by:

ANGLE DISTRIBUTION 3 = 0,0.6,0.75,1.1,0.45,1.5708,0

Polar angles are employed in the coding for emission specification. The angle on the given sample is the angle from the emitting surface normal. The azimuthal angle distribution is typically specified uniform from 0 to  $2\pi$  for two-dimensional calculations. Again, up to 50 point pairs may be used.

The emission energy spectra, angular distributions, and pulse shapes are specified by the above cards input in any order. The last section of inputs draws all this information together.

#### E.4.3 Emission Zones

The emission zones card simply specifies that emission zone information follow. The emission zones are indicated via:

$(z_1, r_1)$  TO  $(z_2, r_2)$  INT i DELAY x TIMES y, ED j, AD k, ADQ3 l.

$z_1, r_1, z_2, r_2$  give the coordinates of the zone. i is the emission intensity time history number reference to be used for the zone, delayed by x seconds and multiplied by y. The DELAY and TIMES factors are optional, j is the energy distribution number to be used for the zone, k is the angle distribution to be used for determining the direction of each particle relative to the surface normal, and l is the distribution reference for the emission electron direction azimuthal angle about the surface normal. Up to 20 emission zones can be specified.

For example, suppose we desire an emission zone position on the top of a cylinder, from the axis of 0.2-m radius and at vertical position (for a particular problem) 0.5 m. We shall reference the previous distributions and input

```
(.5,0) TO (.5,.2) INT 5 TIMES 10, ED7, AD3, ADQ3 2
```

where we have multiplied the current density by 10. We may also want to emit from the side of the cylinder (e.g., radius = 0.2 m) but with reduced intensity and delayed by a couple of nanoseconds:

```
TO (.3,.2) INT 5 DELAY 2E-9 TIMES .1, ED7, AD3, ADQ3 2
```

where  $z_1$  and  $r_1$  for this emission zone are obtained from the previous zone's  $z_2, r_2$ .

Card 16  
END OF INPUT

terminates the input processing.

#### E-4.4 Final Remarks

All cards may be continued on the next card except for zone specifications. Also, blanks make no difference because they are deleted immediately by the coding upon reading the cards. More than one energy, angular, or time distribution can be emitted from a given spatial zone by simply respecifying the same zone coordinates on an additional emission zone card.

The following information is helpful in using the code.

- Angle distributions: polar  $0 - \pi/2$   
azimuthal  $0 - 2\pi$
- Plot file: tape 7
- Movie file: tape 20
- Kinetic energy print is every particle in system including first time step particles
- Zone indices increase in direction of increasing  $z$  or  $r$

## E-5 SAMPLE PROBLEM

A sample ABORC calculation is illustrated in this section. Code inputs and selected outputs are listed to summarize previously defined variables in a test problem. This case was selected as a user's illustration for code input and output interpretation and to provide a benchmark test problem for comparison when conversion to a new computer system is necessitated.

The sample problem has the following characteristics.

Geometry	A cylinder 3 m high x 3 m in diameter
Outer boundary	Cylinder is in an outer cylinder 30 m high by 33 m in diameter
Emission	146/m <sup>2</sup> emitted with a cos $\theta$ polar angular distribution and isotropic azimuthal angular distribution from the top and half the side. The electron energy spectrum is from the QUICKE2 code.
Pulse shape	sin <sup>2</sup>
Pulse length	17-nsec rise time and FWHM
Grid characteristics	
Number of axial zones	64
Number of radial zones	58
Number of emission zones	5
Number of energy bins	3
Particle time step	0.2 nsec
Maximum time of calculation	50 nsec
Minimum zone size	0.02 m
Clear time	100 nsec
Plots	At various points on the top, side, and bottom of the inner cylinder, both the normal electric field and the surface current densities are monitored. Also, other helpful quantities are specified.

### E-5.1 Input Discussion

The input cards to model the problem mentioned above are shown in Figure E-3. The plot code inputs are also shown after the end-of-record



```

BBMAT,81 ,F1M4,TP17N,TC:00N,SID,      T+,59,DT,2,BI3, DZ,02,5 EM,J1,5E2
      =1
      2
      DTPART=,2 E=9,DTPRNT=1,E=9,
      SDEFINE      TMAX= 50,E=7,
      DTPR=20,E=9,40,E=9, 60,E=9,
      FLUENC=1,46E2,
      IOPT(33)=5,20,43,5,0,30,
      P3=      =15,,=14,,=13,,=12,,=11,,=10,,=9,,=8,5,,=7,5,  =7,,
      =6,5,,=5,4,,=5,,=4,6,,=4,2,,=3,8,,=3,4,,=3,,=2,6,,=2,2,,=1,6,,=1,4,,=1,,=,6,
      =,25,,=,045,0,,=,02,,04,,06,,08,,11,,16,,24,
      =,32,,4,,51,,63,,76,,85,,1,1,1,3,1,55,1,0,
      =,2,05,2,3,2,65,3,,3,5,4,,4,5,5,,5,5,6,,7,,8,,9,,10,,11,,12,,13,,14,,15,,
      RG= 0,,2,,35,,45,,55,,65,,75,,85,,95,1,05, 1,15,
      1,25,1,33,1,4,1,45,1,48,1,5,1,52,1,54,1,56,
      1,59,1,615,1,648,1,69,1,745,1,82,1,89,2,,2,15,2,3,
      2,5,2,7,2,9,3,1,3,3,3,5,3,7,3,9,4,1,4,3,
      4,5,4,8,5,2,5,6,6,,6,4,6,6,7,2,7,6,8,5,9,5,10,5,11,5,12,5,13,5,14,5,15,5,
      16,5,
      SEND
CONDUCTORS
=3,      1,5
PLOTS (DZ,005)
KR(0,,75),EZ(,005,,75),KZ(=,5,1,50 ), ER(=,5,1,505)
KZ(=1,5,1,50), ER(=1,5,1,505)
KZ(=2,5,1,50), ER(=2,5,1,505),KR(=1,2 ,75), EZ(=3,2 ,75)
VMAX,VMIN,IFMIT,ILEAVE
EZ(,03,,75),EZ(,05,,75),EZ(,07,,75),EZ(,11,,75), EZ(,17,,75), EZ(,25,,75),
EZ(,5,,75),WKINETIC,WFIELD,END
EMISSION CHARACTERISTICS
AD1=0,,0,,.0875,,1736,,1745,,3420,,2618,,50,,3491,,6428,,4363,,766,
0,5236,,866,,6109,,9397,,6981,,9848,,7854,1,,.8727,,9848,,9599,,9397,
1,047,,866, 1,134,,766, 1,222,,6428, 1,309,,5, 1,396,,342
AD2=0,1,6,28,1,
E11=3,N2( 17N)
ED1 (BINS=3 )=      1,00E+03, 1,32E+16, 1,20E+03, 1,33E+16, 1,60E+03, 1,40E+16,
2,00E+03, 2,64E+15, 2,40E+03, 1,93E+15, 2,80E+03, 1,25E+15, 3,20E+03, 8,08E+14,
3,60E+03, 5,70E+14, 4,00E+03, 3,46E+14, 4,50E+03, 2,10E+14, 5,00E+03, 1,27E+14,
5,50E+03, 7,66E+13, 6,00E+03, 4,63E+13, 6,50E+03, 2,91E+13, 7,60E+03, 1,75E+13,
7,50E+03, 9,98E+12, 8,00E+03, 5,70E+12, 9,00E+03, 1,98E+12, 1,00E+04, 6,08E+11,
1,10E+04, 1,09E+11, 1,20E+04, 1,32E+10
EMISSION ZONES
(0,,0,) TO (0,,1,5)INT1      ,ED1,AD1,ADQ3 2
TO( =,38,1,5) INT1 DELAY .63N TIMES1. ,ED1, AD1, ADQ3 2
TO( =,75,1,5) INT1 DELAY 1,9N TIMES1. ,ED1, AD1, ADQ3 2
TO(=1,13,1,5) INT1 DELAY 3,1N TIMES1. ,ED1, AD1, ADQ3 2
TO( =1,5, 1,5) INT1 DELAY 4,4N TIMES1. , ED1, AD1, ADQ3 2
END OF INPUT
FOR
BBMAT
1

```

1. -09

BEST AVAILABLE COPY

Figure E-5. ABORC input for modeling sample problem

(EOK) card. This plot input causes the current ABORC file to be plotted without comparing it against any other file from a previous calculation.

#### E-5.2 Output Description

Some outputs given by ABORC are listed in this section. Figure E-4 shows quantities printed by the code which are very helpful as input checks. Such items as total number of zones, time steps, plot file sizes, and approximate calculation time give a quick indicator if something is grossly wrong. Minimum zones, time steps, and approximate clear times are also printed.

The mini-print is shown in Figure E-5 for a time of 20 nsec into the simulation. Definitions of the variable names titling the numbers are listed in Table E-3 in the order they appear on the printout, reading from left to right. Some of these variables are most useful in evaluating calculational numerical quality.

The numbers following the labeled variables are the values of the requested plot quantities at this time step. Numerical hash often makes the magnetic field and current density values too noisy to be useful in this un-averaged form, but other quantities are usually well behaved. Basically, these numbers provide a back-up in case the plot file gets lost for some reason.

Spatial distributions of fields and currents at 20 nsec are shown in Figure E-6. Only those portions closest to the axis are listed due to the voluminous output. The axial (z) and radial (r) values are listed to the left and above the tables of values. In the integer-printout tables (H, JZ, JR, and CHARGE IN ZONE), only the index of the radial zone is given due to lack of room. The code inputs must be referred to in these cases for the radial position in real space. Whether to use a zone boundary or center for a given quantity can be determined from Table E-4. The designations "Q1 DIRECTION," "Q2 DIRECTION," "Q3 DIRECTION" refer to axial, radial, and azimuthal directions, respectively.

# SOME INPUT CHECKS

NO. OF PARTICLE TIME STEPS 250  
 NO. OF FIELD TIME STEPS 1250  
 NO. OF ZONES 3648  
 NO. OF TIME STEPS TO BE PUT ON PLOT FILE 625  
 NO. OF WORDS TO BE WRITTEN TO PLOT FILE 1.4375E+04  
 NO. OF FIELD CALCULATIONAL STEPS(ZONE STEPS) 4.5600E+06  
 TIME TO CALCULATE FIELDS(7600 MIN) 6.8400E-01  
 APPROX COST(DOLLARS) 1.8240E+01  
 APPROX COST PER 1000 AVERAGE PARTICLES THIS RUN(DOLLARS) 3.2500E+01  
 CLEAR TIMES ARE LESS THAN 2.0014E-07 1.100E-07 IN THE AXIAL AND RADIAL

Z1	Z2	R2
-1.5000E+01	1.5000E+01	1.6500E+01

THE SMALLEST ZONE IN THE RADIAL DIRECTION IS 2.000000E-02  
 THE SMALLEST ZONE IN THE AXIAL DIRECTION IS 2.000000E-02

PARTICLE TIME STEP= 2.00000E-10 SECONDS

LIGHT TIME STEP= 4.00000E-11 SECONDS

UPDATE PARTICLE POSITIONS EVERY 5 LIGHT TIME STEPS

MAX ALLOWABLE TIME STEP FOR STABILITY IS 4.08144E-11 SECONDS

Figure E-4. ABORC printout of quantities which test the inputs for reasonableness

BEST AVAILABLE COPY

BEST AVAILABLE COPY

```

ASTEP,TIME 501 2.004E-08 NEMIT,NPART 1E 9H4 IEMIT,GCEMIT,I,PSYD,LEAV,CHEK)-2.949E+03-3.100E-05-1.566E-05-4.970E-07 1.603E-02
ENERGIES - EMIT 5.377E-02, KINETIC 1.639E-02, ABSORBED 2.495E-02, FFIELDS 1.021E-02, HFIELDS 2.558E-04, TOTAL FIELDS 1.046E-02
VMAX,POS 5.171E+03 1.200E+00 ECONSERVE 3.6539E-02
ECONSERVE IN 7.3167E-02 15 531 1515 101 GLEAVT-1.524E-05 NABORT,NABRTT 0 0
NLEAV,NLEAVT,NEMITT,NSTEPP 0 0 GABT 0. 0MAX,T,OMIN,T-2.195E-10-2.195E-10-6.873E-08-6.873E-08 V 5.162E+07
VREF,T 0 0 GREF,T 0.
1.0639E+00 3.5787E+04 -5.865E-01 5.7286E+04 -5.198E+00 4.7555E+04 -3.9210E+00 2.3281E+03 -5.3639E-01 -4.6823E+02
5.1632E+03 -2.9190E+02 -2.9810E+03 -2.5753E+03 2.9571E+04 2.7404E+04 2.5361E+04 1.7851E+04 6.2453E+03 1.3148E+03
00661+03 1.6089E-02 1.0421E-02

```

Figure E-5. Example of ABORC mini-print

Table E-3  
MINI-PRINT VARIABLE GLOSSARY

---

NSTEP	Light time step number
TIME	Simulation time (sec)
NEMIT	Number of particles emitted during present time step
NPART	Number of particles being followed at this time
IEMIT	Total emission current at this time (amp)
QEMIT	Cumulative charge emitted up to this time (coulomb)
QINSYD	Total particle charge representing emitted electrons at this time (coulomb)
QLEAV	Total emission electron charge striking and sticking to material surfaces during this time step (coulomb)
QCHEK	Charge conservation check; not entirely correct at present, but small values indicates good conservation of emission charge
ENERGY EMIT	Total cumulative kinetic energy emitted up to this time (joule)
ENERGY KINETIC	Total kinetic energy of all emission electrons at this time (joule)
ENERGY ABSORBED	Total cumulative emission electron energy absorbed by materials up to this time (joule)
ENERGY EFIELDS	Total energy stored in electric field at this time (joule)
ENERGY HFIELDS	Total energy stored in magnetic field at this time (joule)
ENERGY TOTAL FIELDS	Total energy stored in E and H fields at this time (joule)
VMAX	Maximum electric potential anywhere along the axis relative to the bottom of the outer can at this time (volt)
POS	Position of maximum potential along the axis relative to the bottom of the outer can at this time (m)
ECONSERVE	Energy conservation parameter: fraction of energy emitted minus energy in fields minus kinetic energy minus energy absorbed to total energy emitted (dimensionless); small value ( $\sim 0$ ) indicates conservation
ECONSERVE IN	Energy in emission electrons and fields compared to energy emitted minus energy absorbed (dimensionless); small value ( $\sim 0$ ) indicates conservation

---

Table E-3 (cont.)

---

NLEAV	Number of particles being absorbed by material during this time step
LEAVT	Cumulative number of particles absorbed up to this time
NEMITT	Total number of particles emitted up to this time
NSTEPP	Particle time step number
QLEAVT	Cumulative emission electron charge absorbed by conduction surfaces up to this time (coulomb)
NABORT	Number of particles prematurely aborted during this time step; see IOPT(10)
NABORTT	Number of particle re-emissions of electrons occurring during this time step if electron backscattering is being treated
NREFT	Cumulative number of re-emissions of electrons occurring during this time step if electron backscattering is being treated
QREFT	Cumulative amount of charge re-emitted up to this time due to electron backscattering (coulomb)
IQABTT	Cumulative number of particles aborted up to this time due to charge becoming less than QABTF*QMAX, where QMAX is defined below and QABTF is defined in the input description section
QABTT	Cumulative amount of charge aborted up to this time (coulomb); see IQABTT above
QMAX	Charge on the smallest-magnitude particle being followed during this time step (coulomb)
QMAXT	Same as QMAX
QMIN	Charge on the largest-magnitude particle being followed during this time step (coulomb)
QMINT	Same as QMIN
V	Maximum velocity of all particles being followed during this time step (m/sec)

---

```

BEMAT-B1 *FIM4*TP17NATC100N*SI0,
TIME FOR E FIELDS= 2.0000E-08 FOR H FIELDS= 1.9900E-08 TIME STEPS ARE 4.000E-11 STEP NO. 500 NPARTM 1026
CP SEC-TMAXVALB 2.200E-02 CP SEC-TTESTJTB 7.310E-01 NPARTTB 67063 TESTJTB(TCSTJTB*TMXULT) 5.875E-01
TOT CP-TMXULTB 1.185E-01 TOT CP-TTESTJTB 1.68E-01 NPARTTB 67063
TIME= 2.00000E-06

```

	THE E			FIELDS IN THE G1			DIRECTION ARE			(VOLT/M OR AMP/M)		
4	2.00000E-01	3.50000E-01	4.50000E-01	5.50000E-01	6.50000E-01	7.50000E-01	8.50000E-01	9.50000E-01	1.05000E-01	1.15000E-01	1.25000E-01	
1.0500E+01	2.021E-10	-2.225E-09	-1.623E-09	-1.531E-09	-5.307E-09	-6.340E-09	-6.839E-09	-7.334E-09	-7.636E-09	-7.725E-09	-7.725E-09	
5.7500E+00	-2.372E-01	-2.175E-01	-2.047E-01	-1.944E-01	-1.831E-01	-1.715E-01	-1.587E-01	-1.454E-01	-1.318E-01	-1.180E-01	-1.180E-01	
3.2500E+00	-7.364E+01	-6.555E+01	-5.047E+01	-3.667E+01	-2.234E+01	-6.777E+01	-5.308E+01	-3.838E+01	-2.381E+01	-9.947E+01	-4.947E+01	
1.6750E+00	-1.231E+03	-8.237E+02	-6.147E+02	-5.014E+02	-4.061E+02	-3.266E+02	-2.539E+02	-1.900E+02	-1.355E+02	-8.600E+02	-2.392E+02	
1.2000E+00	-3.594E+01	-6.847E+02	-1.037E+03	-1.6024E+03	-1.114E+03	-9.721E+02	-8.187E+02	-6.610E+02	-5.143E+02	-3.600E+02	-2.092E+02	
7.9500E-01	4.931E+01	-8.702E+02	-1.244E+03	-1.600E+03	-1.271E+03	-1.273E+03	-1.225E+03	-1.215E+03	-8.711E+02	-5.433E+02	-2.543E+02	
4.8200E-01	1.552E+03	-8.351E+02	-6.511E+02	-1.734E+02	-1.370E+02	-1.700E+02	-1.502E+02	-1.219E+02	-9.588E+02	-1.190E+03	-1.190E+03	
8.9500E-01	1.821E+03	-1.201E+03	-1.201E+03	-1.427E+03	-1.571E+02	-1.863E+03	-1.965E+03	-1.529E+03	-1.143E+03	-1.139E+03	-1.139E+03	
1.7000E-01	2.164E+10	-2.689E+02	-4.585E+02	-1.855E+03	-1.441E+03	-1.875E+03	-1.923E+03	-1.542E+03	-1.342E+03	-1.015E+03	-7.762E+02	
4.5500E-01	3.427E+02	8.621E+02	1.330E+03	-1.534E+02	-3.104E+03	-2.316E+03	-2.207E+03	-2.015E+03	-1.486E+03	-1.486E+03	-1.486E+03	
1.6000E-01	5.040E+03	1.378E+03	-5.641E+02	-5.847E+02	-1.703E+03	-1.362E+03	-1.665E+03	-1.663E+03	-9.648E+02	-1.684E+02	-1.684E+02	
0.4000E-01	6.616E+03	1.613E+03	3.370E+02	4.820E+02	-1.314E+03	-4.744E+02	1.315E+03	8.675E+02	2.197E+02	9.763E+02	9.763E+02	
2.0000E-01	8.531E+03	2.948E+03	3.356E+03	3.627E+02	2.061E+02	2.785E+02	6.245E+03	4.135E+03	2.317E+03	2.980E+03	2.980E+03	
1.3500E-01	1.041E+04	5.141E+03	5.842E+03	8.261E+03	4.935E+03	3.314E+03	1.070E+04	1.311E+04	1.182E+04	1.051E+04	1.051E+04	
4.5000E-02	1.181E+04	1.027E+04	5.965E+04	1.114E+04	9.261E+02	1.006E+04	1.769E+04	1.991E+04	1.771E+04	1.374E+04	1.374E+04	
7.0000E-02	1.268E+04	2.415E+04	3.204E+04	1.764E+04	5.135E+04	2.375E+04	2.536E+04	2.271E+04	1.968E+04	1.437E+04	1.437E+04	
5.0000E-02	1.505E+04	2.644E+04	3.345E+04	2.005E+04	4.624E+04	2.974E+04	2.740E+04	2.551E+04	2.343E+04	2.061E+04	2.061E+04	
3.0000E-02	3.064E+04	4.441E+04	4.441E+04	2.640E+04	4.791E+04	4.618E+04	2.957E+04	2.551E+04	2.588E+04	2.261E+04	2.261E+04	
1.0000E-02	3.065E+04	4.730E+04	7.604E+04	7.661E+04	4.095E+04	8.141E+04	3.579E+04	3.315E+04	4.028E+04	5.225E+04	5.225E+04	
-2.2500E-02	2.254E-15	2.157E-15	1.614E-15	-2.031E-15	-1.051E-16	-1.618E-07	-1.538E-07	-9.932E-08	-1.314E-08	-1.124E-08	-1.124E-08	
-1.4750E-01	-8.600E-21	3.693E-20	5.844E-20	-1.492E-19	2.121E-20	3.521E-20	-8.106E-20	5.724E-20	2.206E-20	-3.820E-20	-3.820E-20	
-4.2500E-01	-4.254E-30	7.848E-31	5.814E-31	-1.004E-29	-1.841E-31	5.844E-31	-6.716E-30	6.044E-30	5.211E-30	-7.781E-30	-7.781E-30	
-1.0000E-01	-2.557E-04	4.135E-04	1.556E-04	-3.295E-04	-1.377E-04	8.149E-04	-3.233E-04	4.036E-04	3.761E-04	-5.975E-04	-5.975E-04	
-1.2000E+00	-7.950E-51	2.051E-50	-1.549E-50	-1.652E-50	-1.051E-50	-4.374E-51	-2.159E-50	1.960E-50	-3.794E-50	-3.067E-50	-3.067E-50	
-1.6000E+00	-9.978E-51	-1.238E-50	-4.236E-50	-4.740E-50	-1.601E-50	-2.266E-50	-2.633E-50	-3.147E-50	-3.794E-50	-4.613E-50	-4.613E-50	
-2.0000E+00	-2.917E-00	-2.615E-00	-4.236E-00	-4.740E-00	-1.601E-00	-2.266E-00	-2.633E-00	-3.147E-00	-3.794E-00	-4.613E-00	-4.613E-00	
-2.4000E+00	-8.406E-30	-1.011E-29	-1.169E-29	-1.284E-29	-1.441E-29	-1.631E-29	-1.860E-29	-2.137E-29	-2.472E-29	-2.877E-29	-2.877E-29	
-2.8000E+00	-2.344E-19	-2.664E-19	-2.915E-19	-3.175E-19	-3.444E-19	-3.744E-19	-4.143E-19	-4.590E-19	-5.117E-19	-5.736E-19	-5.736E-19	
-3.2000E+00	-7.452E-01	-7.576E-01	-7.576E-01	-7.576E-01	-3.731E+01	-3.794E+01	-3.838E+01	-3.838E+01	-3.838E+01	-3.838E+01	-3.838E+01	
-7.2500E+00	-1.671E-01	-1.616E-01	-1.573E-01	-1.534E-01	-1.497E-01	-1.450E-01	-1.395E-01	-1.339E-01	-1.266E-01	-1.192E-01	-1.192E-01	
-1.0500E+01	-2.054E-10	-2.114E-06	-2.110E-06	-2.057E-06	-2.073E-06	-2.073E-06	-1.983E-06	-1.914E-06	-1.826E-06	-1.720E-06	-1.720E-06	

Figure E-6. Spatial distributions of fields, currents, and charge for ABORC calculations at 20 nsec. This printout is also designated "2-D print" elsewhere in this appendix.





UN ARE (VOLT/M OR AMP/M)  
64 57 FIRST DIMENSION OF ARRAY 100

[illegible]

Figure E-6 (cont.)

[illegible][illegible]

**BEST AVAILABLE COPY**

ORAMP/M2) PRIMARY ELECTRON PARTICLES ONLY

MULT	LY BY	1.E-01	PEAK ABS VALUE	1.257603E+02 INDEX RANGES	65	57 FIRST DIMENSION OF ARRAY 103	24
0.							
6.3000E-01	7	0	0	0	0	0	0
5.1000E-01	0	0	0	0	0	0	0
4.0000E-01	0	0	-4	0	0	0	0
3.2000E-01	0	-2	-12	1	-3	0	0
2.4000E-01	0	-42	-61	1	-17	0	-1
1.6000E-01	-4	-5	139	18	0	0	0
1.1000E-01	-4	49	0	109	0	0	0
8.0000E-02	0	179	113	0	13	0	0
6.0000E-02	167	0	157	0	151	0	0
4.0000E-02	826	0	-84	641	0	0	0
2.0000E-02	0	-662	228	1248	0	0	0
0.	0	-283	309	308	0	0	0
-4.5000E-02	0	0	0	0	0	0	0
-2.5000E-01	0	0	0	0	0	0	0
-6.0000E-01	0	0	0	0	0	0	0
-1.0000E+00	0	0	0	0	0	0	0
-1.4000E+00	0	0	0	0	0	0	0
-1.8000E+00	0	0	0	0	0	0	0

CHARGE IN ZONE (COUL) PRIMARY ELECTRON PARTICLES ONLY

MULTIPLY BY	1.E-08	PEAK ABS VALUE	2.0E+09E-06 INDEX RANGES	65	58 FIRST DIMENSION OF ARRAY 101	24
0.						
4.0000E-01	0	0	0	0	0	0
3.2000E-01	0	0	0	0	0	0
2.4000E-01	0	0	0	0	0	0
1.6000E-01	0	0	0	0	0	0
1.1000E-01	0	0	0	0	0	0
8.0000E-02	0	0	0	0	0	0
6.0000E-02	0	0	0	0	0	0
4.0000E-02	0	0	0	0	0	0
2.0000E-02	0	0	0	0	0	0
0.	0	0	0	0	0	0
-4.5000E-02	0	0	0	0	0	0
-2.5000E-01	0	0	0	0	0	0
-6.0000E-01	0	0	0	0	0	0
-1.0000E+00	0	0	0	0	0	0
-1.4000E+00	0	0	0	0	0	0
-1.8000E+00	0	0	0	0	0	0

Figure E-6 (cont.)

Table E-4  
RELATIVE POSITIONS ON THE GRID WHERE FIELDS,  
CURRENTS, AND CHARGE ARE CALCULATED

Quantity	Axial Position <sup>a</sup>	Radial Position <sup>a</sup>
$E_z$	c	b
$E_r$	b	c
H	c	c
$J_z$	c	b
$J_r$	b	c
CHARGE IN ZONE	b	b

#### E-5.3 PLOTALL Output Description

The plot code output is shown in Figure E-7 as it typically appears at the end of an ABORC calculation. This example is for the case of plotting only one file of data generated by a single ABORC run. Discussion on overlaying additional files of data is given in the following section.

Notice that the plot code inputs are printed, and then most of the ABORC inputs are given. These quantities reside on the plot files, enabling the user to check an old file to determine exactly what ABORC inputs were used to generate it. Also notice that the exact plot positions are listed along with information pertinent to file and plot manipulation.

Finally, sample plots are shown in Figure E-8 for the normal electric field at the top of the cylinder and the surface current density at the middle of the side. The curves are smoothed over 1 nsec. The plot type and exact location on the ABORC grid are given above the plot, along with a convenient plot number and the ABORC title card.

STEPS ON THIS FILE

BEST AVAILABLE COPY

BEST AVAILABLE COPY

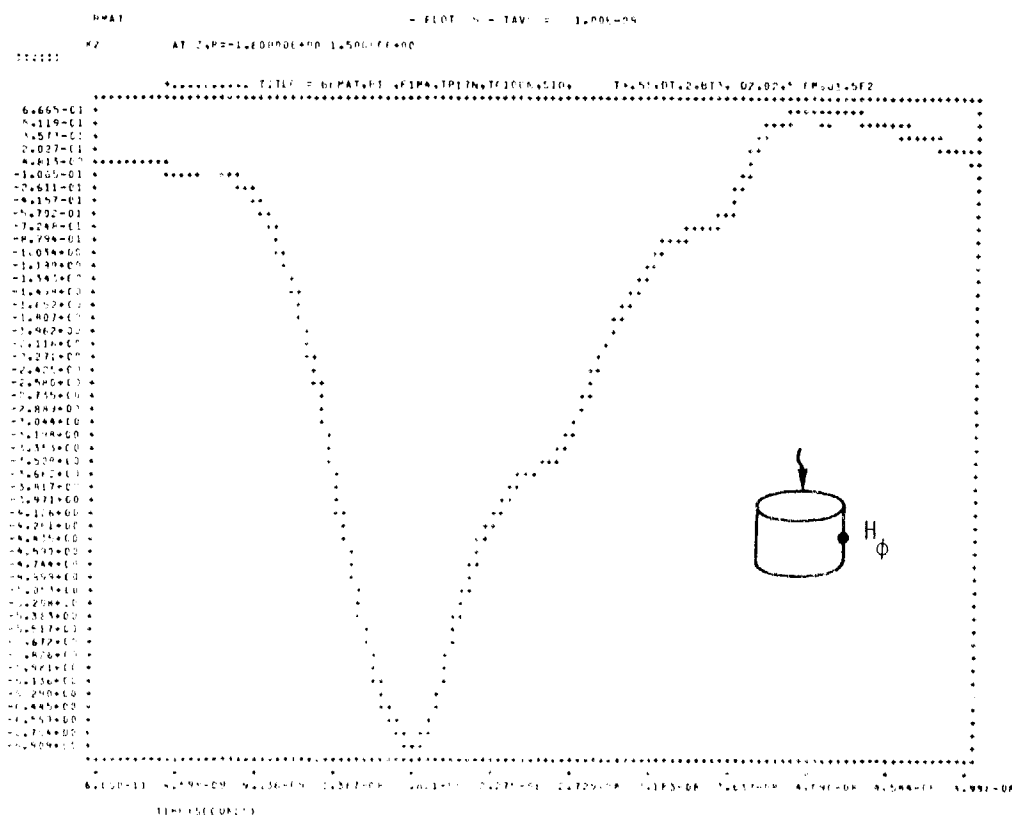
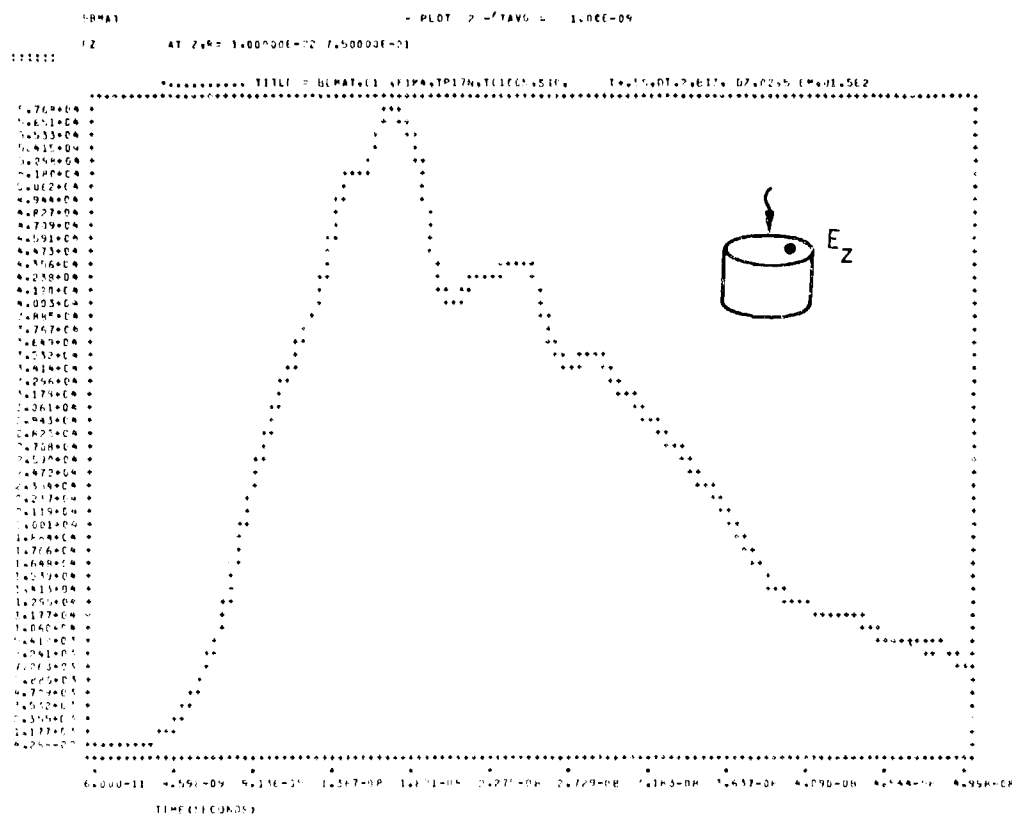


Figure E-8. Sample ABORC plots for electric field at top of cylinder at midpoint and magnetic field at midpoint at side

## E-5 GENERATION OF OVERLAID PLOTS — PLOTALL CODE

A FORTRAN IV computer code called PLOTALL is part of the ABORC computer system. This code operates on ABORC and QUICKE2 (Ref. 1) data files to produce plots of specified quantities. As many as three such files can be overlaid on the same grid and the plots directed to the printer or to a pen-plotter. Computer requirements for these plots are minimal for printer plots and, of course, require a pen-plotter for the higher-resolution plots. Also, plots can be made on CRT or other plotters with appropriate software used with PLOTALL. This section discusses how to generate overlaid plots with the code. Inputs are described and a sample case is discussed. Emphasis is given here to an example of overlaid plot files. An example of plotting a single file is given in the previous section in conjunction with the ABORC sample problem.

While the examples given in this appendix are for ABORC data file manipulation, the capabilities discussed and illustrated also apply to QUICKE2 data files. In the latter case, spectra are plotted rather than time histories, and typically no data-smoothing is performed. PLOTALL capabilities such as comparing curve 1 on file TAPE7 with curve 2 on file TAPE8 are still the same. Most plot runs are done using the negative value for the "number of files" specification [IOPT(1)], however, which allows inputting only two data cards to define the plots once the proper data files are loaded on the system.

An important function performed by the PLOTALL code is that of curve-smoothing. This optional capability is often used in attempts to filter out erroneous high-frequency noise in time history data from ABORC due to particle motion through finite spatial grids. This noise is a byproduct of following too few particles to permit cancellation of statistical fluctuations. The smoothing formula employed by PLOTALL is equivalent to the time-averaging of a voltage pulse entering a circuit with parallel resistance and capacitive elements. The capacitor voltage responds to the incident voltage with a characteristic RC time constant. Similarly, all

---

<sup>1</sup>S. H. Rogers and A. J. Woods, "QUICKE2: An Analytical Electron Emission Code," INTEL-RT 8141-026, June 15, 1976.

curves treated by PLOTALL can be smoothed as if they are voltage pulses, causing a delayed response. The characteristic time is designated as the averaging time and is specified to the code. The equation for the averaging is

$$\frac{df(t)}{dt} + \frac{f(t)}{\tau} = g(t) ,$$

where

$g(t)$  = input function to be time-averaged smoothed,

$\tau$  = characteristic smoothing time,

$f$  = resulting time-smoothed function.

#### E-6.1 PLOTALL Inputs

Inputs to the PLOTALL code are described here, along with a few pointers on required specifications for desired outputs.

In the input card descriptions which follow, the abbreviations D and MAX stand for default and maximum allowed value. Notice the special instructions at the far right of the figures for some of the cards. Additional instructions are given below, along with Table E-5, which lists some constraints on input and calculation variables.

##### Note on Defaults

Card types 4 and 5 must be input in groups of NFILE cards of each type, where NFILE can be from 1 to 3. Values on cards after the first one in each set are assumed to be the value on the first card unless a value appears on the subsequent card. Therefore, defaults listed here pertain only to the first card of the set.

##### Additional Notes and Definitions

- PLOTALL looks for data on files TAPE7, TAPE8, and TAPE , depending on number of files being overlaid.
- Curves on the same file can be overlaid by copying the data to two of the files used by PLOTALL and then specifying appropriate plot positions with the IPPOS cards (card 4).
- "File" is defined as a block of curves generated by one ABORC or one QUICKE2 calculation.
- "Plot" is defined as the figures generated in which one to three curves of the separate "files" are overlaid.



### E-6.2 PLOTALL Sample Problem

A sample problem is considered here. The example is to overlay three separate ABORC results on the same grid. Each file is copied to one of the three used by PLOTALL, TAPE7-9. The inputs to the code are shown in Figure E-9. The spacings indicate that blank cards have been used for specifications for data on TAPE8 and TAPE9. The defaults of plotting every curve on every file and averaging over the same time constant have been employed. An example output of the computer run is given in Figure E-10. Notice the plot title at the top, the plot number given by the code for convenience, the averaging time, the plot type, exact position, and ABORC run titles defining the curves. All of these features are printed automatically, making identification of the plots very positive. Additional features of the PLOTALL code are described in the ABORC sample problem section.

## E-7 GENERATION OF ELECTRON MOTION MOVIES — MOVIE CODE

A FORTRAN IV computer code called MOVIE is part of the ABORC system. This code operates on ABORC and DYNASPHERE (Ref. 2) data files to produce movies showing the motion of particles representing photo-electrons emitted from the object(s). The code requires a file of data (either a permanent file or a tape) produced by invoking the appropriate option in the SGEMP calculation and taking the simple control card procedures necessary for saving the file. This section details to the programmer how to make a movie of ABORC photo-electrons once the file of information is available. Generation of the file is explained above in the ABORC input description section or in the DYNASPHERE user's manual. A brief description is given below of steps necessary to use the MOVIE code, description of code inputs, sample inputs, and discussion of a sample movie frame.

### E-7.1 MOVIE Input Requirements

ABORC provides all the particle position information at each time step, but the MOVIE code is not presently set up to automatically describe the body outlines from the ABORC inputs. Therefore, certain inputs must

<sup>2</sup>A. J. Woods, "User's Manual for the DYNASPHERE SGEMP Computer Code," INTEL-RT 8141-029, April 1976.

# PLOTALL INPUTS

COLUMN FORMAT	1-40 ZABC				
CARD 1	Title of plot run.				
SYMBOL	MASTIL(1-4)				

COLUMN FORMAT	1-2 12	3-4 12	5-6 12	7-8 12	
CARD 2	No. of files to be overlaid. If 0, NFILE = IOPT(1) and no more inputs to PLOTALL are read in. C=1. Max = 3 (NFILE)	No. of plots to be generated. D = Max number on files. Max = 40	0 printer plots only. 1 printer and pen plots. D=0.	Read in NTITL titles of curves if 0. In addition to titles on dump tape. Max = 40 (NTITL)	
SYMBOL	IOPT(1)	IOPT(2)	IOPT(3)	IOPT(4)	

COLUMN FORMAT	9-10 12		13-14 12	15-16 12	
CARD 3 (cont.)	Option which allows non-standard files to be plotted. Not necessary for ABORC files. D=0.		DEBUG Print out data in first IOPT(7) or so. Buffer reads from files if 0. D=0.	DEBUG Checks time averaging on first file if 0. Plot averaged and unaveraged curves are overlaid. D=0.	
SYMBOL	IOPT(5)		IOPT(7)	IOPT(8)	

COLUMN FORMAT	17-18 12	19-20 12	21-22 12	23-24 12
CARD 2 (cont.)	DEBUG Print out data just before call plot routines if > 0. D=0.	Plot every NPTSKP points. D=1. (NPTSKP)	<0 do not print. ≥0 print every IPRINT time points. D=0. (IPRINT) Value of zero causes about 50 points for each curve to be printed.	Print every NPRAVG points of averaged data if > 0. D=0. (NPRAVG) Not operational at present.
SYMBOL	IOPT(9)	IOPT(10)	IOPT(11)	IOPT(12)

COLUMN FORMAT	1-10	11-20
CARD 3	Consider only data for time > TSTART. ★ D=0. (sec)	Consider only data for time ≤ TFIN. ★ D=∞. (sec)
SYMBOL	TSTART	TFIN

COLUMN FORMAT	1-80 4Q12
CARD 4	Positions of curves on file to be plotted. D = every curve up to NPTMX [IOPT(2)]. Starting with #1, Max = 40. See note on defaults
SYMBOL	

\* DELAY is added to the time for each data point, then TSTART and TFIN are checked.

**BEST AVAILABLE COPY**

CARD 5	1-10 E10	11-20 E10	21-30 E10		Read in NFILE card 5's.
	Average data on this file over -AY seconds. Don't average (see default note)	Multiply data on this file by FNORM. (see default note) D=1.	Delay data on this file by DELAY sec- onds in plots. D=0. *		
CARD 6	1-10 A10	11-20 A10			Read in NTITL cards if IOPT(4)>0.
	Curve title for plot #1. (in addition to plot title and pos- ition) D=blank.	Curve title for plot #2. D=blank.	etc.		
CARD 7					
CARD 8					
CARD 9					
CARD 10					

[illegible]

Table E-5  
MINIMUM AND MAXIMUM ALLOWED VALUES OF PLOTALL  
INPUT AND CALCULATIONAL VARIABLES

Quantity	Minimum Value Allowed	Maximum Value Allowed
Number of different files overlaid	1	3
Number of different plots	1	40
Number of point pairs on one plot	2	4000

BBMAT,REFQ SENS  
3

2,      -09

Figure E-9. Sample PLOTALL input card. These cards indicate that three files of data are to be overlaid and averaged over 2 nsec. There are three blank cards after the "3" and two blank cards after the "2,-09" card.

**BEST AVAILABLE COPY**



Figure E-10. Sample output of computer run

be specified to MOVIE if an outline of the object(s) is desired on the frame. Other options such as spatial/temporal plots, which can appear on the frame along with the particle motion, must also be specified to the code. These capabilities can be invoked using straightforward procedures described in Table E-6. Obviously, the additional steps of special control card procedures are needed to direct the calculations to the proper disposal station of the computer, but these commands are entirely installation-specific and so are not discussed here. The capabilities of specifying time histories or spatial distributions of plot quantities along with particle trajectories exist only on ABORC MOVIE files. DYNASPHERE movies contain only particle trajectories, and the spherical surfaces are obtained automatically from the data file. All of the inputs described in Table E-6 are still defined, but some are only dummies.

#### E-7.2 Sample MOVIE Code Inputs

A sample of MOVIE code inputs is shown in Figure E-11. Note that this input does not produce the sample frame shown in Figure E-12.

#### E-7.3 Sample MOVIE Frame

A sample frame generated by the MOVIE code is shown in Figure E-12. The axis of the object is at the left side of the frame. At this time of 48 nsec (shown at bottom center), the electrons have moved far away from the object. This case was for low fluence, so no space-charge-limiting occurred. The graph on the right shows the magnetic field near the boom of the object. Any quantity available on the data file could have been specified here. The large title at the top would appear in the position of the first title card shown in Figure E-11, while the smaller title under the graph would be input in the second title card input given in the example. The small title underneath the main title on the frame is the title card used in the ABORC run, which is automatically obtained from the MOVIE file by the coding.

Table E-6  
INPUTS FOR MOVIE CODE

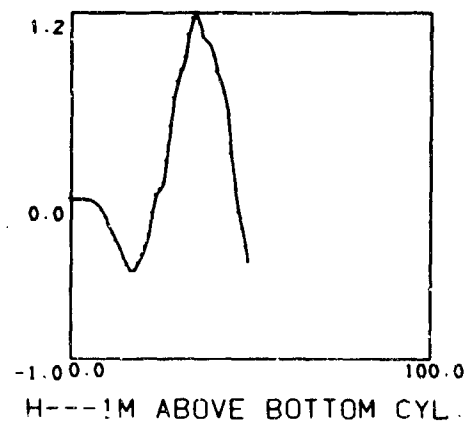
Card(s)	Columns	Format	Variable	Description
1	1-32	8A4	MOVTIT(I)	Movie title (placed at top of each frame).
2	1-10	I10	IPART	>0 to plot trajectory of particles. ≤0 no particles plotted.
2	11-20	I10	NGRAPH	Number of curves to be plotted in graph if IPOS ≤ 0; number of points on graph if IPOS > 0; NGRAPH = 15. ABORC only.
2	21-30	I10	IPOS	>0 plot graph quantities versus position (or other measure). ≤0 plot graph quantities versus time. ABORC only.
3	1-24	6A4	GRATIT(I)	Graph title (placed below graph). ABORC only.
4	1-80	8I10	IGRAPH(I)	File numbers of data to be plotted on graph (files are read from ABORC plot tape); 1 to NGRAPH values up to 3 allowed. ABORC only.
(Use card 5 only if IPOS = 0)				
5	1-80	8E10.3	POS(I)	Position (or other measure) of graph quantity I; 1 to NGRAPH values.
6	1-10	E10.3	TAV	Time to average quantities over (nsec). ABORC only.
6	11-20	E10.3	FGEOM	Factor to reduce bound of geometry by.
7	1-10	I10	IREP	Number of times to repeat each movie frame.
8	1-10	I10	NCLOSE	>0 if close-up of part of the body desired (give only the geometry of that part) ≤0 whole body.
8	11-20	I10	NXY	Total number of points to define geometry of body (only intersection points need be given); ABORC only.
8	21-30	I10	NG	Number of groups in which to construct body (points in each group are connected); 1 ≤ NG ≤ 4; ABORC only.
8	31-70	rI10	NP(I)	Number of points in each group; 1 to NG values; ABORC only.
9	1-80	8E10.3	EP(I)	E-coordinate of points defining body; 1 to NXY values; ABORC only.
10	1-80	8E10.3	RP(I)	R-coordinate of points defining body; 1 to NXY values; ABORC only.



		OUTSIDE OBJ RESPONSE	1
		2	
		ENRM VS. X	1
.005	.	.0125	
.1	.	.1	
	3		
	1		
.7875		.615	14
.889	.	.855	
.26	.	.26	
.26	.	.26	
		.813	
		.855	
		.27	
		.27	

Figure E-11. Sample MOVIE code inputs

DUMBBELL--1M BOOM--LOW FLUENCE  
DUM/10/ . FLU=1.E-5. BRAD POEM.DELMEQ.T+.SSIDE EM..COS.30X30 TANK.B4 .DT.2



TIME = 48.0 NS

Figure E-12. Sample movie frame produced by MCVIE code

## DISTRIBUTION LIST

### DEPARTMENT OF DEFENSE

Director  
Defense Advanced Rsch. Proj. Agency  
ATTN: NMR

Director  
Defense Communications Agency  
ATTN: NMR

Defense Documentation Center  
Cameron Station  
12 cy ATTN: TC

Director  
Defense Intelligence Agency  
ATTN: DB-4C

Director  
Defense Nuclear Agency  
2 cy ATTN: RAEV  
3 cy ATTN: TITL, Tech. Library  
ATTN: TISI, Archives  
ATTN: DDST

Dir. of Defense Rsch. & Engineering  
Department of Defense  
ATTN: S&SS (OS)

Commander  
Field Command  
Defense Nuclear Agency  
ATTN: FCFR  
ATTN: FCLMC

Director  
Interservice Nuclear Weapons School  
ATTN: Document Control

Director  
Joint Strat. Target Planning Staff, JCS  
ATTN: JLTW-2

Chief  
Livermore Division, Field Command, DNA  
Lawrence Livermore Laboratory  
ATTN: FCPRL

National Communications System  
Office of the Manager  
ATTN: NCS-TS

Director  
National Security Agency  
ATTN: R-425

OJCS/J-3  
ATTN: J-3, RLTA Br., WWMCCS Plans Div.

OJCS/J-5  
ATTN: J-5, Plans & Policy Nuc. Div.

### DEPARTMENT OF THE ARMY

Director  
BMD Advanced Tech. Center  
Huntsville Office  
ATTN: RDMH-O

Commander  
BMD System Command  
ATTN: BDMSC-TEN

Dep. Chief of Staff for Rsch. Dev. & Acq.  
Department of the Army  
ATTN: DAMA-CSM-N

Commander  
Harry Diamond Laboratories  
ATTN: DRXDO-TI, Tech. Lib.  
ATTN: DRXDO-RCC, Raine Gilbert  
ATTN: DRXDO-RCC, John A. Rosado  
ATTN: DRXDO-NP

Commander  
Picatinny Arsenal  
ATTN: SARPA  
ATTN: SMUPA

Commander  
Redstone Scientific Information Center  
US Army Missile Command  
ATTN: Chief, Documents

Chief  
US Army Communications Sys. Agency  
ATTN: SCCM-AD-SV, Library

Commander  
US Army Electronics Command  
ATTN: DRSEL

Commander  
US Army Foreign Science & Tech. Center  
ATTN: DRXST-ISI

### DEPARTMENT OF THE NAVY

Chief of Naval Operations  
Navy Department  
ATTN: Code 604C3

Chief of Naval Research  
Navy Department  
ATTN: Henry Mullaney, Code 427

Director  
Naval Research Laboratory  
ATTN: Code 7701  
ATTN: Code 5410, John Davis

Officer-in-Charge  
Naval Surface Weapons Center  
ATTN: Code WA501, Navy Nuc. Prgms. Off.

DEPARTMENT OF THE NAVY (Continued)

Director  
Strategic Systems Project Office  
Navy Department  
ATTN: NSP

DEPARTMENT OF THE AIR FORCE

AF Geophysics Laboratory, AFSC  
ATTN: Charles Pike

AF Materials Laboratory, AFSC  
ATTN: Library

AF Weapons Laboratory, AFSC  
ATTN: SUL  
2 cy ATTN: NTS  
2 cy ATTN: DYC

Hq. USAF/RD  
ATTN: RDQSM

Commander  
Rome Air Development Center, AFSC  
ATTN: Edward A. Burke

SAMSO/DY  
ATTN: DYS

SAMSO/MN  
ATTN: MNNH  
ATTN: MNNG

SAMSO/SK  
ATTN: SKF

SAMSO/XR  
ATTN: XRS

Commander in Chief  
Strategic Air Command  
ATTN: XPFS  
ATTN: NRI-STINFO, Library

ENERGY RESEARCH & DEVELOPMENT ADMINISTRATION

University of California  
Lawrence Livermore Laboratory  
ATTN: Tech. Info. Dept. L-3

Los Alamos Scientific Laboratory  
ATTN: Doc. Con. for Reports Lib.

Sandia Laboratories  
Livermore Laboratory  
ATTN: Doc. Con. for Theodore A. Dellin

Sandia Laboratories  
ATTN: Doc. Con. for 3141, Sandia Rpt. Coll.

OTHER GOVERNMENT AGENCY

NA  
Lewis Research Center  
ATTN: Carolyn Purvis  
ATTN: Library  
ATTN: N. J. Stevens

DEPARTMENT OF DEFENSE CONTRACTORS

Aerospace Corporation  
ATTN: V. Josephson  
ATTN: Frank Hai  
ATTN: Julian Reinheimer  
ATTN: Library

Avco Research & Systems Group  
ATTN: Research Lib., A830, Rm. 7201

The Boeing Company  
ATTN: Preston Geren

University of California at San Diego  
ATTN: Sherman DeForest

Computer Sciences Corporation  
ATTN: Alvin T. Schiff

Dr. Eugene P. DePlomb  
ATTN: Eugene P. DePlomb

Dikewood Industries, Inc.  
ATTN: Tech. Lib.  
ATTN: K. Lee

EG&G, Inc.  
Albuquerque Division  
ATTN: Technical Library

Ford Aerospace & Communications Corp.  
ATTN: Library  
ATTN: Donald R. McMorow, MS G30

General Electric Company  
Space Division  
Valley Forge Space Center  
ATTN: Joseph C. Peden, VFSC, Rm. 4230M

General Electric Company  
TEMPO-Center for Advanced Studies  
ATTN: William McNamara  
ATTN: DASIAIC

Hughes Aircraft Company  
Centinela & Teale  
ATTN: Tech. Lib.

Hughes Aircraft Company, El Segundo Site  
ATTN: William W. Scott, MS A1080  
ATTN: Edward C. Smith, MS A620

Institute for Defense Analyses  
ATTN: IDA, Librarian

IRT Corporation  
ATTN: Technical Library  
ATTN: Dennis Swift  
ATTN: Andrew J. Woods  
ATTN: Thomas N. Belmer

Jaycor  
ATTN: Eric P. Wenaas  
ATTN: Library

Jaycor  
ATTN: Robert Sullivan

Johns Hopkins University  
Applied Physics Laboratory  
ATTN: Peter E. Partridge

DEPARTMENT OF DEFENSE CONTRACTORS (Continued)

Kaman Sciences Corporation  
ATTN: W. Foster Rich  
ATTN: Library  
ATTN: Jerry I. Lubell

Lockheed Missiles & Space Company, Inc.  
ATTN: Dept. 85-85

McDonnell Douglas Corporation  
ATTN: Stanley Schneider

Mission Research Corporation  
ATTN: Roger Stettner  
ATTN: Conrad L. Longmire

Mission Research Corporation-San Diego  
ATTN: Library  
ATTN: V. A. J. Van Lint

R & D Associates  
ATTN: Technical Library  
ATTN: Leonard Schlessinger

DEPARTMENT OF DEFENSE CONTRACTORS (Continued)

Rockwell International Corporation  
ATTN: Technical Library

Science Applications, Incorporated  
ATTN: William L. Chadsey

Simulation Physics, Inc.  
ATTN: Roger G. Little

Stanford Research Institute  
ATTN: Library

Systems, Science & Software, Inc.  
ATTN: Technical Library  
ATTN: Andrew R. Wilson

TRW Defense & Space Sys. Group  
2 cy ATTN: Robert M. Webb, R1-2410  
ATTN: Tech. Info. Center/S-1930